FINITE AMPLITUDE UNSTEADY SLENDER BODY THEORY AND EXPERIMENTS

Thesis by

George Thomas Yates

In Partial Fulfillment of the Requirements

for the Degree of

Doctor of Philosophy

California Institute of Technology

Pasadena, California

1977

(Submitted September 23, 1976)

"I am the wiser in respect to all knowledge and the better qualified for all fortunes for knowing that there is a minnow in that brook."

— Thoreau

ACKNOWLEDGMENTS

I would like to extend my deepest appreciation to Professor Theodore Y. T. Wu. His guidance and encouragement were essential elements in the development of this work, and for his continued assistance I am most sincerely grateful.

I am also indebted to Dr. Allen T. Chwang for his interesting discussions on some of the theoretical issues and for his assistance in several of the computational results. Thanks also go to Dr. Anthony T. Cheung for helping with the figures. Special thanks are due to Mr. Glenn Bowlus and Mr. Pui Lam for their help in the construction of the experimental apparatus and the subsequent data acquisition and reduction.

For her patient transcribing of my handwriting and for her skillful preparation of this manuscript, I am greatly indebted to Helen Burrus. Thanks also go to Cecilia Lin for preparation of the figures.

Appreciation for financial assistance is due to the Institute's Graduate Research and Teaching Assistantships. The National Science Foundation and the Office of Naval Research are also acknowledged for their financial support of this investigation.

ABSTRACT

A theoretical study is carried out of the potential flow about slender bodies. Several theoretical models are discussed and new developments are directed toward a finite amplitude theory where flow singularities are distributed along the body centerline, which may undergo arbitrary body motion and the body cross section is presently restricted to being circular. Guided by the example of a toroidal ring, for which simple symmetry in shape makes a highly accurate solution possible, the general theory is developed and results are given for the force and rate of work done by the fluid on the moving body. An example with application to the anguilliform mode of aquatic animal propulsion is given and compared to observations on a swimming eel (Synbranchus marmoratus).

Next, an experimental investigation is discussed, where a truly three-dimensional body (modeled after a Chinook salmon) was used to examine the basic slender body assumptions. Pressure measurements were made on the model surface using a set of high sensitivity pressure transducers, and several theoretical solutions are evaluated and compared with the measured pressure distribution.

TABLE OF CONTENTS

LIST OF FIGURES

LIST OF FIGURES (cont'd)

I. INTRODUCTION

Acting both as a casual observer and as a scientific investigator, man has long been fascinated by the movement of fish and of other aquatic animals. Researchers have approached the subject from a variety of different perspectives as shown by the diverse background of the participants at a recent symposium on swimming and flying in nature (Wu et al., 1975), and cooperation between disciplines has proved mutually beneficial. Reviewing the literature and the approaches taken by the various investigators is itself a major endeavor and reference is made here to the reviews of Lighthill (1969) and Webb (1975).

Extensive use of potential flow theory is made and before beginning the detailed discussions a word regarding its validity in such problems is in order. The Reynolds number for fish swimming generally lies in the range $10^4 < Re < 10^8$, and at such high Reynolds numbers the effects of viscosity are confined to a thin boundary layer adjacent to the body surface. Since the streamlined shape of fish should give rise to gentle pressure gradients, the boundary layer should not be prone to flow separation. The boundary layer is expected to thicken continually along the body in the flow direction reaching at the worst only a few per cent of the body length in the tail region. The flow outside of this boundary layer can be treated by potential flow theory and the pressure field computed by such inviscid theories remains constant across the boundary layer and generates the thrust on the body which must overcome the drag arising from the viscous shear stresses of the fluid on the body in the boundary layer region.

The approach taken in this dissertation is to use the data which is already available on aquatic animal swimming to shed light on fundamental problems in fluid mechanics. To this end an extension of the slender body theory is made to allow for finite amplitude body motion and to account for body centerline curvature. Although the theory is done in the context of aquatic animal propulsion the results are equally applicable to problems in ship hydrodynamics (Letcher, 1975). For example, chapter IV has direct application to anchor, towing, and mooring lines, and with appropriate modifications to ship maneuverability and to ship oscillatory flow interactions (Newman, 1975).

The discussion begins in chapter II with a review of the classical slender body theory, followed by a treatment of a center plane singularity method which is developed with the aid of an exact potential theory solution for ellipsoidal body shapes. Here the exact potential solution serves two purposes; first as a reliable check on the results from slender body theory and second as a guiding example for the development of new theories.

Chapters III and IV are devoted to the development of a new finite amplitude slender body solution using singularity distributions along the body centerline. Treatment of the toroidal ring in chapter III was found instructive in the theory improvement and is included to illustrate the method used in chapter IV, where a body of circular cross section is considered undergoing plane finite amplitude undulations. The body is only required to have a small cross section as compared to the body centerline radius of curvature and to the overall

length. New results are obtained illustrating the influence of body centerline curvature on the local flow quantities, and the resulting sectional force per unit arc length modifies the previous results based on the classical concept of the induced mass of the body (Lighthill, 1960b). Sectional force, sectional rate of work, total force, and total rate of work are found as well as the specific cost of transport which is used to predict an optimum mode of swimming for an example relevant to the swimming of an eel.

Some experimental results are presented in chapters V and VI, for use in evaluating the theories presented in chapter II and IV and to indicate areas of future work. In chapter V a rigid fiberglass model shaped and dimensioned after a Chinook salmon, was towed down a twenty-five-foot-long towing tank and measurements of the local pressures were taken and compared to the theoretical predictions of chapter II. Another set of observations (chapter VI) were made on living organisms while swimming freely in otherwise still water. The motion was recorded on video tape and 16 mm movie film, from which the swimming parameters were extracted for use in the theoretical calculations of chapter IV.

II. SLENDER BODY THEORY AND A COMPARISON TO EXACT POTENTIAL THEORIES

Potential flow theories have had a rich and rewarding history in the development of hydrodynamics, and this chapter deals briefly with several, with a special interest in their application to long slender bodies in an axial or near axial flow. Treatment of the theories is brief and intended primarily for their mutual comparison and for later use in assessing their validity against some experimental results, and detailed development of the theories is available in the literature.

In the first section the classical slender body theory approach is outlined. As a check on the theory's accuracy, the second section deals with an exact treatment for potential flow about a triaxial ellipsoid. Next, using the experience gained through this exact solution a center plane singularity distribution solution method is reviewed. The results from section 2. 1 and 2. 3 have application to a wide range of body shapes while the exact solution of section 2. 2 is restricted to ellipsoidal bodies, and hence comparisons of the general body theories is restricted to this class of ellipsoidal bodies.

2. 1 Slender body theory

Slender body theory was first extensively worked on in the context of aerodynamics by M. Munk (1924a, 1924b) and subsequently by Jones (1946a, 1946b) and Ward (1955). Lighthill (1960a) reviews this early work in his forty-eighth Wilbur Wright Memorial Lecture, and has henceforth pioneered much of the ensuing developments (Lighthill, 1960b, 1970, 1971).

Following such now-classical works we consider a slender fish-shaped body swimming with a mean forward velocity U in the negative x-direction. The body has a symmetric thickness function $g(x, y)$ measured from its centerplane; its transverse undulation from the mean forward direction is prescribed by $h(x, t)$ (see figure 2. 1), and the slenderness assumption requires that both g and h be small compared to the body length. The coordinate system is fixed on the stretched-straight body centerline and is moving with the body. According to Lighthill's theory (1960b), the velocity potential may be expressed in the body frame of reference as

$$\Phi = Ux + \Phi_o + \Phi_1 \qquad (2.1.1)$$

where $Ux + \Phi_o$ is the solution of the so-called stretched-straight problem (with $h \equiv 0$), and Φ_1 is the solution to the remaining problem. The stretched-straight problem is now classic and will not be repeated here.

The latter problem for Φ_1 is a two-dimensional problem in the cross flow plane and can be solved by using the complex potential, $f(\zeta)$, where $\zeta = y + iz$ (Newman and Wu, 1973). For the case of no vortex shedding anterior to the tail,

$$f(\zeta) = iV[(\eta^2 - \beta^2)^{\frac{1}{2}} - \zeta - c_o(x)] \qquad (2.1.2)$$

where,

$$V(x, t) = \frac{\partial h}{\partial t} + U \frac{\partial h}{\partial x} \quad , \qquad (2.1.3)$$

and $\eta = \eta_r + i\eta_i$ is the complex plane in which the elliptic cross section is mapped conformally into a slit along the η_r axis from $-\beta$ to $+\beta$. Assuming the body cross section is now elliptic, we obtain

$$g(x, y) = \frac{A(x)}{B(x)} \sqrt{B^2(x) - y^2} \qquad (2.1.4)$$

and

$$\beta = A+B, \qquad 4c^2 = B^2 - A^2 \qquad (2.1.5)$$

$$\eta = \frac{\zeta + \sqrt{\zeta^2 - 4c^2}}{2} + \frac{\frac{1}{2}\beta^2}{\zeta + \sqrt{\zeta^2 - 4c^2}} \qquad (2.1.6)$$

The flow velocity and the pressure can be computed from

$$\Phi_1 = \mathrm{Re}\{f(\zeta)\} \ . \qquad (2.1.7)$$

Pressures calculated in this way are compared to the pressures computed from exact potential flows over ellipsoids translating at a constant angle of attack (figure 2.2 and 2.3) given in the next section.

2.2 Exact potential flow solution for a triaxial ellipsoid

The exact solution to the velocity potential of a triaxial ellipsoid in arbitrary translational and rotational motions through an incompressible, inviscid fluid of infinite extent has been known (see e.g., Havelock, 1931) and can be expressed in a variety of forms. Wu and Chwang (1974) represent the solution as a constant volume distribution of doublets and show how the singularities and their region of distribution may be varied to lead to alternate solution forms. For

example, by using Maclaurin's theorem developed in connection with gravitational potentials of ellipsoids (MacMillan, 1958), the doublet distribution over the ellipsoid volume may be reduced to a distribution over any interior confocal ellipsoid with the new strength increased by the factor of the volume ratio of the two ellipsoids. As a limiting case, the confocal ellipsoid reduces to the center plane ellipse and the doublet strength becomes an ellipsoidal distribution. This center plane doublet distribution has been instructive in developing a solution for more general bodies and will be discussed further in the next section.

$$\varphi(x) = -2\pi a_1 a_2 a_3 \beta_i x_i \int_{\lambda}^{\infty} \frac{du}{(a_1^2 + u)\,\Delta(u)} \qquad (2.2.1)$$

for the ellipsoid

$$\sum_{i=1}^{3} (x_i/a_i)^2 = 1 \qquad (a_1 > a_2 > a_3)\ , \qquad (2.2.2)$$

where

$$\beta_i = U_i/[2\pi(2-\alpha_i)] \qquad (i = 1, 2, 3)\ , \qquad (2.2.3)$$

$$\alpha_i = a_1 a_2 a_3 \int_{o}^{\infty} \frac{du}{(a_i^2 + u)\,\Delta(u)}\ , \qquad (2.2.4)$$

$$\Delta(u) = [(a_1^2 + u)(a_2^2 + u)(a_3^2 + u)]^{\frac{1}{2}}\ , \qquad (2.2.5)$$

and λ is the largest root of

$$\sum_{i=1}^{3} \frac{x_i^2}{a_i^2 + \lambda} = 1 \quad . \qquad (2.2.6)$$

This representation has been used to calculate the velocity $\underline{u} = \nabla\varphi$, and the pressure from the Bernoulli equation. When the flow quantities are evaluated on the body surface there remains only one integral to be calculated, namely a_i. Though this integral may also be expressed in terms of the incomplete elliptic integrals of the first and second kind, in the calculations made here it was computed numerically on an IBM 370/158 computer, using Simpson's rule.

It is now possible to compare the pressure jump across a slender body as calculated by slender body theory (section 2.1) and by the exact potential solution for a spheroid (figure 2.2) and a triaxial ellipsoid (figure 2.3). In both plots the incident flow makes a five-degree angle of attack with respect to the long axis of the body (the x-axis). The body length has been taken as unity, and the y-axis has been scaled by the maximum body extent at each cross section. The good agreement between the theories indicates a possible wider application of the slender body theory to more general body geometries. This will be checked later when experimental pressure measurements are available on such general bodies and the theories again assessed (chapter V).

2.3 Solution by singularity distributions on the center plane of body symmetry.

As was noted in the previous section the potential flow solution

about a triaxial ellipsoid can be represented by an ellipsoidal doublet distribution on the focal ellipse. Using this as a guide Wu and Chwang (1974) developed a center plane singularity solution technique for bodies which exhibit a plane of symmetry.

For the case of such a body undergoing simple translation the choice of a doublet distribution on a central plane region S_o gives the velocity potential

$$\varphi = \int_{S_o} \beta_i(\xi, \eta) \frac{\partial}{\partial x_i} \left(\frac{1}{R}\right) d\xi d\eta \qquad (2.3.1)$$

where

$$R = [(x-\xi)^2 + (y-\eta)^2 + z^2]^{\frac{1}{2}} \qquad (2.3.2)$$

Application of the boundary condition that there be no normal flow on the body surface S_b

$$\frac{\partial \varphi}{\partial n} = \underline{U} \cdot \underline{n} \qquad (\underline{x} \in S_b) \qquad (2.3.3)$$

yields the following integral equation, to be solved for the doublet strength $\underline{\beta}$,

$$\int_{S_o} \beta_i(\xi, \eta) K_i(x, y, z; \xi, \eta) d\xi d\eta = U_j n_j \qquad (\underline{x} \in S_b) \qquad (2.3.4)$$

where

$$K_i(x, y, z; \xi, \eta) = n_j \frac{\partial}{\partial x_j} \frac{\partial}{\partial x_i} \left(\frac{1}{R}\right) . \qquad (2.3.5)$$

Since the region of integration is unknown, this integral equation is

strictly speaking nonlinear, and theory for this kind of integral equation is in its infancy. For bodies with nonstationary transverse curvature on the plan form, the parametric representation for the boundary points of S_o is taken as,

$$x_o^2 = x(x + \zeta\, \zeta_x) \quad \text{and} \quad y_o^2 = y(y + \zeta\, \zeta_y) \qquad (2.3.6)$$

where the body surface S_b is defined by the function $\zeta(x, y)$ through

$$z = \pm\, \zeta(x, y) \qquad (\underline{x} \in S_b) \quad . \qquad (2.3.7)$$

It should be noted that this parametric representation (2.3.6) is an unproven rule which works successfully in the cases tested.

Having chosen the region S_o it remains only to solve an integral equation of the first kind. This was done numerically on an IBM 370/158 computer. The region S_o was broken into N small areas of dimension Δx by Δy on which the doublet strength is assumed constant. The integrals over the Δx by Δy areas can be computed analytically and together with the boundary condition (2.3.3) applied at N points on the body surface results in a system of N linear equations. Solving the system of equations involves a matrix inversion and was sensitive to the manner in which the region S_o was divided, and the doublet strength computed in this way was found to oscillate depending on the S_o division. Having a known solution for a triaxial ellipsoid proved helpful in finding the proper division of S_o, and best agreement was obtained when S_o was divided into regions in the same ratio as the body major and minor axis, resulting in square areas

Δx by Δy. Resulting pressure coefficients, which tend to smooth out any variations in the doublet strengths, conform to the exact solution results.

In future application of this center plane singularity method to arbitrary double models where an exact solution is not available for comparison we can only utilize this experience and choose the region S_o in a similar manner. This method has the advantage over other singularity distribution methods, such as surface source distributions in that all the singular points are internal to the body and hence eliminate complications often encountered with boundary singularities in computations of wave resistance. Further applications of this method seems promising particularly in conjunction with developments in solving such integral equations of the first kind.

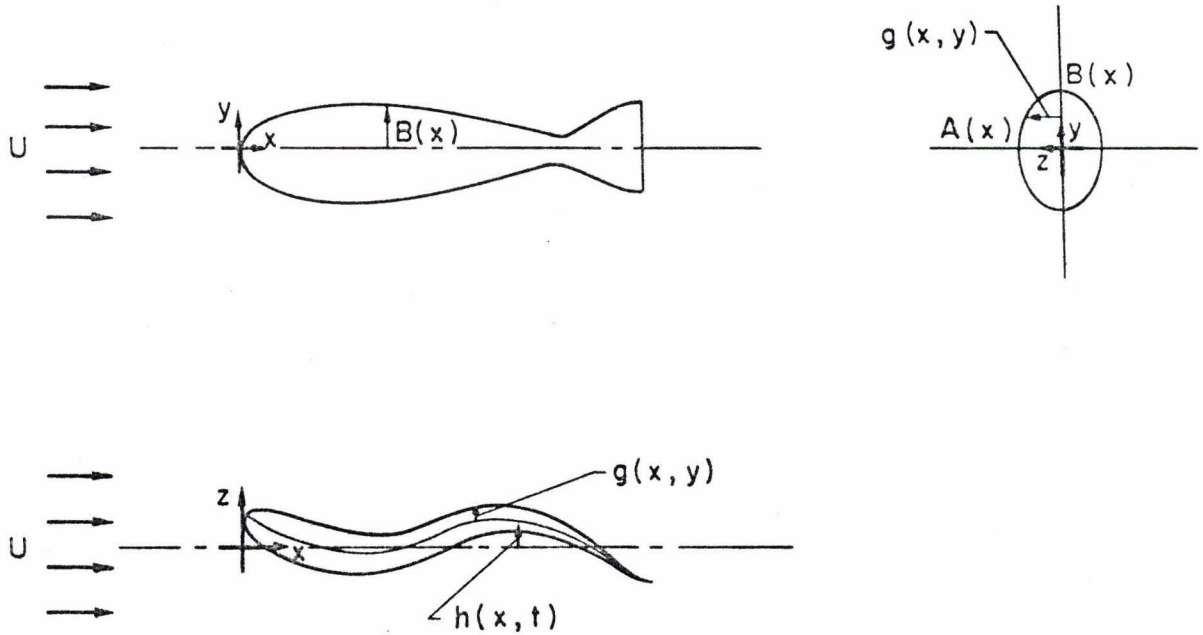

Figure 2. 1. Illustration of the body geometry and the coordinate system used.

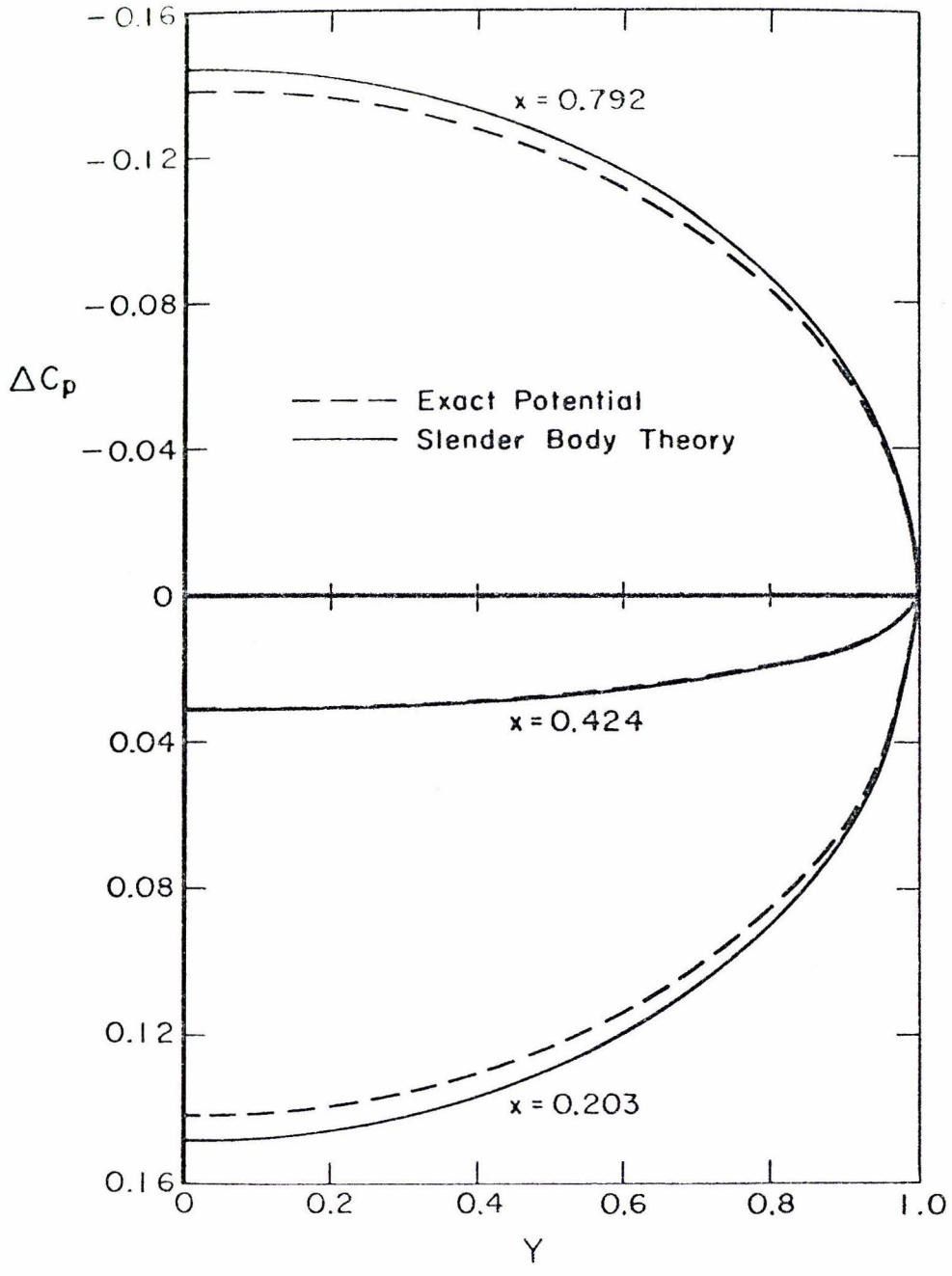

Figure 2.2. ΔC_p is plotted over a given cross section at several locations for two theories (spheroid: $a_1 = 0.5$, $a_2 = a_3 = 0.1434$.

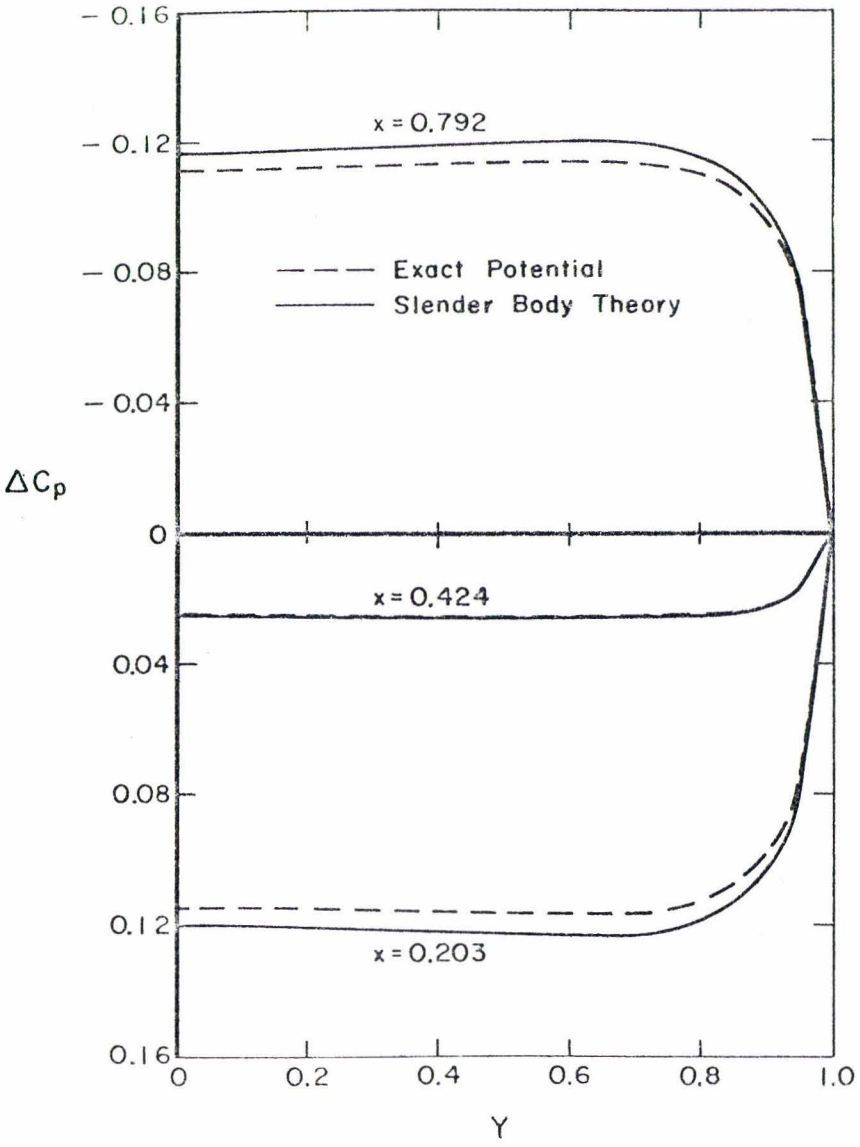

Figure 2.3. ΔC_p is plotted over a given cross section at several locations for two theories (ellipsoid: $a_1 = 0.5$, $a_2 = 0.1434$, $a_3 = 0.0896$.

III. FINITE AMPLITUDE SLENDER BODY THEORY: THE TOROIDAL RING

In order to widen the range of application of slender body theories by removing the restriction of small amplitude, Lighthill (1971) developed a large amplitude elongated body theory by extending his (1970) physical interpretation of the perturbation results. Use was made of a Lagrangian description of the body motion and momentum conservation was used in evaluating sectional forces, in conjunction with a time-varying control volume with a rearward facing surface which translates and rotates with the tail section.

In this chapter and in the next a solution technique using singularity distributions along the body centerline is developed for bodies with circular cross section in arbitrary planar body motion. A local frame of reference is used to facilitate application of the boundary conditions and the effects of nonzero body centerline curvature result in a first-order correction to the velocity potential. The resulting potential is valid uniformly throughout the fluid domain and is expanded close to the body in the slenderness ratio (body radius/body overall length) to give local flow quantities.

The toroidal ring, whose body cross section is everywhere circular, was chosen as the simplest body shape for the primary investigation of finite amplitude slender body theory. The torus is especially well suited for this study since it retains the new features of finite amplitude and of body curvature, while it lacks ends and has an axis of rotational symmetry. Later, more general body geometries

with flexible shape and variable cross section will be considered, but for the first step, this simple model is chosen to illustrate the main approach and to exhibit the new features of the solution.

The arbitrary motion of a torus through an ideal (inviscid and incompressible) fluid consists of three components: a translation along and a translation perpendicular to its axis of rotational symmetry, which will be called the central axis, and a rotation about an axis perpendicular to the central axis and lying in the meridional plane of the body. These three modes of motion will be called broadwise translation, edge-on translation, and on-edge rotation respectively. In addition, two other solutions will be given: first for a torus which is uniformly expanding radially, and then for a torus with a line distribution of sinks on the central axis. Figure 3.1 shows the torus and coordinates used. The torus radius, a, will be called the major radius and the cross sectional radius, b, will be called the minor radius. It is assumed throughout that the ratio of the minor to major radius is small ($\epsilon = \frac{b}{a} \ll 1$).

3.1 Broadwise translation of a toroidal ring

We first consider the translational motion of a toroidal ring moving with velocity U (which may depend on time, t) parallel to its central axis (z-axis). This motion is taken as the simplest for the torus, and two methods of solution are pursued in this case. The first method has general application to more arbitrarily shaped slender bodies, and illustrates some of the features not seen by the second method. Although the second method is limited to use only

with the toroidal rings, it does expedite their solutions. Both methods will be developed here but only the second method will be used in the remaining examples for the ring. The first method will again be used when the finite amplitude flexible motion is considered in chapter IV.

Both methods rely on the choice of appropriate distribution of flow singularities. Since the major radius, a, is assumed large compared to the minor radius, b, we would expect the first-order solution to be that of flow past an infinitely long, straight circular cylinder of radius b. This suggests that the solution may be represented, to the first approximation, by a distribution of doublets along the centroid circle of radius a, and pointing in the direction of the motion. The velocity potential for such a distribution is

$$\varphi(\underline{x}, t) = -\int_0^{2\pi} \frac{\underline{\beta} \cdot (\underline{x} - \underline{x}')}{R^3} \, a d\theta' \quad , \tag{3.1.1}$$

where

$$R = [z^2 + r^2 + a^2 - 2ar\cos(\theta-\theta')]^{\frac{1}{2}} \tag{3.1.2}$$

is the distance between the field point $\underline{x} = (r\cos\theta,\ r\sin\theta, z)$ and the source point $\underline{x}' = (a\cos\theta',\ a\sin\theta', 0)$ on the line doublet at $r = a$.

The first method of solution is now developed to illustrate the method which will be used later for arbitrary body shapes. This example is instructive since it not only demonstrates the solution technique for arbitrary body centerlines, but also identifies the contribution to the solution from the local body curvature and that from the induced flow of the far body.

The distribution of singularities given by equation (3. 1. 1) is taken as the leading order approximation. To evaluate this integral we break it up into two parts, the first being an integral over the singularities close to the point of interest, and the second being the integrated effect of the singularities far from the specified field point. Such a decomposition of φ can be expressed as

$$\varphi = -a\beta r_1 \sin\psi \left[\int_{-\gamma}^{+\gamma} \frac{d\theta'}{R^3} + \int_{\gamma}^{2\pi-\gamma} \frac{d\theta'}{R^3} \right] \qquad (3.1.3)$$

where R is given in equation (3. 1. 2), r_1 and r_2 denote the least and greatest distance, respectively, of the point $\underline{x}$ from the centroid circle, or

$$r_1^2 = z^2 + (r-a)^2 \quad , \qquad r_2^2 = z^2 + (r+a)^2 \quad . \qquad (3.1.4)$$

The range 2γ, of the first integral, will be chosen such that $b \ll a\gamma \ll a$. It should be noted that γ is an otherwise arbitrary parameter, introduced into the problem primarily to facilitate the evaluation of the integrals asymptotically for the field point $\underline{x}$ lying in the vicinity of the torus, in such a way that it does not appear in the final expression for $\varphi(\underline{x}, t)$ (e. g., $\gamma = \epsilon^{\frac{1}{4}}$ facilitates computations).

The first integral in equation (3. 1. 3) will be called the near body or local curvature integral, and its integrand may be expanded in powers of θ' as

$$\frac{a^3}{R^3} \simeq \left(\frac{r}{a}\theta'^2 + \frac{r_1^2}{a^2}\right)^{-3/2} + \frac{1}{8}\frac{\frac{r}{a}\theta'^4[1 + O(\theta'^2)]}{\left[\frac{r}{a}\theta'^2 + \frac{r_1^2}{a^2}\right]^{5/2}}$$

$$+ O\left(\theta'^8\left[\frac{r}{a}\theta'^2 + \frac{r_1^2}{a^2}\right]^{-7/2}\right) \quad . \tag{3.1.5}$$

By symmetry of R about $\theta' = 0$, the range of integration is reduced, and it remains only to evaluate the two integrals,

$$I_1 = \int_0^\gamma \frac{d\theta'}{R_*^3} \quad \text{and} \quad I_2 = \int_0^\gamma \frac{\theta'^4 d\theta'}{R_*^5} \tag{3.1.6}$$

where

$$R_* = \left[\frac{r}{a}\theta'^2 + \frac{r_1^2}{a^2}\right]^{\frac{1}{2}} \quad . \tag{3.1.7}$$

These integrals are easily evaluated, and in the vicinity of the toroid surface, where $r_1 = O(b)$, they may be expanded in powers of $r_1/a\gamma$

$$I_1 \simeq \frac{a^2}{r_1^2}\left[1 - \frac{r_1}{2a}\cos\psi + \frac{3}{8}\frac{r_1^2}{a^2}\cos^2\psi\right.$$

$$\left. - \frac{1}{2}\frac{r_1^2}{a^2\gamma^2} + O\left(\frac{r_1^3}{a^3}, \frac{r_1^4}{a^4\gamma^4}\right)\right] \quad , \tag{3.1.8}$$

$$I_2 \simeq \log\frac{2\gamma a}{r_1} - \frac{4}{3} + O\left(\frac{r_1}{a}, \gamma^2\right) \quad . \tag{3.1.9}$$

These expansions combine to give the potential due to the near body singularities

$$\varphi_n = -2a\beta r_1 \sin\psi \int_0^\gamma \frac{d\theta'}{R^3}$$

$$\simeq -\frac{2\beta}{r_1} \sin\psi \left[1 - \frac{r_1}{2a} \cos\psi + \frac{r_1^2}{8a^2}\left(\log \frac{2\gamma a}{r_1} + \frac{3}{2} \cos 2\psi + \frac{1}{6}\right)\right.$$

$$\left. - \frac{1}{2} \frac{r_1^2}{a^2\gamma^2} + O\left(\frac{r_1^3}{a^3} \log \frac{r_1}{a}, \frac{r_1^4}{a^4\gamma^4}\right)\right] . \qquad (3.1.10)$$

Note that as the curvature goes to zero $\left(\frac{r_1}{a} \to 0\right)$ the solution of the two-dimensional cylinder is recovered from the first term. The second and third term represent the leading-order corrections due to the local body curvature.

If we denote by $\underline{e}_z$ and $\underline{e}_{r_1}$ the unit vectors in the directions of increasing z and r_1, respectively, the boundary condition requiring no normal component of flow velocity relative to the translating toroidal ring becomes

$$\frac{\partial\varphi}{\partial r_1} = U\, \underline{e}_z \cdot \underline{e}_{r_1} = U \sin\psi \quad (r_1 = b) . \qquad (3.1.11)$$

The near body potential (3.1.10) nearly satisfies this with $\beta = \frac{Ub^2}{2}$ since at $r_1 = b$,

$$\frac{\partial\varphi_n}{\partial r_1} = \frac{2\beta}{b^2} \sin\psi \left[1 - \frac{\epsilon^2}{8}\left(\log \frac{2\gamma}{\epsilon} + \frac{3}{2} \cos 2\psi - \frac{5}{6}\right) + \frac{\epsilon^2}{2\gamma^2}\right.$$

$$\left. + O(\epsilon^3 \log\epsilon, \epsilon^4/\gamma^4)\right] . \qquad (3.1.12)$$

We emphasize that the curvature affects the boundary condition first at the order of $\epsilon^2 \log \epsilon$, while it affects the potential, the tangential velocity and hence the surface pressure at order ϵ.

For calculating the far-field doublets contribution to φ, namely,

$$\varphi_f = - a\beta r_1 \sin\psi \int_{\gamma}^{2\pi-\gamma} \frac{d\theta'}{R^3} \quad , \tag{3.1.13}$$

the integrand can be expanded in powers of $r_1/a\theta'$ and r_1/a from the outset. In the most adverse case $r_1/a\theta'$ is bounded above by $r_1/a\gamma$, which has already been assumed small. Hence,

$$\frac{a^3}{R^3} \simeq (\frac{2r}{a})^{-3/2} \left\{ (1-\cos\theta')^{-3/2} - \frac{3}{4} \frac{r_1^2}{a^2} (1-\cos\theta')^{-5/2} [1 + O(\frac{r_1}{a})] + O(\frac{r_1^4}{a^4 \gamma^2}) \right\} \quad . \tag{3.1.14}$$

Again taking advantage of the symmetry of R, this time about $\theta' = \pi$, we need evaluate only the two integrals

$$\int_{\gamma}^{\pi} \frac{d\theta'}{(1-\cos\theta')^{3/2}} \simeq \frac{1}{\sqrt{2}} [\frac{2}{\gamma} - \frac{1}{2} \log \frac{\gamma}{4} - \frac{1}{12} + O(\gamma^2)] \quad , \tag{3.1.15}$$

and

$$\int_{\gamma}^{\pi} \frac{d\theta'}{(1-\cos\theta')^{5/2}} \simeq \sqrt{2} [\frac{1}{\gamma^4} + \frac{5}{12} \frac{1}{\gamma^2} + O(\log \gamma)] \quad . \tag{3.1.16}$$

Making use of these expansions we obtain for the potential due to the doublets distributed over the distant body center line the representation

$$\varphi_f \simeq \frac{2\beta}{r_1} \sin\psi \left[\frac{r_1^2}{8a^2} \left(\log \frac{\gamma}{4} + \frac{1}{6}\right) - \frac{r_1^2}{2a^2\gamma^2} + O\left(\frac{r_1^4}{a^4\gamma^4}\right)\right] , \quad (3.1.17)$$

which has a contribution to the normal velocity on the toroid surface given by

$$\frac{\partial \varphi_f}{\partial r_1} \simeq \frac{2\beta}{b^2} \sin\psi \left[\frac{\epsilon^2}{8} \left(\log \frac{\gamma}{4} + \frac{1}{6}\right) - \frac{\epsilon^2}{2\gamma^2} + O\left(\frac{\epsilon^4}{\gamma^4}\right)\right] . \quad (3.1.18)$$

Equation (3.1.17) combines with (3.1.10) to give

$$\varphi \simeq -\frac{2\beta}{r_1} \sin\psi \left[1 - \frac{r_1}{2a} \cos\psi + \frac{r_1^2}{8a^2}\left(\log \frac{8a}{r_1} + \frac{3}{2} \cos 2\psi\right)\right.$$

$$\left. + O\left(\frac{r_1^3}{a^3} \log \frac{r_1}{a}\right)\right] . \quad (3.1.19)$$

This result is independent of the choice of γ, as it should be, and immediately gives

$$\frac{\partial \varphi}{\partial r_1} = \frac{2\beta}{b^2} \sin\psi \left[1 - \frac{\epsilon^2}{8}\left(\log \frac{8}{\epsilon} + \frac{3}{2} \cos 2\psi - 1\right)\right.$$

$$\left. + O(\epsilon^3 \log \epsilon)\right] , \quad (3.1.20)$$

which already satisfies (3.1.11) up to order ϵ, and it is the $\cos 2\psi$ term in (3.1.20) that requires an even higher order correction to the

solution. This term may be made to satisfy the boundary condition if certain higher order singularity distributions are included, as we shall do later.

To begin the discussion of the second method of solution, we return to the potential represented by a distribution of doublets directed in the flow direction and on the meridian circle (3. 1. 1). Evaluation of this integral is accomplished by considering the uniform ring distribution of sources, expressed as

$$\varphi_s(\underline{x},t) = -ma\int_0^{2\pi} \frac{d\theta'}{R} \quad , \tag{3. 1. 21}$$

where R is the same as in equation (3. 1. 2) and m is the constant source strength. Using the variables r_1 and r_2 as defined in equation (3. 1. 3), and after some simple changes of the integration variable, we obtain

$$\varphi_s = -4ma\int_0^{\pi/2} \frac{d\theta'}{(r_2^2 - 4ar\sin^2\theta')^{\frac{1}{2}}} = -\frac{4ma}{r_2}K(k), \tag{3. 1. 22}$$

where $K(k)$ denotes the complete elliptic integral of the first kind, with argument k, and

$$k^2 = \frac{4ar}{r_2^2} = 1 - \left(\frac{r_1}{r_2}\right)^2 = 1 - k'^2 , \qquad k' = \frac{r_1}{r_2} \quad . \tag{3. 1. 23}$$

The potential for the uniform doublet distribution on the centroid circle of strength β and oriented in the z-direction can be

immediately derived by differentiation of the ring source potential, (3. 1. 21) giving

$$\varphi = 4\beta a \frac{\partial}{\partial z}\left[\frac{1}{r_2} K(k)\right] = -\frac{4\beta a z}{r_2 r_1^2} E(k) \quad , \tag{3. 1. 24}$$

where $E(k)$ denotes the complete elliptic integral of the second kind, and in obtaining the last expression in (3. 1. 24) use has been made of the formula

$$\frac{d}{dk} K(k) = \frac{1}{k}\left(\frac{E}{k'^2} - K\right) \quad . \tag{3. 1. 25}$$

To facilitate our evaluation of the boundary condition we will also use the curvilinear orthogonal coordinate system (r_1, θ, ψ) defined by (see figure 3. 1)

$$\begin{aligned} x &= (a + r_1 \cos\psi)\cos\theta \quad , \\ y &= (a + r_1 \cos\psi)\sin\theta \quad , \qquad z = r_1 \sin\psi \quad , \end{aligned} \tag{3. 1. 26}$$

and expand the expression (3. 1. 24) for small values of r_1/a and $k' = (r_1/r_2)$. Thus we obtain in the neighborhood of the toroidal ring

$$\begin{aligned} k' = \frac{r_1}{2a}\Big[1 - \frac{r_1}{2a}\cos\psi + \frac{r_1^2}{8a^2}(3\cos^2\psi - 1) \\ + \frac{r_1^3}{16a^3}\cos\psi\,(3 - 5\cos^2\psi) + O\Big(\frac{r_1^4}{a^4}\Big)\Big] \quad , \end{aligned} \tag{3. 1. 27}$$

and accordingly,

$$\varphi = -\frac{2\beta}{r_1}\sin\psi\ \left[1 - \frac{r_1}{2a}\cos\psi + \frac{r_1^2}{8a^2}\left(\log\frac{8a}{r_1} + \frac{3}{2}\cos 2\psi\right)\right.$$

$$\left. + O\left(\frac{r_1^3}{a^3}\log\frac{a}{r_1}\right)\right] \quad . \tag{3.1.28}$$

This result is the same as (3.1.19) obtained from the first method. Application of the boundary condition (3.1.11) to (3.1.28) yields

$$U = \frac{2\beta}{b^2}\left[1 - \frac{\epsilon^2}{8}\left(\log\frac{8}{\epsilon} - 1 + \frac{3}{2}\cos 2\psi\right) + O(\epsilon^3\log\epsilon)\right] , \tag{3.1.29}$$

where

$$\epsilon = \frac{b}{a} \tag{3.1.30}$$

is considered to be small. Since the order ϵ^2 term in (3.1.29) depends on the angle ψ, the doublet strength β can only be determined up to this order as

$$\beta = \frac{1}{2}Ub^2\left[1 + \frac{\epsilon^2}{8}\log\frac{8}{\epsilon} + O(\epsilon^2)\right] \quad . \tag{3.1.31}$$

Strictly speaking, the second term should be combined with the term of order ϵ^2 to give the error of order $\epsilon^2\log\epsilon$ relative to the leading term $\beta = \frac{1}{2}Ub^2$. In order to improve the solution to include order ϵ^2 one may superimpose on the doublet ring appropriate higher order singularities, which by implication of (3.1.29) have strength of ϵ^2 with respect to β. Again drawing on the results from the infinite straight-line distribution that are expected to give leading order behavior, we are led to the choice of an octupole distribution.

The proper octupole is suggested immediately when the z derivatives of φ are taken

$$\frac{\partial^2 \varphi}{\partial z^2} = \frac{4\beta}{r_1^3}\left[\sin 3\psi + O\left(\frac{r_1}{a}\right)\right] \quad . \tag{3.1.32}$$

The z differentiation is performed while holding x and y fixed, and noting that r_1 and ψ are functions of z. The octupole potential therefore assumed the form

$$\varphi = \frac{\partial^3}{\partial z^3} \int_0^{2\pi} \left(-\frac{A}{R}\right) a\,d\theta' \quad , \tag{3.1.33}$$

and its strength A is chosen such that it will cancel the $\cos 2\psi$ term in equation (3.1.29). This requirement is satisfied if

$$A = \beta\left(\frac{b\epsilon}{8}\right)^2 \quad . \tag{3.1.34}$$

The combined potential of the doublet and octupole ring distributions now gives

$$\begin{aligned}\varphi(\underline{x}, t) = -\frac{Ub^2}{r_1}\Big[&\sin\psi - \frac{r_1}{4a}\sin 2\psi + \frac{r_1^2}{8a^2}\sin\psi\left(\log\frac{8a}{r_1} - \frac{3}{4}\right) \\ &+ \frac{\epsilon^2}{8}\sin\psi\left(\log\frac{8}{\epsilon} - \frac{7}{4}\right) + \frac{3}{32}\frac{r_1^2}{a^2}\sin 3\psi \\ &+ \frac{1}{32}\frac{b^2\epsilon^2}{r_1^2}\sin 3\psi + O\left(\frac{r_1^3}{a^3}\log\frac{r_1}{a}\right)\Big] \quad ,\end{aligned} \tag{3.1.35}$$

and the doublet strength is determined more precisely as

$$\beta = \frac{Ub^2}{2}\left[1 + \frac{\epsilon^2}{8}\left(\log\frac{8}{\epsilon} - \frac{7}{4}\right) + O(\epsilon^3 \log \epsilon)\right] \quad . \qquad (3.1.36)$$

While the curvature of the ring centerline has little effect on the value of β, for it first appears in the term of order $\epsilon^2 \log \epsilon$, its effect on the velocity field, however, arises as early as in the term of order ϵ. For example, the local velocity in the body frame of reference has at the torus surface the value

$$\begin{aligned} \underline{u}_b &= \nabla(\varphi - Uz) \\ &= \underline{e}_\psi U\left[-2\cos\psi + \frac{\epsilon}{2}\cos 2\psi - \frac{\epsilon^2}{4}\cos\psi\left(\log\frac{8}{\epsilon} - \frac{5}{4}\right)\right. \\ &\quad \left. - \frac{3}{8}\epsilon^2 \cos 3\psi + O(\epsilon^3 \log \epsilon)\right] \quad . \qquad (3.1.37) \end{aligned}$$

The centerline curvature effect is thus seen to increase on the aperture side and to decrease on the outward side the magnitude of the tangential velocity at the torus surface. This modified velocity field will have such an impact on the pressure distribution and sectional force coefficient as to result in a new feature in force distribution that can be of significance in the general case of unsteady flow involving slender body motions of finite amplitude. In fact, the pressure, p, is given by the Bernouilli equation

$$\frac{p}{\rho} + \frac{\partial\varphi}{\partial t} + \frac{1}{2}(u_b^2 - U^2) = \frac{p_\infty}{\rho} \quad , \qquad (3.1.38)$$

where p_∞ is the pressure at infinity, ρ the constant fluid density, and the time derivative of φ is evaluated with respect to the body

frame of reference. From the above result we obtain the pressure distribution over the toroid surface as

$$\frac{p-p_\infty}{\rho} = \frac{dU}{dt} b \left[\sin\psi - \frac{\epsilon}{2} \sin\psi \cos\psi + \frac{\epsilon^2}{4} \sin\psi \left(\log \frac{8}{\epsilon} - \frac{5}{4}\right) \right.$$

$$\left. + \frac{\epsilon^2}{8} \sin 3\psi + O(\epsilon^3 \log \epsilon) \right] \qquad (3.1.39)$$

$$+ U^2 \left[\frac{1}{2} - 2\cos^2\psi + \epsilon \cos\psi \cos 2\psi - \frac{\epsilon^2}{8} \right.$$

$$\left. - \frac{\epsilon^2}{2} \cos^2\psi \left(\log \frac{8}{\epsilon} - \frac{27}{4}\right) - \frac{7}{2}\epsilon^2 \cos^4\psi + O(\epsilon^3 \log \epsilon) \right] ,$$

which has an error of $O(\epsilon^3 \log \epsilon)$. The contribution of this pressure to the differential force acting on a meridional segment of the toroid subtending a differential angle $d\theta$ about θ is given by

$$d\underline{F} = -\int p\underline{n}\, dS = -bd\theta \int_0^{2\pi} p\underline{e}_{r_1} (a + b\cos\psi) d\psi ,$$

since the unit vector normal to the toroid surface is $\underline{n} = \underline{e}_{r_1}$, and $ds_\theta = (a + b\cos\psi)d\theta$ and $ds_\psi = bd\psi$ are the differential arc lengths in the directions of θ and ψ, respectively, over the toroid surface. The result of integration yields for the differential force per unit arc length of the centroid circle,

$$\underline{\mathcal{F}} = -\underline{e}_z \rho\pi b^2 \frac{dU}{dt} \left[1 + \frac{\epsilon^2}{4} \left(\log \frac{8}{\epsilon} - \frac{7}{4}\right) + O(\epsilon^3 \log \epsilon) \right]$$

$$+ \underline{e}_r \frac{1}{2} \rho \frac{\pi b^2}{a} U^2 \left[1 + O(\epsilon^2 \log \epsilon) \right] , \qquad (3.1.40)$$

where $\underline{e}_r$ denotes the unit radial vector parallel to the plane of $z = 0$, or

$$\underline{e}_r = \underline{e}_x \cos\theta + \underline{e}_y \sin\theta. \tag{3.1.41}$$

Thus, when the torus accelerates in the z-direction, every segment of the torus experiences a uniform drag due to the induced mass of the fluid and a uniform outward pull

$$\mathcal{F}_r = \frac{\pi}{2}\rho\frac{b^2}{a}U^2 \quad , \tag{3.1.42}$$

which depends on the instantaneous velocity U and vanishes as the radius of curvature, a, of the body centerline becomes infinite, although $\underline{\mathcal{F}}\cdot\underline{e}_r$ has no net resultant for the whole ring. The reason for the radial force $\mathcal{F}_r$ pointing outward, rather than inward, is because the lower (negative) pressure on the aperture side of the ring acts on much smaller areas than that which is exposed to the higher (but still negative) pressure on the outside equatorial belt.

The sectional induced mass (per unit central arc length of the torus) referred to the normal component of local acceleration is

$$m_{33} = \rho\pi b^2\left[1 + \frac{\epsilon^2}{4}\left(\log\frac{8}{\epsilon} - \frac{7}{4}\right) + O(\epsilon^3\log\epsilon)\right] \quad . \tag{3.1.43}$$

Integrating the sectional force $\underline{\mathcal{F}}$ along the meridian circle gives the total force on the toroidal ring

$$\begin{aligned}\underline{F} &= \int_0^{2\pi} \underline{\mathcal{F}}\, a\,d\theta \\ &= -\underline{e}_x \rho V_b \frac{dU}{dt}\left[1 + \frac{\epsilon^2}{4}\left(\log\frac{8}{\epsilon} - \frac{7}{4}\right) + O(\epsilon^3\log\epsilon)\right] \quad ,\end{aligned} \tag{3.1.44}$$

where

$$V_b = 2\pi^2 ab^2 \qquad (3.1.45)$$

is the volume occupied by the toroid ring. The total induced mass is then

$$M_{33} = \rho V_b [1 + \frac{\epsilon^2}{4}(\log \frac{8}{\epsilon} - \frac{7}{4}) + O(\epsilon^3 \log \epsilon)] \quad , \qquad (3.1.46)$$

which is clearly equal to the line integral of the sectional induced mass m_{33} given by (3.1.43).

The total moment of force about the toroid ring center of mass $(0, 0, 0)$ is easily obtained

$$\underline{M} = \int_0^{2\pi} (\underline{e}_r \times \underline{\mathcal{F}}) a^2 d\theta = 0 \quad , \qquad (3.1.47)$$

as it must be from the flow symmetry.

The total force and moment can be determined in another way, namely, by making use of the fluid momentum and the fluid angular momentum

$$\underline{I} = -\rho \int_S \varphi \underline{n} \, dS \qquad (3.1.48)$$

and

$$\underline{J} = -\rho \int_S (\underline{x} \times \underline{n}) \varphi \, dS \quad . \qquad (3.1.49)$$

Substitution of (3.1.35) into these two expressions gives

$$\underline{I} = \underline{e}_z \rho V_b U [1 + \frac{\epsilon^2}{4}(\log \frac{8}{\epsilon} - \frac{7}{4}) + O(\epsilon^3 \log \epsilon)] \qquad (3.1.50)$$

and

$$\underline{J} = 0 . \qquad (3.1.51)$$

The total force and moment on the body are

$$\underline{F} = -\frac{d}{dt}\underline{I} \qquad \text{and} \qquad \underline{M} = -\frac{d}{dt}\underline{J} , \qquad (3.1.52)$$

and this result is the same as equation (3.1.44) and equation (3.1.47) arrived at from integration of the local pressure distribution over the body surface.

As an alternative method of finding m_{33}, we can also apply G.I. Taylor's theorem that relates the total doublet strength β_T and the body volume V_b to the flow momentum according to

$$I = 4\pi\rho\beta_T - \rho V_b U = M_{33} U . \qquad (3.1.53)$$

In the present case, V_b is given by (3.1.45) and

$$\beta_T = \pi a b^2 U \left[1 + \frac{\epsilon^2}{8}\left(\log\frac{8}{\epsilon} - \frac{7}{4}\right) + O(\epsilon^3 \log\epsilon)\right] , \qquad (3.1.54)$$

hence, by (3.1.53),

$$M_{33} = \rho V_b \left[1 + \frac{\epsilon^2}{8}\left(\log\frac{8}{\epsilon} - \frac{7}{4}\right) + O(\epsilon^3 \log\epsilon)\right] , \qquad (3.1.55)$$

exactly the same as in (3.1.46) and it also gives the correct flow momentum (3.1.50).

3.2 Edge-on translation

Now suppose the toroidal ring is moving in its own plane (e.g., in the x-direction) with velocity

$$\underline{U} = V(t)\,\underline{e}_x = V(t)\,(\underline{e}_r \cos\theta - \underline{e}_\theta \sin\theta) , \qquad (3.2.1)$$

where $\underline{e}_r$ and $\underline{e}_\theta$ are unit vectors along the r and θ coordinate, respectively,

$$\underline{e}_r = \underline{e}_x \cos\theta + \underline{e}_y \sin\theta, \qquad \underline{e}_\theta = \underline{e}_y \cos\theta - \underline{e}_x \sin\theta. \tag{3.2.2}$$

The boundary condition that the velocity has no normal component relative to the moving toroid requires

$$\frac{\partial\varphi}{\partial r_1} = V\underline{e}_x \cdot \underline{e}_{r_1} = V\frac{\partial y}{\partial r_1} = V\cos\psi\cos\theta \quad (r_1 = b) . \tag{3.2.3}$$

For the solution of φ we seek again the representation of a doublet distribution along the centroid circle at r = a. Since the undisturbed flow relative to body sections has both normal and tangential components, both of which vary from one body section to another, we shall assume that the doublet strength (per unit arc length), $\underline{\beta}$, has also both normal and tangential components in order to account for the sectional variation of the flow, that is

$$\underline{\beta}(\theta) = \underline{e}_r\beta_n(\theta) + \underline{e}_\theta\beta_s(\theta) \qquad (0 \leqslant \theta \leqslant 2\pi) . \tag{3.2.4}$$

In fact, it turns out, as can be verified a posteriori, that $\partial\varphi/\partial r_1$ will not satisfy at $r_1 = b$ the specified dependence on ψ and θ as prescribed in (3.2.3) unless

$$\beta_n(\theta) = \hat{\beta}_n\cos\theta, \qquad \beta_s(\theta) = \hat{\beta}_s\sin\theta \tag{3.2.5}$$

with $\hat{\beta}_n$ and $\hat{\beta}_s$ being two constants, which we now assume.

The velocity potential can then be written as

$$\varphi(\underline{x}) = -a\int_0^{2\pi} \frac{\underline{\beta}(\theta')\cdot(\underline{x}-\underline{x}')}{R^3}\,d\theta' \quad , \tag{3.2.6}$$

where R is given by (3.1.2), and $\underline{x}, \underline{x}'$ are also there defined. With the above form of $\underline{\beta}$, we have

$$\underline{\beta}\cdot(\underline{x}-\underline{x}') = \hat{\beta}_n \cos\theta'[r\cos(\theta-\theta')-a] + \hat{\beta}_s r\sin\theta'\sin(\theta-\theta') \quad , \tag{3.2.7}$$

and accordingly, after some simplification and integrations by parts.

$$\varphi = \frac{2\cos\theta}{r_2}\left\{ -(\hat{\beta}_n + 2\hat{\beta}_s)\int_0^{\pi/2} \frac{\cos 2\theta\, d\theta}{[1-k^2\sin^2\theta]^{\frac{1}{2}}} \right.$$

$$\left. + \frac{2a\hat{\beta}_n}{r_2^2}\left(\frac{r_1^2}{2a} + r - a\right)\int_0^{\pi/2} \frac{\cos 2\theta\, d\theta}{[1-k^2\sin^2\theta]^{3/2}} \right\} \quad , \tag{3.2.8}$$

where r_1, r_2 are defined by (3.1.4) and k by (3.1.23). These integrals can also be expressed in terms of the complete elliptic integrals as

$$\varphi = \frac{2\cos\theta}{r_2}\left\{ (\hat{\beta}_n + 2\hat{\beta}_s)\left[\left(\frac{2}{k^2} - 1\right)K - \frac{2}{k^2}E\right] \right.$$

$$\left. - \hat{\beta}_n\left(1 + \frac{2a\cos\psi}{r_1}\right)\left[\left(\frac{2}{k^2} - 1\right)E - 2\left(\frac{k'}{k}\right)^2 K\right] \right\} \quad , \tag{3.2.9}$$

in which the elliptic integrals K and E have the argument k.

In the vicinity of the toroid surface, where r_1/a and k' are small, expansion of (3.2.9) together with use of (3.1.27) yields

$$\varphi = \cos\theta\left\{\frac{\hat{\beta}_n+2\hat{\beta}_s}{a}\left[\log\frac{8a}{r_1} - 2 + O\left(\frac{r_1}{a}\log\frac{a}{r_1}\right)\right]\right.$$

$$- \frac{2\hat{\beta}_n}{r_1}\left[\cos\psi + \frac{r_1}{2a}\sin^2\psi - \frac{3}{8}\frac{r_1^2}{a^2}\left(\log\frac{8a}{r_1} - \frac{11}{12}\right)\cos\psi\right.$$

$$\left.\left. + \frac{3}{32}\frac{r_1^2}{a^2}\cos 3\psi + O\left(\frac{r_1^3}{a^3}\log\frac{a}{r_1}\right)\right]\right\} \quad . \qquad (3.2.10)$$

Since the $\cos 3\psi$ term in this equation will prevent the above φ from satisfying the boundary condition (3.2.3) in the order ϵ^2, a remedy is sought by introducing an octupole distribution of a higher order strength than the doublets. From our previous experience the octupole was chosen to cancel the anomalous angular dependence introduced by the local curvature by the normal doublet distribution. The proper octupole can be derived by suitable differentiation of the source potential with respect to r, however, it is more direct to differentiate with respect to the parameter a. Taking

$$\varphi_o = -a\int_o^{2\pi} A\frac{d^3}{da^3}\left(\frac{1}{R}\right)d\theta' \qquad (3.2.11)$$

and choosing the octupole strength A such that the $\cos 3\psi$ term is eliminated from the boundary condition gives

$$A = \hat{\beta}_n \cos\theta' \left(\frac{b\epsilon}{8}\right)^2 \quad . \qquad (3.2.12)$$

Superposing this octupole potential as a higher order correction to the doublet ring distributions, (3.2.10), leads to a normal component of flow velocity at the toroid surface given by

$$\frac{\partial \varphi}{\partial r_1} = \cos\theta \left\{ -\left(\frac{\hat{\beta}_n + 2\hat{\beta}_s}{ab}\right)\left[1 + O(\epsilon \log \epsilon)\right] \right.$$

$$\left. + \frac{2\hat{\beta}_n}{b^2}\cos\psi\left[1 + \frac{3}{8}\epsilon^2\left(\log\frac{8}{\epsilon} - \frac{23}{12}\right) + O(\epsilon^3 \log \epsilon)\right]\right\} . \tag{3.2.13}$$

In order that condition (3.2.3) is satisfied, we must have

$$\hat{\beta}_s = -\frac{1}{2}\hat{\beta}_n \tag{3.2.14}$$

and

$$\hat{\beta}_n = \frac{1}{2} Vb^2\left[1 - \frac{3}{8}\epsilon^2\left(\log\frac{8}{\epsilon} - \frac{23}{12}\right) + O(\epsilon^3 \log \epsilon)\right] . \tag{3.2.15}$$

From (3.2.5) and (3.2.15) we see that the leading term of the normal component of the doublet, namely $\beta_n = \frac{1}{2} b^2 V \cos\theta$, would again be as expected from local two-dimensional theory; its actual strength, as indicated by (3.2.15), is slightly reduced under the effect of curvature of the centroid line. It is further of interest to observe that a tangential component of doublet distribution, with strength given by (3.2.14) and hence being of the same order as β_n, is required so that the local source-like term (the first term on the right-hand side of (3.2.10)) can be annihilated. Thus (3.2.10) becomes, for $r_1/a \ll 1$,

$$\varphi = -Vb^2 \frac{\cos\theta}{r_1}\left\{ \cos\psi + \frac{r_1}{2a}\sin^2\psi - \frac{3}{8}\left(\frac{r_1}{a}\right)^2\left(\log\frac{8a}{r_1} - \frac{11}{12}\right)\cos\psi \right.$$

$$- \frac{3}{8}\left(\frac{b}{a}\right)^2\left(\log\frac{8a}{b} - \frac{23}{12}\right)\cos\psi + \frac{\cos 3\psi}{32}\left(\frac{3r_1^2}{a^2} + \frac{b^4}{a^2 r_1^2}\right)$$

$$\left. + O\left(\frac{r_1^3}{a^3}\log\frac{r_1}{a}\right)\right\} . \tag{3.2.16}$$

It then follows that the flow velocity at the toroid surface has in the body frame of reference the value

$$\underline{u}_b = \underline{e}_\psi \frac{1}{b} \frac{\partial}{\partial \psi} (\varphi - Vx) + \underline{e}_\theta \frac{1}{(a+b\cos\psi)} \frac{\partial}{\partial \theta} (\varphi - Vx) \quad (r_1 = b)$$

$$= \underline{e}_\psi 2V\cos\theta[\sin\psi - \frac{\epsilon}{2}\sin\psi\cos\psi + \frac{\epsilon^2}{8}\sin\psi(-3\log\frac{8}{\epsilon} - \frac{17}{4})$$

$$+ \frac{3\epsilon^2}{16}\sin 3\psi + O(\epsilon^3\log\epsilon)] \qquad (3.2.17)$$

$$+ \underline{e}_\theta V\sin\theta[1 + \epsilon\cos\psi + \frac{\epsilon^2}{2}(-2 + 3\sin^2\psi) + O(\epsilon^3\log\epsilon)] \ ,$$

where $\epsilon = b/a$.

The pressure distribution over the toroid surface can be calculated by using (3.1.38) in which U is to be replaced by V, $u_b^2 = \underline{u}_b \cdot \underline{u}_b$, with $\underline{u}_b$ given above, and

$$\frac{\partial\varphi}{\partial t} = (\frac{\varphi}{V})\frac{dV}{dt} \qquad (r_1 = b) \qquad (3.2.18)$$

with φ given by (3.2.16). Using this pressure we obtain the differential force per unit arc length of the centroid circle as

$$\underline{\mathcal{F}} = -\underline{e}_r \rho\pi b^2(\dot{V}\cos\theta)[1 - \frac{3}{4}\epsilon^2(\log\frac{8}{\epsilon} - \frac{19}{12}) + O(\epsilon^3\log\epsilon)]$$

$$+ \underline{e}_r \rho\pi \frac{b^2}{a} V^2[1 - \frac{3}{2}\cos^2\theta + O(\epsilon^2\log\epsilon)] \ , \qquad (3.2.19)$$

of which the error is of order $\epsilon^3\log\epsilon$. The first term on the right-hand side shows that the sectional induced mass is

$$m_{11} = m_{22} = \rho\pi b^2 \left[1 - \frac{3}{4}\epsilon^2 \left(\log \frac{8}{\epsilon} - \frac{19}{12}\right) + O(\epsilon^3 \log \epsilon)\right] \tag{3.2.20}$$

if referred to the normal component of the local acceleration, and curvature decreases this induced mass at order $\epsilon^2 \log \epsilon$. In addition, the curvature effect again results in an outward traction which now depends on the meridian angle θ, but has no net resultant due to the obvious flow symmetry. Finally, upon integration of the differential force we obtain for the total force acting on an accelerating ring.

$$\underline{F} = \int_0^{2\pi} \underline{\mathcal{F}}\, a d\theta = -\underline{e}_x \rho\pi^2 a b^2 \frac{dV}{dt}\left[1 - \frac{3}{4}\epsilon^2 \left(\log \frac{8}{\epsilon} - \frac{19}{12}\right) + O(\epsilon^3 \log \epsilon)\right] . \tag{3.2.21}$$

The modification of the total force due to the curvature is of high order and tends to reduce slightly the force experience by the toroid ring as compared with a circular cylinder of equal length. The induced mass follows immediately and for this case is

$$M_{11} = M_{22} = \frac{1}{2}\rho V_b \left[1 - \frac{3}{4}\epsilon^2 \left(\log \frac{8}{\epsilon} - \frac{19}{12}\right) + O(\epsilon^3 \log \epsilon)\right] . \tag{3.2.22}$$

The moment of force about the center of mass $(0, 0, 0)$ is

$$\underline{M} = \int_0^{2\pi} (\underline{e}_r \times \underline{\mathcal{F}}) a^2 d\theta = 0 . \tag{3.2.23}$$

The fluid impulse computed by equation (3.1.48) with equation (3.2.16) is

$$\underline{I} = \underline{e}_x \frac{1}{2} \rho V_b V[1 - \frac{3}{4}\epsilon^2(\log \frac{8}{\epsilon} - \frac{19}{12}) + O(\epsilon^3 \log \epsilon)] \tag{3.2.24}$$

and $F = \frac{-d\underline{I}}{dt}$ gives (3.2.21) again. The fluid angular momentum is zero as is the moment of force in this case.

3.3 On-edge rotation

Now suppose the toroidal ring is rotating with angular velocity Ω about the x-axis,

$$\underline{\Omega} = \Omega(t)\, \underline{e}_x. \tag{3.3.1}$$

The boundary condition that there be no normal flow velocity relative to the toroid surface requires that,

$$\frac{\partial \varphi}{\partial r_1} = \underline{\Omega} \times \underline{x} \cdot \underline{e}_{r_1} = a\,\Omega \sin\theta \sin\psi \quad (r_1 = b). \tag{3.3.2}$$

For the solution of φ we seek again the representation of a doublet distribution on the centroid circle. With the coordinate system (x, y, z) fixed in the body, the local incident flow is always along the z-axis and varies in magnitude in proportion to $\sin\theta$. Therefore, as a first attempt at φ we take a doublet strength with the same functional behavior,

$$\underline{\beta}(\theta') = \beta \sin\theta'\, \underline{e}_z, \tag{3.3.3}$$

which gives rise to the velocity potential,

$$\varphi(\underline{x}, t) = -a \int_0^{2\pi} \frac{\underline{\beta}(\theta') \cdot (\underline{x} - \underline{x}')}{R^3}\, d\theta' \tag{3.3.4}$$

with $\underline{x}$, $\underline{x}'$, and R given earlier. With the above form of $\underline{\beta}$, we have

$$\underline{\beta}(\theta') \cdot (\underline{x} - \underline{x}') = \beta x \sin\theta' \qquad (3.3.5)$$

and hence

$$\varphi = -a\beta x \int_0^{2\pi} \frac{\sin\theta'}{R^3}\, d\theta' \quad . \qquad (3.3.6)$$

After a similar change of variables as in the section 3.1 and some simplification, the potential can be expressed in terms of the complete elliptic integrals E and K having the argument k.

$$\varphi = \frac{4}{3}\frac{a\beta x \sin\theta}{r_2 r_1^2}\left[\left(\frac{2}{k^2} - 1\right)K + \left(2 - \frac{1}{k^2}\right)E - \frac{1}{k'^2}\left(1 + \frac{1}{k^2}\right)E\right] \qquad (3.3.7)$$

where r_1, r_2, k, and k' are given by (3.1.4) and (3.1.23).

Near the toroid surface, where r_1/a and k' are small, φ can be expanded to give

$$\varphi = -\frac{2\beta\sin\theta}{r_1}\left[\sin\psi - \frac{r_1}{4a}\sin 2\psi + \frac{3}{32}\frac{r_1^2}{a^2}\sin 3\psi + \frac{r_1^2}{8a^2}\sin\psi\left(-3\log\frac{8a}{r_1} + \frac{13}{4}\right) O\left(\frac{r_1^3}{a^3}\log\frac{r_1}{a}\right)\right] , \qquad (3.3.8)$$

and the resulting normal component of velocity on the toroid surface is

$$\frac{\partial\varphi}{\partial r_1} = \frac{2\beta\sin\theta}{b^2}\left[\sin\psi + \frac{\epsilon^2}{8}\sin\psi\left(3\log\frac{8}{\epsilon} - \frac{25}{4}\right) - \frac{3}{32}\epsilon^2\sin 3\psi + O(\epsilon^3\log\epsilon)\right] \quad (r_1 = b) \qquad (3.3.9)$$

where $\epsilon = b/a$. The boundary condition can be satisfied to the order of $\epsilon^2 \log \epsilon$. Again the sin 3ψ term prevents the boundary condition to be satisfied to the order of ϵ^2. However, the addition of a octupole distribution on the centroid axis can be chosen so as to annihilate this term and render the boundary condition valid up to order $\epsilon^3 \log \epsilon$ terms. The proper octupole is suggested immediately when z derivatives of φ are taken.

$$\frac{\partial^2 \varphi}{\partial z^2} = \frac{4\beta \sin\theta}{r_1^3} \left[\sin 3\psi + O\left(\frac{r_1}{a}\right) \right] . \tag{3.3.10}$$

The z differentiation is performed while holding x and y fixed, and thus r_1 and ψ are functions of z. The octupole with the velocity potential

$$\varphi_o = \frac{\partial^3}{\partial z^3} \int_o^{2\pi} \left(\frac{A}{R}\right) a d\theta' \tag{3.3.11}$$

is chosen, and its strength is chosen so that on the toroid surface the sin 3ψ terms in equation (3.3.9) is cancelled,

$$A = \beta \left(\frac{b\epsilon}{8}\right)^2 \sin\theta'. \tag{3.3.12}$$

Application of the boundary condition (3.3.2) then gives the doublet strength

$$\beta = \frac{a\Omega b^2}{2} \left[1 + \frac{\epsilon^2}{8} \left(-3 \log \frac{8}{\epsilon} + \frac{25}{4}\right) + O(\epsilon^3 \log \epsilon) \right] \tag{3.3.13}$$

and the potential of the doublet and octupole ring distributions are superimposed to give

$$\varphi(\underline{x},t) = -\frac{b^2}{r_1}(a\Omega\sin\theta)[\sin\psi - \frac{r_1}{4a}\sin 2\psi + \frac{r_1^2}{8a^2}\sin\psi(-3\log\frac{8a}{r_1} + \frac{13}{4}) + \frac{3}{32}\frac{r_1^2}{a^2}\sin 3\psi + \frac{1}{32}\frac{b^4}{a^2 r_1^2}\sin 3\psi + O(\frac{r_1^3}{a^3}\log\frac{r_1}{a})] \quad . \qquad (3.3.14)$$

The flow velocity on the toroid surface in the body frame of reference follows immediately

$$\begin{aligned}\underline{u}_b &= \nabla\varphi - \underline{\Omega}\times\underline{x} \qquad (r_1 = b)\\ &= \underline{e}_\psi(-a\Omega\sin\theta)[2\cos\psi + \frac{\epsilon}{2}(2\sin^2\psi + 1) \\ &\quad + \frac{\epsilon^2}{8}\cos\psi(-6\log\frac{8}{\epsilon} + \frac{19}{2}) + \frac{3\epsilon^2}{8}\cos 3\psi + O(\epsilon^3\log\epsilon)] \qquad (3.3.15)\\ &\quad + \underline{e}_\theta(a\Omega\cos\theta)[\frac{3}{2}\epsilon^2\cos\psi\sin\psi + O(\epsilon^3\log\epsilon)] \quad .\end{aligned}$$

The pressure distribution over the toroid surface can be found from (3.1.38) in which U^2 is replaced by $(\underline{\Omega}\times\underline{x})\cdot(\underline{\Omega}\times\underline{x})$, $u_b^2 = \underline{u}_b\cdot\underline{u}_b$ is given above, and

$$\frac{\partial\varphi}{\partial t} = (\frac{\varphi}{\Omega})\frac{d\Omega}{dt} \qquad (r_1 = b) \qquad (3.3.16)$$

with φ given in (3. 3. 14). Using this pressure we can calculate the sectional force, i. e., the force acting on the toroid per unit arc length of the centroid circle, as

$$\underline{\mathcal{F}} = \underline{e}_z \rho\pi b^2 (a \frac{d\Omega}{dt} \sin\theta)[1 - \frac{3}{4}\epsilon^2(\log\frac{8}{\epsilon} - \frac{17}{12}) + O(\epsilon^3 \log\epsilon)]$$

$$+ \underline{e}_r \frac{3}{2}\pi\rho b(a\Omega\sin\theta)^2[\epsilon + O(\epsilon^3\log\epsilon)] \qquad (3.3.17)$$

The first term shows that the sectional induced mass is

$$m_{44} = m_{55} = \rho\pi b^2[1 - \frac{3}{4}\epsilon^2(\log\frac{8}{\epsilon} - \frac{17}{12}) + O(\epsilon^3\log\epsilon)] \qquad (3.3.18)$$

if referred to the normal component of the local acceleration, with a curvature correction entering at order $\epsilon^2 \log\epsilon$, tending to reduce the induced mass of a straight circular cylinder. The leading order effect of centroid curvature is in the second term, which is a radially outward traction having no net force on the body due to its symmetry. Integrating the sectional force along the centroid circle gives the total force on the torus, which by symmetry of the motion is $\underline{F} = 0$.

The moment of force about the toroid center of mass (the origin in our coordinate system) in this case will be nonzero. The sectional torque, or moment of the toroid surface forces about the origin is

$$\underline{\mathcal{T}} = \int_0^{2\pi} (-p\underline{e}_{r_1} \times \underline{x})(1 + \epsilon\cos\psi)\, b\, d\psi \qquad (3.3.19)$$

$$= \underline{e}_\theta \rho\pi a b^2 (a\dot{\Omega}\sin\theta)[1 - \frac{3}{4}\epsilon^2(\log\frac{8}{\epsilon} - \frac{17}{12}) + O(\epsilon^3\log\epsilon)] \ .$$

This gives rise finally to the total moment of force about the center of mass

$$\underline{M} = \int_0^{2\pi} \underline{\gamma}\, a d\theta$$

$$= -\underline{e}_y \rho\pi^2 a^2 b^2 (a\dot{\Omega})[1 - \frac{3}{4}\epsilon^2(\log\frac{8}{\epsilon} - \frac{17}{12}) + O(\epsilon^3 \log\epsilon)] \quad . \tag{3.3.20}$$

The effect of curvature is of a high order and will slightly decrease the torque experienced by the toroidal ring. The total induced mass of the ring in this case is

$$M_{44} = M_{55} = \frac{1}{2}\rho a^2 V_b[1 - \frac{3}{4}\epsilon^2(\log\frac{8}{\epsilon} - \frac{17}{12}) + O(\epsilon^3\log\epsilon)] \tag{3.3.21}$$

where $V_b = 2\pi^2 a b^2$ is the volume of the toroidal ring.

The fluid momentum and the fluid angular momentum from equation (3.1.48) and (3.1.49), respectively, with the potential (3.3.14) gives

$$\underline{I} = O \tag{3.3.22}$$

and

$$\underline{J} = \underline{e}_x \frac{1}{2}\rho V_b(a^2\Omega)[1 - \frac{3}{4}\epsilon^2(\log\frac{8}{\epsilon} - \frac{17}{12}) + O(\epsilon^3\log\epsilon)] \quad . \tag{3.3.23}$$

The resulting force and moment of force about the toroid center of mass follow directly by a time derivative and compare to the result (3.3.20).

3.4 Induced mass tensor for a toroidal ring

For a rigid body moving with arbitrary translation and rotation the induced mass tensor is useful in finding both the forces experienced by the body and its kinetic energy. The kinetic energy in the fluid is

$$T = \frac{1}{2}\rho \int_V \underline{u} \cdot \underline{u}\, dV = \frac{1}{2}\rho \int_V \nabla\cdot(\varphi\nabla\varphi)dV = -\frac{1}{2}\rho\int_S (\varphi\nabla\varphi)\cdot \underline{n}dS \tag{3.4.1}$$

where V is the volume which the fluid occupies and the equation $\nabla^2\varphi = 0$ has been used in writing the second expression. If φ is now supposed to be a linear combination of translation along the three coordinate axes and rotation about these axes, it may be written

$$\varphi = U_\alpha \phi_\alpha \qquad (\alpha = 1, 2, \ldots, 6) \tag{3.4.2}$$

where U_1, U_2 and U_3 are the translational velocities along x, y, and z, respectively, and U_4, U_5 and U_6 are the angular velocities about the same axes, respectively. The kinetic energy may be written

$$2T = M_{\alpha\beta} U_\alpha U_\beta \tag{3.4.3}$$

where the added mass tensor is

$$M_{\alpha\beta} = -\rho\int_S \phi_\alpha \frac{\partial\phi_\beta}{\partial n}\, dS\ . \tag{3.4.4}$$

Symmetry of the six-by-six tensor reduces the number of independent

elements from 36 to 21. Further body symmetries of the toroid ring leave only nine nonzero elements, and only three nontrivial values.

$$M_{\alpha\beta} = \begin{bmatrix} A & A & 0 & 0 & 0 & 0 \\ A & A & 0 & 0 & 0 & 0 \\ 0 & 0 & B & 0 & 0 & 0 \\ 0 & 0 & 0 & C & C & 0 \\ 0 & 0 & 0 & C & C & 0 \\ 0 & 0 & 0 & 0 & 0 & 0 \end{bmatrix} \qquad (3.4.5)$$

where

$$A = \frac{1}{2}\rho V_b\left[1 - \frac{3}{4}\epsilon^2\left(\log\frac{8}{\epsilon} - \frac{19}{12}\right) + O(\epsilon^3 \log\epsilon)\right] \qquad (3.4.6)$$

$$B = \rho V_b\left[1 + \frac{1}{4}\epsilon^2\left(\log\frac{8}{\epsilon} - \frac{7}{4}\right) + O(\epsilon^3 \log\epsilon)\right] \qquad (3.4.7)$$

$$C = \frac{1}{2}a^2 V_b\left[1 - \frac{3}{4}\epsilon^2\left(\log\frac{8}{\epsilon} - \frac{17}{12}\right) + O(\epsilon^3 \log\epsilon)\right] . \qquad (3.4.8)$$

3.5 Radially expanding ring

Next we consider the case of a toroidal ring whose center of mass always remains at a fixed point in space but whose major and minor radii are allowed to be functions of time ($a = a(t)$ and $b = b(t)$). This case was investigated, with the hope of shedding light on the types of singularities needed in solving flows over more general bodies where the local radius of curvature may have a time dependence. Since the volume of the toroidal ring is now changing we expect the need for source distributions, in addition to a radially directed

doublet in representing the flow. The local coordinate system (r_1, θ, ψ) is again employed, and now it is fixed on the centroid circle and moving with velocity $\underline{u} = \dot{a}\underline{e}_r$, where $\dot{a} = \frac{da}{dt}$. The boundary condition that the velocity has no normal component relative to the expanding toroid requires

$$\frac{\partial \varphi}{\partial r_1} = \dot{a}\cos\psi + \dot{b} \qquad (r_1 = b), \tag{3.5.1}$$

where $\dot{b} = \frac{db}{dt}$. Since the problem is linear, it may be decomposed into a solution, $\varphi = \varphi_1 + \varphi_2$, where φ_1 and φ_2 are both harmonic functions and φ_1 satisfies the boundary condition

$$\frac{\partial \phi_1}{\partial r_1} = \dot{a}\cos\psi \qquad (r_1 = b) \tag{3.5.2}$$

and ϕ_2 satisfies

$$\frac{\partial \phi_2}{\partial r_1} = \dot{b} \qquad (r_1 = b) \tag{3.5.3}$$

and thus their sum satisfies (3.5.1).

As a first attempt at the solution of φ_1, we pick a doublet distribution along the meridional circle directed radially.

$$\varphi_1 = -\int_0^{2\pi} \frac{\underline{\beta} \cdot (\underline{x} - \underline{x}')}{R^3} a d\theta', \qquad \underline{\beta} = \beta_1 \underline{e}_r \tag{3.5.4}$$

$$\underline{\beta} \cdot (\underline{x} - \underline{x}') = \beta_1[-a + r\cos(\theta - \theta')] \tag{3.5.5}$$

Following the already established procedure, this integral is expressed in complete elliptic integrals E and K (with argument k) as

$$\varphi_1 = \frac{4a^2\beta_1}{r_2 r_1^2}\left\{ E - \frac{r}{a}\left[\left(\frac{2}{k^2} - 1\right) E - \frac{2k'^2}{k^2} K\right]\right\} \qquad (3.5.6)$$

where r_1, r_2, k, and k' have all been given earlier (3.1.4) and (3.1.23).

In the vicinity of the toroid surface, where r_1/a and k' are small, expansion of this expression together with (3.1.27) yields

$$\varphi_1 = -\frac{2\beta_1}{r_1}\left[\cos\psi + \frac{r_1}{2a}\left(-\log\frac{8a}{r_1} + \sin^2\psi\right)\right.$$
$$+ \frac{3r_1^2}{8a^2}\cos\psi\left(\log\frac{8a}{r_1} - \frac{13}{12}\right) + \frac{3}{32}\frac{r_1^2}{a^2}\cos 3\psi$$
$$\left. + O\left(\frac{r_1^3}{a^3}\log\frac{r_1}{a}\right)\right] . \qquad (3.5.7)$$

The second term on the right-hand side is a source like term of exactly the same nature as that which arose from the normal distribution of doublets when discussing the ring in edge-on translation. There a tangential doublet was used to cancel this term, here a source distribution is employed.

$$\varphi_s = \int_0^{2\pi} -\frac{m_1}{R}\, a d\theta' = -\frac{4am_1}{r_2} K(k) . \qquad (3.5.8)$$

Taking the same limit as was used in obtaining (3.5.7)

$$\varphi_s = -2m_1\left[\log\frac{8a}{r_1} + \frac{r_1}{2a}\cos\psi\left(1 - \log\frac{8a}{r_1}\right) + O\left(\frac{r_1^2}{a^2}\log\frac{r_1}{a}\right)\right] . \qquad (3.5.9)$$

The undesired source like behavior is eliminated by choosing

$$m_1 = \frac{\beta_1}{2a} \tag{3.5.10}$$

and the superposition of the two singularity distributions gives the potential

$$\varphi_1 = -\frac{2\beta_1}{r_1}\left[\cos\psi + \frac{r_1}{2a}\sin^2\psi + \frac{r_1^2}{8a^2}\cos\psi\left(\log\frac{8a}{r_1} - \frac{5}{4}\right)\right.$$
$$\left. + \frac{3}{32}\frac{r_1^2}{a^2}\cos 3\psi + O\left(\frac{r_1^3}{a^3}\log\frac{r_1}{a}\right)\right] . \tag{3.5.11}$$

The $\cos 3\psi$ term prevents the boundary condition to be satisfied to order ϵ^2, and an octupole is sought to cancel this term. An octupole with radial derivatives is called for, and the easiest to be evaluated is

$$\varphi_o = \int_o^{2\pi} -A\frac{d^3}{da^3}\left(\frac{1}{R}\right) a\,d\theta' . \tag{3.5.12}$$

This octupole has already been treated in section 3.2 and from equation (3.2.13) and the boundary condition (3.5.2), the octupole strength must be taken as

$$A = \beta_1\left(\frac{b\epsilon}{8}\right)^2 , \tag{3.5.13}$$

where $\epsilon = b/a$. This boundary condition also gives the doublet strength as

$$\beta_1 = \frac{\dot{a}b^2}{2}\left[1 + \frac{\epsilon^2}{8}\left(\log\frac{8}{\epsilon} - \frac{9}{4}\right) + O(\epsilon^3\log\epsilon)\right] . \tag{3.5.14}$$

Substituting back into the expression for the potential, and including all the singularities (doublet, source, and octupole), we get,

$$\varphi_1(\underline{x}, t) = -\frac{\dot{a}b^2}{r_1}\left[\cos\psi + \frac{r_1}{2a}\sin^2\psi + \frac{r_1^2}{8a^2}\cos\psi\left(\log\frac{8a}{r_1} - \frac{5}{4}\right)\right.$$

$$+ \frac{\epsilon^2}{8}\cos\psi\left(\log\frac{8}{\epsilon} - \frac{9}{4}\right) + \frac{1}{32}\left(\frac{3r_1^2}{a^2} + \frac{b^4}{a^2 r_1^2}\right)\cos 3\psi$$

$$\left. + O\left(\frac{r_1^3}{a^3}\log\frac{r_1}{a}\right)\right] . \qquad (3.5.15)$$

It then follows that the flow velocity at the toroid surface has in the body frame of reference the value

$$\underline{u}_b = \nabla\varphi - \dot{a}\underline{e}_r \qquad (r_1 = b)$$

$$= \underline{e}_\psi\, \dot{a}\left[2\sin\psi - \epsilon\sin\psi\cos\psi + \frac{\epsilon^2}{8}\sin\psi\left(2\log\frac{8}{\epsilon} - \frac{7}{2}\right)\right.$$

$$\left. + \frac{3}{8}\epsilon^2\sin 3\psi + O(\epsilon^3\log\epsilon)\right] . \qquad (3.5.16)$$

For the solution of φ_2, we first take a source distribution along the meridional circle

$$\varphi_s = \int_0^{2\pi} -\frac{m_2 a\, d\theta'}{R} \qquad (3.5.17)$$

This potential was just considered in (3.5.8) and (3.5.9) and we use these results directly. Carrying out the expansion to a higher order yields

$$\varphi_s = -2m_2 \left\{ \log \frac{8a}{r_1} + \frac{r_1}{2a} \cos\psi \left(1 - \log \frac{8a}{r_1}\right) \right.$$

$$\left. + \frac{r_1^2}{8a^2} \left[\left(3\cos^2\psi - \frac{1}{2}\right) \log \frac{8a}{r_1} - 4\cos^2\psi + \frac{1}{2} \right] + O\left(\frac{r_1^3}{a^3} \log \frac{r_1}{a}\right) \right\}$$

(3.5.18)

and hence

$$\frac{\partial \varphi_s}{\partial r_1} = \frac{2m_2}{r_1} \left\{ 1 - \frac{r_1}{a} \cos\psi \left(1 - \frac{1}{2} \log \frac{8a}{r_1}\right) \right.$$

$$- \frac{r_1^2}{4a^2} \left[\left(3\cos^2\psi - \frac{1}{2}\right) \log \frac{8a}{r_1} - \frac{11}{2} \cos^2\psi + \frac{3}{4} \right]$$

$$\left. + O\left(\frac{r_1^3}{a^3} \log \frac{r_1}{a}\right) \right\} . \qquad (3.5.19)$$

The second term in these last two equations can be eliminated by a doublet distribution directed along $\underline{e}_r$. Using the result of (3.5.7) replacing β_1 by β_2 gives

$$\varphi_d = -\int_0^{2\pi} \frac{\underline{\beta} \cdot (\underline{x} - \underline{x}')}{R^3} a\,d\theta' \qquad \underline{\beta} = \beta_2 \underline{e}_r \qquad (3.5.20)$$

and

$$\frac{\partial \varphi_d}{\partial r_1} = \frac{2\beta_2}{r_1^2} \left[\cos\psi - \frac{r_1}{2a} + O\left(\frac{r_1^2}{a^2} \log \frac{r_1}{a}\right)\right] . \qquad (3.5.21)$$

On $r_1 = b$ (3.5.3) gives

$$\beta_2 = b\epsilon\, m_2 \left(1 - \frac{1}{2} \log \frac{8}{\epsilon}\right) , \qquad (3.5.22)$$

and

$$\left(\frac{\partial \varphi_s}{\partial r_1} + \frac{\partial \varphi_d}{\partial r_1}\right) = \frac{2m_2}{b}\left[1 - \frac{\epsilon^2}{8}\cos 2\psi\left(3\log\frac{8}{\epsilon} - \frac{11}{2}\right)\right.$$

$$\left. + O(\epsilon^3 \log \epsilon)\right] . \qquad (3.5.23)$$

The $\cos 2\psi$ term prevents the boundary condition from being satisfied to the order of ϵ^2, and a quadrupole is sought to cancel this term. A quadrupole with radial derivatives is called for which can be expressed as

$$\varphi_q = \int_0^{2\pi} - A_q \frac{d^2}{da^2}\left(\frac{1}{R}\right) a\,d\theta' \qquad (3.5.24)$$

$$= -\frac{2A_q}{r_1^2}\left[\cos 2\psi + O\left(\frac{r_1}{a}\right)\right] ,$$

hence

$$\frac{\partial \varphi_q}{\partial r_1} = \frac{4A_q}{b^3}\left[\cos 2\psi + O(\epsilon)\right] \qquad (r_1 = b) . \qquad (3.5.25)$$

If we chose

$$A_q = \frac{m_2}{16} b^2 \epsilon^2 \left(3\log\frac{8}{\epsilon} - \frac{11}{2}\right) , \qquad (3.5.26)$$

then combining these three distributions of singularities gives

$$\varphi_2 = \varphi_s + \varphi_d + \varphi_q = -2m_2\Big\{\log\frac{8a}{r_1} + \frac{r_1}{2a}\cos\psi(1 - \log\frac{8a}{r_1})$$

$$+ \frac{r_1^2}{8a^2}\left[(3\cos^2\psi - \frac{1}{2})\log\frac{8a}{r_1} - 4\cos^2\psi + \frac{1}{2}\right]$$

$$+ \frac{b}{r_1}\epsilon\cos\psi(1 - \log\frac{8}{\epsilon}) + \frac{\epsilon^2}{2}(1 - \frac{1}{2}\log\frac{8}{\epsilon})(-\log\frac{8a}{r_1} + \sin^2\psi)$$

$$+ \frac{1}{16}\frac{b^2\epsilon^2}{r_1^2}(3\log\frac{8}{\epsilon} - \frac{11}{2})\cos 2\psi + O(\frac{r_1^3}{a^3}\log\frac{r_1}{a})\Big\} \quad . \tag{3.5.27}$$

On $r_1 = b$ condition (3.5.3) is used to determine m_2 as

$$m_2 = \frac{b\dot{b}}{2} \quad . \tag{3.5.28}$$

Accordingly,

$$\frac{1}{b}\frac{\partial\varphi_2}{\partial\psi} = \dot{b}\left[\frac{3}{2}\epsilon\sin\psi(1 - \log\frac{8}{\epsilon}) + \epsilon^2\sin\psi\cos\psi(2\log\frac{8}{\epsilon} - \frac{27}{8})\right.$$

$$\left. + O(\epsilon^3\log\epsilon)\right] \qquad (r_1 = b) \quad . \tag{3.5.29}$$

Combining φ_1 and φ_2 gives the general solution of an expanding major and minor radius and the solution consists of distribution of the following singularities along the meridional radius,

source: $$m = \frac{b\dot{b}}{2} + \frac{\dot{a}b^2}{4a}\left[1 + O(\epsilon^2\log\epsilon)\right] , \tag{3.5.30}$$

doublet: $\underline{\beta} = \beta \underline{e}_r$

$$\beta = \frac{\dot{b} b^3}{2a}\left(1 - \frac{1}{2}\log\frac{8}{\epsilon}\right) + \frac{\dot{a} b^2}{2}\left[1 + \frac{\epsilon^2}{8}\left(\log\frac{8}{\epsilon} - \frac{9}{4}\right) + O(\epsilon^3 \log \epsilon)\right] , \tag{3.5.31}$$

quadrupole: $$A_q = \frac{\dot{b} b^3 \epsilon^2}{32}\left(3 \log\frac{8}{\epsilon} - \frac{11}{2}\right) , \tag{3.5.32}$$

octupole: $$A_o = \left(\frac{b\epsilon}{8}\right)^2 \frac{\dot{a} b^2}{2}\left[1 + \frac{\epsilon^2}{8}\left(\log\frac{8}{\epsilon} - \frac{9}{4}\right) + O(\epsilon^3 \log \epsilon)\right] . \tag{3.5.33}$$

If we consider the special case when the volume of the torus remains constant, that is when $\dot{a}b = -2\dot{b}a$, the resulting singularity strengths are

$$m = 0, \tag{3.5.34}$$

$$\beta = \frac{\dot{a} b^2}{2}\left[1 + \frac{3}{8}\epsilon^2\left(\log\frac{8}{\epsilon} - \frac{25}{12}\right) + O(\epsilon^3 \log \epsilon)\right] , \tag{3.5.35}$$

$$A_q = \dot{a} b^3 [O(\epsilon^3 \log \epsilon)] , \tag{3.5.36}$$

and A_o is unchanged. Note that even though we are allowing the minor radius to change with time there is no source distribution needed, since the source-like behavior of the ring distribution of doublets is exactly that required by the time rate of change of b, and further agrees with the fact that since the torus volume is constant there can be no net source strength.

As a second special case we take $\dot{a} \neq 0$ and $\dot{b} = 0$. The pressure distribution over the toroid surface can be calculated by using (3. 1. 38) in which U is to be replaced by $\dot{a}$, with $\underline{u}_b$ given above and

$$\frac{\partial \varphi}{\partial t} = (\frac{\varphi}{\dot{a}})\ \ddot{a}\ , \tag{3. 5. 37}$$

with φ given by (3. 5. 15). Using this pressure the sectional force per unit length of the centroid circle is

$$\underline{\mathcal{F}} = -\underline{e}_r \rho\pi b^2 \ddot{a}\ [1 + \frac{\epsilon^2}{4}(\log\frac{8}{\epsilon} - \frac{5}{4}) + O(\epsilon^3 \log\epsilon)]$$

$$-\underline{e}_r \frac{1}{2}\ \frac{\rho\pi b^2}{a}\ (\dot{a})^2\ [1 + O(\epsilon^2 \log\epsilon)] \tag{3. 5. 38}$$

In this case the symmetry renders the total force and moment of force about the center of mass equal to zero. The sectional induced mass is

$$m = \rho\pi b^2[1 + \frac{\epsilon^2}{4}(\log\frac{8}{\epsilon} - \frac{5}{4}) + O(\epsilon^3 \log\epsilon)] \tag{3. 5. 39}$$

if referred to the normal component of the local acceleration, and the curvature effect increases this induced mass but only at the rather high order of $\epsilon^2 \log\epsilon$.

The total source strength is

$$Q = \int_0^{2\pi} ma\, d\theta = \pi\frac{b^2}{2}\ \dot{a}[1 + \frac{\epsilon^2}{8}(\log\frac{8}{\epsilon} - \frac{9}{4}) + O(\epsilon^3 \log\epsilon)]\ . \tag{3. 5. 40}$$

In this case the toroid is not a rigid body and hence the nonzero source strength is permitted and is indeed necessary. Furthermore,

$$Q = \frac{1}{4\pi} \int_S (\nabla\varphi \cdot \underline{n})\, dS$$

$$= \frac{1}{4\pi} \int_0^{2\pi} a\, d\theta \int_0^{2\pi} \frac{\partial\varphi}{\partial r_1}\, b(1 + \epsilon \cos\psi)\, d\psi$$

$$= \frac{\pi b^2}{2} \dot{a} \left[1 + O(\epsilon^3 \log \epsilon)\right] . \qquad (3.5.41)$$

3.6 Line distribution of sinks on the central axis

We now superimpose a purely radial flow on the toroid ring fixed in space. The imposed flow is that created by an infinitely long straight line distribution of sinks. The resulting velocity field is

$$\underline{U} = -\frac{2a}{r}\, \underline{e}_r \qquad (3.6.1)$$

where a is the sink strength. If $a > 0$ the flow is radially inward, and if $a < 0$ the flow is radially outward (a source). The boundary condition that there be no normal component to the velocity on the toroid surface requires

$$\frac{\partial\varphi}{\partial r_1} = -\underline{U} \cdot \underline{e}_{r_1} \qquad (r_1 = b)$$

$$= \frac{2a}{a} \left[\cos\psi - \frac{\epsilon}{2}(1 + \cos 2\psi) + \frac{\epsilon^2}{4}(3\cos\psi + \cos 3\psi) + O(\epsilon^3)\right] . \qquad (3.6.2)$$

The terms on the right-hand side are a result of the $1/r$ dependence in the velocity created by the central axis distribution of sinks. A solution is sought by distributing singularities on the meridial circle, and the first choice is radially directed doublets, $\underline{\beta} = \beta \underline{e}_r$. This distribution of singularities has been worked out already (section 3. 5) and the velocity component normal to the toroid surface and evaluated on that surface is

$$\frac{\partial \varphi}{\partial r_1} = \frac{2\beta}{b^2}\left[\cos\psi - \frac{\epsilon}{2} - \frac{3}{8}\epsilon^2 \cos\psi\left(\log\frac{8}{\epsilon} - \frac{25}{12}\right)\right.$$

$$\left. - \frac{3}{32}\epsilon^2 \cos 3\psi + O(\epsilon^3 \log \epsilon)\right] \qquad (3.6.3)$$

where $\epsilon = b/a$. Note that the second term in this expansion is the source-like behavior of the doublet ring and that it is needed to satisfy the boundary condition (3. 6. 2) where a similar term occurs. This means that there is no longer any need for a source distribution or equivalently a tangential doublet distribution. The $\frac{\epsilon}{2}\cos 2\psi$ term in (3. 6. 2), although it has a source-like dependence on r, cannot be constructed from sources because of its ψ dependence, and must be satisfied by a higher order singularity with a higher order strength. The $\cos 2\psi$ dependence leads to the quadrupole

$$\varphi_q = -aA_q \int_0^{2\pi} \frac{d^2}{da^2}\left(\frac{1}{R}\right) d\theta' \quad . \qquad (3.6.4)$$

This can be expressed in complete elliptic integrals and expanded

in powers of the small parameter r_1/a and k' in the vicinity of the toroid surface to give

$$\varphi_q = -\frac{2A_q}{r_1^2}\left[\cos 2\psi - \frac{r_1}{4a}(\cos\psi + \cos 3\psi) + O(\frac{r_1^2}{a^2}\log\frac{r_1}{a})\right] \tag{3.6.5}$$

and following immediately

$$\frac{\partial\varphi_q}{\partial r_1} = \frac{4A_q}{b^3}\left[\cos 2\psi - \frac{\epsilon}{8}(\cos\psi + \cos 3\psi) + O(\epsilon^2\log\epsilon)\right] \qquad (r_1 = b)\ . \tag{3.6.6}$$

The appearance of the $\cos 3\psi$ terms necessitates the use of the octupole

$$\varphi_o = -aA_o\int_o^{2\pi}\frac{d^3}{da^3}\left(\frac{1}{R}\right)d\theta' \ . \tag{3.6.7}$$

Expressing this integral in terms of complete elliptic integrals and expanding for small r_1/a and k' near the toroid surface leads to

$$\varphi_o = -\frac{4A_o}{r_1^3}\left[\cos 3\psi + O(\frac{r_1}{a})\right] \ , \tag{3.6.8}$$

and

$$\frac{\partial\varphi_o}{\partial r_1} = \frac{12A_o}{b^4}\left[\cos 3\psi + O(\epsilon)\right] \qquad (r_1 = b)\ . \tag{3.6.9}$$

Superimposing the potentials φ, φ_q, and φ_o and requiring their sum to satisfy the boundary condition (3.6.2) implies

$$A_q = - \frac{ab^2\epsilon^2}{4} \tag{3.6.10}$$

$$A_o = (\frac{\epsilon b}{8})^2 \ (\beta + \frac{2ab^2}{a}) \tag{3.6.11}$$

$$\beta = \frac{ab^2}{a}[\,1 + \frac{3}{8}\epsilon^2(\log\frac{8}{\epsilon} - \frac{1}{4}) + O(\epsilon^3 \log\epsilon)] \tag{3.6.12}$$

and

$$\varphi(\underline{x}, t) = - \frac{2ab^2}{ar_1}\,[\cos\psi + \frac{r_1}{2a}(-\log\frac{8a}{r_1} + \sin^2\psi) - \frac{b^2}{4ar_1}\cos 2\psi$$

$$+ \frac{3r_1^2}{8a^2}\cos\psi(\log\frac{8a}{r_1} - \frac{13}{12}) + \frac{3b^2}{8a^2}\cos\psi\,(\log\frac{8}{\epsilon} - \frac{1}{4})$$

$$+ \frac{1}{32}\cos 3\psi(\frac{3r_1^2}{a^2} + 2\epsilon^2 + \frac{3b^2\epsilon^2}{r_1^2}) + O(\frac{r_1^3}{a^3}\log\frac{r_1}{a})]\,. \tag{3.6.13}$$

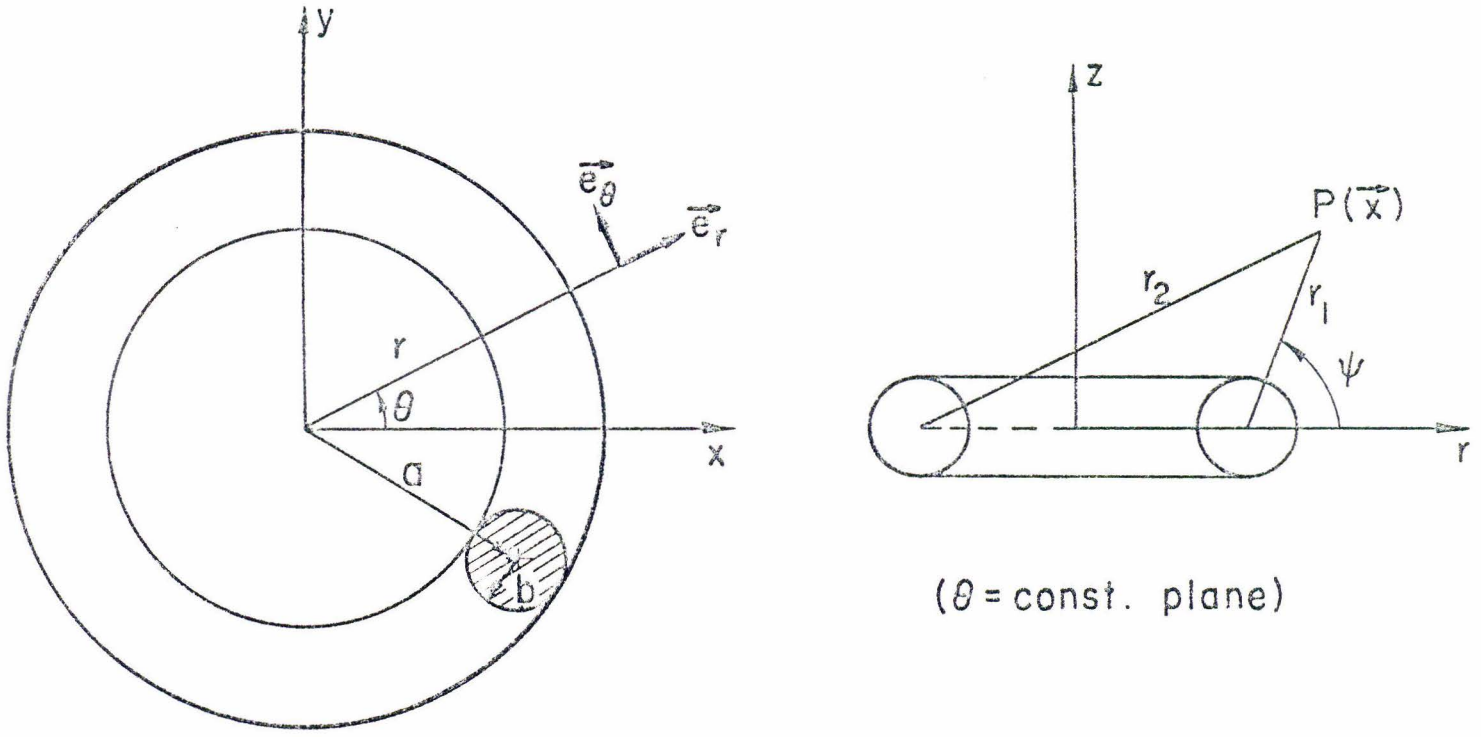

Figure 3. 1. The coordinate system for the toroidal ring problem.

IV. FINITE AMPLITUDE MOTION OF A FLEXIBLE SLENDER BODY

As a typical case of the undulatory motions that most elongated aquatic animals make to propel themselves through water, especially when the viscous effect is unimportant except in drag calculations, we consider the potential flow generated by a flexible slender body moving in an arbitrary manner through an ideal fluid originally at rest. For simplicity we assume that the body has circular cross sections, of local radius $b(s)$ where s denotes the arc length along the body centerline and the body may perform a planar, but otherwise arbitrary motion. Thus the present case is more relevant to anguilliform motion, but the method would also be akin, with suitable extensions of the theory, to studies on carangiform propulsion (though such extensions are not included here).

4.1 General theory

Large-amplitude motions of the slender body in the plane say $z = 0$ can be generally described in the parametric form

$$x = x(s,t), \qquad y = y(s,t) \qquad (0 < s < \ell), \qquad (4.1.1)$$

which specifies the instantaneous position of a point on the body centerline at an arc length s from the anterior tip, and ℓ is the body length. The parametric functions will be assumed twice continuously differentiable in s and t. This motion may be either generated by an extraneous agency, or, in self-swimming animals, due to swimming actions and the resultant fluid action, including involuntary recoils. The body centerline will be assumed to be inextensible so

that

$$(\frac{\partial x}{\partial s})^2 + (\frac{\partial y}{\partial s})^2 = 1 \quad . \tag{4.1.2}$$

Under this condition the unit vectors tangential and normal to the body centerline can be written

$$\underline{e}_s = (\frac{\partial x}{\partial s}, \frac{\partial y}{\partial s}, 0), \qquad \underline{e}_n = (\frac{\partial y}{\partial s}, -\frac{\partial x}{\partial s}, 0) \quad , \tag{4.1.3}$$

so that $(\underline{e}_n, \underline{e}_s, \underline{e}_z)$ form a right-hand system of orthogonal vectors, and the centerline has the instantaneous radius of curvature $|a|$ where

$$a(s,t) = (\frac{\partial^2 y}{\partial s^2} \frac{\partial x}{\partial s} - \frac{\partial^2 x}{\partial s^2} \frac{\partial y}{\partial s})^{-1} \quad . \tag{4.1.4}$$

The center of curvature of the line at station s lies on the positive (or negative) side of the n-axis if a is negative (or positive), as shown in figure 4.1. (The present sign convention is adopted in order to make direct comparison with the results of the torus problem.) The velocity of the centerline in planar motion is given by

$$\underline{V}(s,t) = (\frac{\partial x}{\partial t}, \frac{\partial y}{\partial t}, 0) \quad , \tag{4.1.5}$$

which can be arbitrarily assigned provided it will always keep the radius of curvature $|a|$ large compared to the local body radius b and it satisfies the inextensibility condition (4.1.2) for all t. As in our discussion on the problem of torus, it is convenient to decompose $\underline{V}$ into the components normal and tangential to the body centerline,

$$\underline{V}(s,t) = V_s(s,t,)\,\underline{e}_s + V_n(s,t)\,\underline{e}_n \quad , \tag{4.1.6}$$

where

$$V_s = \frac{\partial x}{\partial t}\frac{\partial x}{\partial s} + \frac{\partial y}{\partial t}\frac{\partial y}{\partial s} \quad , \qquad V_n = \frac{\partial x}{\partial t}\frac{\partial y}{\partial s} - \frac{\partial y}{\partial t}\frac{\partial x}{\partial s} \quad . \tag{4.1.7}$$

In addition to this translational motion $\underline{V}$, the body at an arc length s, or more precisely a coordinate system with its origin fixed at s and having its axis directed along $(\underline{e}_s, \underline{e}_n, \underline{e}_z)$, also undergoes a rotation about the z-axis, $\underline{\Omega} = \Omega\,\underline{e}_z$, and

$$\Omega = \underline{e}_s \cdot \frac{\partial}{\partial t}\underline{e}_n = -\,\underline{e}_n \cdot \frac{\partial}{\partial t}\underline{e}_s = x_s y_{st} - y_s x_{sy} \quad . \tag{4.1.8}$$

The velocity experienced by a material point on the body surface is then

$$\begin{aligned} \underline{U}_b &= \underline{V} + \underline{\Omega} \times b\,\underline{e}_{r_l} \\ &= V_n \underline{e}_n + (V_s + \Omega b \cos\psi)\,\underline{e}_s \qquad (4.1.9) \\ &= U_n \underline{e}_n + U_s \underline{e}_s \end{aligned}$$

where $U_n = V_n$ and $U_s = V_s + \Omega b \cos\psi$.

For the velocity potential we seek again the representation of a line doublet distributed along the body centerline from $s = 0$ to ℓ and moving with it for all t. The unknown doublet strength (per unit

length of s) will also be decomposed, for the convenience of calculation, into the normal and tangential components

$$\underline{\beta} = \beta_s(s,t)\,\underline{e}_s + \beta_n(s,t)\,\underline{e}_n \qquad (0 < s < \ell). \tag{4.1.10}$$

In case the body end is blunt, a more accurate account of the local flow requires the doublet line to start from a point ($s = 0$) at a short distance, of the order of the radius of curvature of the body surface at the end, from the body end, but this feature is already known (e.g., Wu and Chwang, 1974) to be of secondary importance. There is no need to include in the construction of solution an additional line source since β_s, the tangential component of the line doublet, is easily seen (by integration of the integral representation (4.1.11) by parts) to be equivalent to a line source distribution. The velocity potential can then be expressed as

$$\varphi(\underline{x},t) = -\int_0^{\ell} \frac{\underline{\beta}(s,t)\cdot(\underline{x}-\underline{x}')}{R^3}\,ds, \tag{4.1.11}$$

where $\underline{x}'$ is a point on the centerline prescribed by (4.1.1) and $R = |\underline{x}-\underline{x}'|$. The doublet strength $\underline{\beta}$ is to be determined by applying the boundary condition

$$[\nabla\varphi - \underline{U}_b(s,t)]\cdot\underline{\nu}(\underline{x},t) = 0 \qquad (\underline{x} \text{ on } S(s,t)), \tag{4.1.12}$$

where $\underline{\nu}(\underline{x},t)$ denote the normal vector of the body surface at station s, at which the body cross section is assumed to remain circular (for

every s) and its boundary is denoted by $S(s,t)$, and $\underline{U}_b(s,t)$ is given by equation (4. 1. 9).

In the same way that (3. 1. 1) was split into the two integrals of (3. 1. 3) (now letting c/a assume the roll of γ), we evaluate the asymptotic representation of $\varphi(\underline{x},t)$ for $\underline{x}$ in the vicinity of $S(s,t)$ by decomposing the integral in (4. 1. 11) into three parts

$$\varphi = -\left(\int_0^{s_o-c} + \int_{s_o-c}^{s_o+c} + \int_{s_o+c}^{\ell} \right) \frac{\underline{\beta} \cdot (\underline{x} - \underline{x}')}{R^3} \, ds \equiv \varphi_1 + \varphi_o + \varphi_2 \, , \tag{4. 1. 13}$$

where s_o is the value of s determined in such a way that the plane containing the vector $\underline{e}_n(s_o,t)$ and parallel to the z-axis (hence perpendicular to $\underline{e}_s(s_o,t)$ also contains the specific point $\underline{x}$ in question, and the range $2c$ of the integral φ_o will be chosen such that $b \ll c \ll$ (a or ℓ). This choice implies that within the range of integration for φ_o, the centerline curvature will not have any significant departure from its value at s_o, and this segment of body would therefore behave like a segment of the torus discussed previously. The location of s_o is assumed to be sufficiently far from either end, and the end solution is not further prusued here.

Of the three parts of φ, φ_o is the most important since both φ_1 and φ_2 cannot make more than a minor contribution to the value of φ on account of the greater distance, from s_o, of the doublets that represent φ_1 and φ_2. To facilitate the calculation of φ_o, we introduce a local system of cartesian coordinates (ξ, η, ζ), with the origin at s_o, the ξ- and η-axis coinciding with $\underline{e}_n$ and $\underline{e}_s$ at s_o,

respectively, and with $\zeta = z$. We shall also employ, alternatively for convenience, a system of curvilinear coordinates (r_1, ψ, θ) defined by

$$r_1 = (\xi^2 + \zeta^2)^{\frac{1}{2}}, \quad \psi = \tan^{-1}(\zeta/\xi) \ , \quad s - s_o = a\theta \ . \qquad (4.1.14)$$

Note that θ is in the same or opposite sense to that of s according as $a > 0$ or $a < 0$. When expressed in terms of these coordinates, we have

$$\underline{x} = [r_1 \cos\psi, 0, \quad r_1 \sin\psi] \ ,$$

$$\underline{x}' = [-a(1 - \cos\theta), \quad a \sin\theta, 0] \ . \qquad (4.1.15)$$

where the square brackets denote the components of a vector with respect to the system $[\xi, \eta, \zeta]$. Also we have

$$\underline{e}_n(\theta) = [\cos\theta, \ \sin\theta, 0] \ , \quad \underline{e}_s = [-\sin\theta, \ \cos\theta, 0] \ . \qquad (4.1.16)$$

It therefore follows that

$$R = |\underline{x} - \underline{x}'| = [r_1^2 + 2a(a + r_1\cos\psi)(1 - \cos\theta)]^{\frac{1}{2}} \ , \qquad (4.1.17)$$

and

$$\underline{\beta} \cdot (\underline{x} - \underline{x}') = -\beta_n[(a + r_1\cos\psi)(1 - \cos\theta) - r_1\cos\psi]$$

$$-\beta_s(a + r_1\cos\psi)\sin\theta \qquad (4.1.18)$$

$$= -\beta_n\left[\frac{R^2 - r_1^2}{2a} - r_1\cos\psi\right] - \beta_s(a + r_1\cos\psi)\sin\theta \ .$$

Upon substituting (4. 1. 17) and (4. 1. 18) into the integrand of φ_o, we have

$$\varphi_o = -a\int_{-a}^{a} \frac{\underline{\beta}\cdot(\underline{x}-\underline{x}')}{R^3}\,d\theta = -(a\,r_1\cos\psi + \frac{1}{2}\,r_1^2)\int_{-a}^{a}\frac{\beta_n\,d\theta}{R^3}$$

$$+\int_{-a}^{a}(\frac{1}{2}\beta_n + \frac{d\beta_s}{d\theta})\,\frac{d\theta}{R} - \left[\frac{\beta_s(\theta)}{R}\right]_{-a}^{a}, \qquad (4.1.19)$$

in which the integral with β_s has been integrated by parts, and

$$a = c/a << 1 \qquad (4.1.20)$$

by assumption. Since θ is small within the range of integration, we may expand $(1 - \cos\theta)$; $\beta_n(\theta)$ and $\beta_s(\theta)$ for small θ,

$$(1 - \cos\theta) = \frac{\theta^2}{2}\,(1 - \frac{1}{12}\,\theta^2 + \ldots),$$

$$\beta_n(\theta) = \beta_n(0) + \theta\beta_n'(0) + \frac{1}{2}\,\theta^2\beta_n''(0) + \ldots,$$

with a similar equation for $\beta_s(\theta)$. Here the primes over β denote differentiation with respect to θ. Obviously, the terms $\theta\beta_n'(0)$ and $\theta\beta_s''(0)$ in these expansions, being odd in θ, have no contribution to the integrals in (4. 1. 19) since R is even in θ. Thus we see that the error committed through neglecting the second and higher terms in the above expansions will introduce a factor $[1 + O(a^2 \log a)]$ to the final result so obtained (the additional factor log a in the order term arises from the integral of R^{-1}). Accordingly, we need to be concerned only with the following two integrals

$$I_1 = \int_{-a}^{a} \frac{d\theta}{R_*} , \qquad I_2 = \int_{-a}^{a} \frac{d\theta}{R_*^3} , \tag{4.1.21}$$

where

$$R_* = [\, r_1^2 + a^2(1 + \frac{r_1}{a} \cos\psi)\theta^2 \,]^{\frac{1}{2}} . \tag{4.1.22}$$

These elementary integrals can further be expanded for small values of r_1/c where r_1 is sufficiently close to the body so that $r_1 \sim O(b)$, giving

$$I_1 \simeq \frac{2}{a}(1 + \frac{r_1}{a}\cos\psi)^{-\frac{1}{2}} \left\{ \log \frac{2c}{r_1} \, (1 + \frac{r_1}{a}\cos\psi)^{\frac{1}{2}} + O(\frac{r_1}{c})^2 \right\}$$

$$\simeq \frac{2}{a}\left\{ \log \frac{2c}{r_1} + O(\frac{r_1}{a} \log \frac{c}{r_1}) \right\} , \tag{4.1.23}$$

$$I_2 \simeq \frac{2}{ar_1^2}(1 + \frac{r_1}{a}\cos\psi)^{-\frac{1}{2}} \left\{ 1 + O(\frac{r_1}{c})^2 \right\}$$

$$\simeq \frac{2}{ar_1^2} \left\{ 1 - \frac{r_1}{2a}\cos\psi + O(\frac{r_1}{c})^2 \right\} . \tag{4.1.24}$$

The order term in (4.1.24) will hold provided $(r_1/c)^2$ is of a higher order than (r_1/a). By a similar expansion procedure, the last term in (4.1.19) becomes $-2d\beta_s/ds$ evaluated at s_o. We then see that in the leading terms of these expansions, only the first term of I_1 depends on the limits of integration involving c, whose value is no more precisely prescribed than by its order of magnitude only. This

somewhat indefinite (constant) term, namely log c, is expected, in principle, to be cancelled out when the asymptotic expansions of φ_1 and φ_2 are combined with that of φ_o in the final account for φ. Although such expansions of φ_1 and φ_2 require the prescription of the velocity $\underline{V}(s,t)$ of the entire centerline, the fact that both φ_1 and φ_2 exist at the origin of (ξ, η, ζ) and are regular in its neighborhood may be used to infer that for small values of r_1/c and $|s - s_o|/c$,

$$\varphi_1 \simeq \frac{\beta}{c}\left\{ A_o + \frac{r_1}{c}(A_1 \cos\psi + A_2 \sin\psi) + O(\frac{r_1}{c})^2 \right\} , \tag{4.1.25}$$

and a similar expansion holds for φ_2, where the coefficients A_o, A_1, and A_2 may depend on c, and are of order $\log(c/\ell)$. Here β represents a bound estimate of $\underline{\beta}(s)$ over the centerline; the factor (β/c) and the order estimates of A_o, A_1, and A_2 can be obtained by an approximate evaluation of the lengths involved in the integrand of φ_1 and φ_2. The foregoing argument is nevertheless sufficient for the doublet strength to be determined to its leading order.

Compiling the asymptotic expansions for the various terms, we have

$$\begin{aligned} \varphi \simeq\ & [\frac{1}{a}\beta_n + 2\frac{\partial}{\partial s}\beta_s(s)]\left\{\log\frac{2c}{r_1} + B_o + O(\frac{r_1}{a}\log\frac{c}{r_1})\right\} \\ & - 2\beta_n\left\{\frac{1}{r_1}\cos\psi + \frac{1}{2a}\sin^2\psi + B_1 + O(\frac{r_1}{c^2}\log\frac{c}{\ell})\right\} \end{aligned} \tag{4.1.26}$$

where B_o and B_1 may depend on c and s, with their magnitude estimated to be of order $\log(c/\ell)$, but are independent of r_1 and ψ.

Here the subscript of s_o has been dropped as understood. Now, since the body surface at station s, at which $r_1 = b(s)$, has the normal vector given by

$$\underline{\nu} = \underline{e}_{r_1} - \underline{e}_s \frac{db}{ds} = \underline{e}_\xi \cos\psi + \underline{e}_\zeta \sin\psi - \underline{e}_\eta \frac{db}{ds} , \tag{4.1.27}$$

the boundary condition (4.1.12) becomes

$$\frac{\partial\varphi}{\partial r_1} - \frac{\partial\varphi}{\partial s}\frac{db}{ds} = (V_n - \Omega b \frac{db}{ds}) \cos\psi - V_s \frac{db}{ds} \qquad (r_1 = b), \tag{4.1.28}$$

which is satisfied by (4.1.26) if

$$\beta_n = \frac{1}{2} (V_n - \Omega b \frac{db}{ds}) b^2 \tag{4.1.29}$$

with a relative error of order $(b^2/a^2) \log (b/a)$, and

$$\frac{\partial\beta_s}{\partial s} = \frac{1}{2} V_s(s,t)\, b \frac{db}{ds} - \frac{1}{2a} \beta_n \tag{4.1.30}$$

with a relative error of order $(b/a) \log (b/a)$. Thus to leading order the local flow field is represented by a normal doublet, of strength

$$\beta_n \simeq \frac{1}{2} V_n b^2 \tag{4.1.31}$$

as predicted on two-dimensional theory, plus a source strength $V_s bb'$ as in the small amplitude slender body theory, plus the centerline curvature effect which remains the same as in the flow past a torus.

Substitution of the doublet strength (4. 1. 29) and (4. 1. 30) into (4. 1. 26) yield the velocity potential

$$\varphi(\underline{x}, t) = V_s\, b \frac{db}{ds} \left(\log \frac{2c}{r_1} + B_o\right) - b^2 (V_n - \Omega b \frac{db}{ds})(\frac{1}{r_1} \cos\psi + \frac{1}{2a} \sin^2\psi + B_1) \tag{4. 1. 32}$$

where terms of relative order $(b/a)^2 \log (\ell /b)$ have been neglected. From this the flow velocity on the body surface can be calculated relative to the body frame (i. e., the frame translating with $\underline{V}$ and rotating with $\underline{\Omega}$)

$$\begin{aligned} \underline{u}_b &= \nabla\varphi - (\underline{V} + \underline{\Omega} \times b\underline{e}_{r_1}) \qquad (r_1 = b) \\ &= -\underline{e}_{r_1}(V_s b' + \Omega b b' \cos\psi) + \underline{e}_\psi \sin\psi (V_n - V_n \frac{b}{a} \cos\psi - \Omega b b') \\ &\quad - \underline{e}_s [V_s + (\Omega b + \frac{\partial V_n}{\partial s} b + 2V_n b') \cos\psi] \end{aligned} \tag{4. 1. 33}$$

where $b' = \frac{db}{ds}$. The effect of variable cross section (the terms having b') comes in at the same order as the curvature, and the far body effects (the terms B_o and B_1) give only higher order corrections to $\underline{u}_b$. Writing the Bernoulli equation in the moving body frame at s gives the pressure distribution on the body surface.

$$-\frac{p}{\rho} = \frac{\partial\varphi}{\partial t} + \frac{1}{2}[u_b^2 - V_n^2 - (V_s + \Omega b \cos\psi)^2] \tag{4. 1. 34}$$

where $u_b^2 = \underline{u}_b \cdot \underline{u}_b$, the time derivative of φ is taken with respect to the local body frame of reference, and the pressure at infinity has been gaged to zero.

From the pressure field the sectional force per unit arc length is calculated as

$$\underline{\mathcal{F}}(s,t) = -b\int_0^{2\pi} p\underline{\nu}\,(1+\frac{b}{a}\cos\psi)d\psi$$

$$= \underline{e}_n\,[-(\frac{\partial}{\partial t} - V_s\frac{\partial}{\partial s})(\rho\pi b^2 V_n) - \rho\pi b^2\,(\frac{V_n^2}{2a} - \dot{\Omega}\,bb')]$$

$$- \underline{e}_s\,\frac{V_n^2}{2}\,\frac{\partial}{\partial s}\,(\rho\pi b^2) \quad . \qquad (4.1.35)$$

The first term represents the material derivative of the normal component of the flow momentum based on the tangential component, $V_s(s,t)$, of the body velocity rather than on the mean forward velocity U, as in the previous theories. The contribution of the centrifugal acceleration, V_n^2/a, results in a normal component of force which vanishes for straight bodies. The angular acceleration of the body surface $\dot{\Omega}\,b$, which need not be assumed small, contributes to the normal force if $b'(s) \neq 0$. A force in the axial direction occurs because of changes in cross sectional area $\rho\pi b^2$. The present result reduces to that of small-amplitude theory, but clearly indicates departure from it due to finite-amplitude and centerline-curvature effects. As shown in the above result, these effects bring forth new

contributions to the sectional forces in addition to the classical concept based on the induced mass of the body.

As a special case, the sectional force (4. 1. 35) reduces to the result (3. 2. 19) for a toroidal ring undergoing edge-on translation, by setting $\underline{e}_n = \underline{e}_r$, $V_n = V \cos\theta$, $V_s = V \sin\theta$, and $b' = 0$.

At a given material point on the body centerline the sectional force exerted by the fluid on the body is time averaged over one beat cycle and then integrated over the entire body length to give the total mean propulsive force on the flexible slender body as

$$\underline{F} = \int_0^{\ell} [\frac{1}{T} \int_0^{T} \underline{\mathcal{F}} dt] \, ds \qquad (4. 1. 36)$$

where T is the period of the undulation. To proceed further it is necessary to specify the body centerline time history, and to retain the generality of this section that calculation is not done now but is rather saved for the next section where several examples are considered.

Having obtained the local pressure field and the sectional force on the body we can now also find the rate at which work is done by the elongated body. This rate of work is of interest since it must be supplied by the swimming organisms musculature and certainly must lie within the capabilities of the organism.

The rate of doing work by the body on the fluid per unit arc length (the sectional power) is given by

$$\mathcal{P} = b \int^{2\pi} (p \, \underline{\nu} \cdot \underline{U}_b)(1 + \frac{b}{a} \cos\psi) \, d\psi \qquad (4. 1. 37)$$

where $\underline{\nu}$, $\underline{U}_b$, and p are given by equations (4. 1. 27), (4. 1. 8), and (4. 1. 34) respectively. Taking the scalar product

$$\underline{\nu} \cdot \underline{U}_b = \underline{\nu} \cdot \underline{V} - b' \Omega b \cos \psi \quad , \tag{4. 1. 38}$$

and substituting it into (4. 1. 37) gives

$$\mathcal{P} = b \int_0^{2\pi} (p \underline{\nu} \cdot \underline{V})(1 + \epsilon \cos \psi)\, d\psi$$

$$- \int_0^{2\pi} b' \Omega b^2 p \cos \psi (1 + \epsilon \cos \psi)\, d\psi \quad . \tag{4. 1. 39}$$

The first term in this equation is the scalar product of the sectional force with the velocity of the body centerline, and the second term is a contribution due to the local change in cross section and the rotation of the body section. Performing the integration indicated in the second term using the pressure from equation (4. 1. 34) and neglecting higher order terms gives

$$\mathcal{P} = -\underline{\mathcal{F}} \cdot \underline{V} - \Omega b \dot{V}_n b' \rho \pi b^2 \tag{4. 1. 40}$$

The total mean power required of the swimming organism is obtained by a time average at a fixed material point over one beat cycle and then an integration over the entire body length.

$$P = \int_0^{\ell} [\frac{1}{T} \int_0^{T} \mathcal{P}\, dt]\, ds. \tag{4. 1. 41}$$

In order to summarize the results of this section the salient features are combined in the form of a theorem

Theorem I.

For an elongated flexible body having circular cross sections of radius $b(s)$, which varies continuously with the arc length s measured along its inextensible centerline whose motion through an incompressible, inviscid fluid originally at rest, is prescribed over a time range of t by arbitrary single-valued functions $x = x'(s,t)$, $y = y'(s,t)$, and $z = 0$ for every point on the centerline such that its radius of curvature, $|a|$, is large compared to maximum b, the velocity potential of the resulting potential flow is

$$\varphi(\underline{x},t) = \int_0^{\ell} \frac{\partial \beta_s}{\partial s} \frac{ds}{R}$$

$$- \int_0^{\ell} \left[(x-x') \frac{\partial y'}{\partial s} - (y-y') \frac{\partial x'}{\partial s} \right] \frac{\beta_n}{R^3} ds \qquad (4.1.42)$$

where

$$R(\underline{x};s,t) = \left[(x-x')^2 + (y-y')^2 + z^2 \right)^{\frac{1}{2}} ,$$

$$\beta_n(s,t) = \frac{1}{2}(V_n - \Omega b \frac{db}{ds}) b^2, \quad \frac{\partial \beta_s}{\partial s} = \frac{1}{2} V_s b \frac{db}{ds} - \frac{1}{2a} \beta_n ,$$

$$V_n = \frac{\partial x'}{\partial t} \frac{\partial y'}{\partial s} - \frac{\partial y'}{\partial t} \frac{\partial x'}{\partial s} ,$$

$$V_s = \frac{\partial x'}{\partial t} \frac{\partial x'}{\partial s} + \frac{\partial y'}{\partial t} \frac{\partial y'}{\partial s} ,$$

$$\Omega = \frac{\partial x'}{\partial s} \frac{\partial^2 y'}{\partial s \partial t} - \frac{\partial y'}{\partial s} \frac{\partial^2 x'}{\partial s \partial t}$$

and

$$a = \left(\frac{\partial^2 y'}{\partial s^2}\,\frac{\partial x'}{\partial s} - \frac{\partial^2 x'}{\partial s^2}\,\frac{\partial y'}{\partial s}\right)^{-1} .$$

Proof: The proof is almost immediate upon noting that

$$\underline{\beta} \cdot (\underline{x}-\underline{x}') = \beta_n\left[(x-x')\,\frac{\partial y'}{\partial s} - (y-y')\,\frac{\partial x'}{\partial s}\right] - \beta_s \frac{\partial}{\partial s}\left[\frac{1}{2} R^2\right] ,$$

followed by integrating the term with β_s in the integral representation (4. 1. 11) by parts, assuming that the tangential doublet strength β_s vanishes at $s = 0$ and ℓ, which is valid for the end with paraboloidal or less blunt shapes (see, e. g., Wu & Chwang, 1974). The conditions $\beta_s(0) = 0$ and $\beta_s(\ell) = 0$ are in fact required by the condition on zero total source strength for closed bodies.

The above solution, (4. 1. 42), of φ is uniformly valid throughout the flow field, and is accurate with a relative error of order $(b/a) \log (\ell/b)$.

4. 2 Special case; anguilliform swimming

The swimming of long slender organisms at high Reynolds number with no fins from which vorticity is likely to be shed has presented difficulty in previous thrust calculations. Small amplitude slender body theories (except Lighthill, 1960b) rely on the shedding of vorticity for the generation of thrust, and the thrust is given by the time rate of change of the added mass at the sharp trailing edge shedding a vortex sheet which is transported by the mean flow downstream. For an inviscid fluid in which no vorticity is allowed the

problem of thrust generation seems uncertain especially in light of D'Alembert's paradox, which states that for steady motions in potential flows there can be no net force on a body. Clearly no paradox really exists here since the admission of unsteady flows renders D'Alembert's observation nonapplicable. Saffman (1967) has shown a simple example of the generation of a nonzero mean force for deformable bodies in a perfect fluid. The just developed theory for unsteady finite amplitude motion of a flexible slender body is another example of such thrust generating motions in potential flows. In this section a special case of this theory is worked out showing a motion similar to that observed in aquatic animal swimming (anguilliform) which produces the mean forward thrust, needed to overcome the viscous drag. Comparison of the theoretical results with observations on anguilliform swimming (Gray, 1933a, b and chapter VI) gives reasonable agreement, and points out areas where further refinements are needed in the theory.

Let us now specify a body shape and work out an example which has general application to anguilliform aquatic animal swimming. We shall give our body a mean forward velocity U in the negative x direction, and further suppose that the body centerline be given by $y = h(x,t)$ in an (x,y) frame moving with the mean forward velocity. The body cross section is circular with radius $b(s)$, and in the notation of Theorem I,

$$\begin{aligned} x' &= -Ut + x(s,t) \\ y' &= h(x,t) \quad . \end{aligned} \tag{4.2.1}$$

Such a geometry is still quite general and permits a wide class of body motions (figure 4.2). The position vector of a point at s on the body centerline is $\underline{x} = [x(s,t),\ h(x(s,t),t),\ 0]$ and its rate of change along the arc length s, is given as

$$\frac{d\underline{x}}{ds} = \frac{\partial \underline{x}}{\partial x}\ \frac{\partial x}{\partial s} = x_s(1, h_x, 0) = \underline{e}_s, \tag{4.2.2}$$

where

$$x_s = \left(\frac{\partial x}{\partial s}\right)_t , \qquad h_x = \left(\frac{\partial h}{\partial x}\right)_t . \tag{4.2.3}$$

For brevity we adopt the subscript notation to denote differentation. When a subscript t appears operating on x or y it is assumed that the arc length s is held fixed, and when t appears operating on h it is assumed that x is held fixed in the differentiation

$$x_t = \left(\frac{\partial x}{\partial t}\right)_s , \qquad h_t = \left(\frac{\partial h}{\partial t}\right)_x . \tag{4.2.4}$$

The condition of inextensibility of the body centerline requires that

$$x_s^2 + y_s^2 + z_s^2 = 1 , \tag{4.2.5}$$

and in our case it follows that

$$x_s = (1 + h_x^2)^{-\frac{1}{2}} . \tag{4.2.6}$$

It also follows that

$$s(x,t) = \int_o^s ds = \int_o^{x(s,t)} \frac{\partial s}{\partial x}\, dx$$

$$= \int_o^{x(s,t)} \sqrt{1 + h_x^2}\, dx \quad , \qquad (4.2.7)$$

and

$$\frac{ds}{dt} = x_t \sqrt{1 + h_x^2} + \int_o^{x(s,t)} \frac{h_x h_{xt}}{\sqrt{1+h_x^2}}\, dx \quad . \qquad (4.2.8)$$

Since $\frac{ds}{dt} = 0$, this implies

$$x_t = \frac{-1}{\sqrt{1+h_x^2}} \int_o^{x(s,t)} \frac{h_x h_{xt}}{\sqrt{1+h_x^2}}\, dx \quad , \qquad (4.2.9)$$

and

$$x_{tt} = - \frac{x_t h_t (x_t h_{xx} + 2h_{xt})}{1 + h_x^2}$$

$$- \frac{1}{\sqrt{1+h_x^2}} \int_o^{x(s,t)} \frac{h_{xt}^2 + h_x h_{xtt} + h_x^3 h_{xtt}}{(1 + h_x^2)^{3/2}}\, dx \quad . \qquad (4.2.10)$$

In the above it was found to be convenient to assume that the body head ($s = 0$) was situated at $x = 0$ for all times, and that the head is moving with a constant velocity $(-U \underline{e}_x)$. This restriction may be removed by simply replacing the lower limit in equation (4.2.8) and

(4. 2. 9) by $x_o(s,t)$ and adding a term with its time derivative, but for simplicity we shall set $x_o \equiv 0$.

With the quantities x_t and x_s known, the flow quantities specified by Theorem I can be easily obtained as

$$V_n = - x_s V_o \quad , \tag{4. 2. 11}$$

$$(\frac{\partial V_n}{\partial t})_s = - x_{st} V_o - x_s (V_{ot} + x_t V_{ox}) \quad , \tag{4. 2. 12}$$

$$(\frac{\partial V_n}{\partial s})_t = x_{ss} V_o + x_s^2 V_{ox} \quad , \tag{4. 2. 13}$$

$$V_s = -U x_s + x_s [x_t (1 + h_x^2) + h_x h_t] \quad , \tag{4. 2. 14}$$

$$\kappa = \frac{1}{a} = x_s^3 h_{xx} \quad , \tag{4. 2. 15}$$

$$\Omega = x_s^2 (x_t h_{xx} + h_{xt}) \quad , \tag{4. 2. 16}$$

where

$$x_{st} = - \frac{h_x (h_t h_{xx} + h_{xt})}{(1 + h_x^2)^{3/2}} \quad , \tag{4. 2. 17}$$

$$x_{ss} = - \frac{h_x h_{xx}}{(1 + h_x^2)^2} \quad , \tag{4. 2. 18}$$

and

$$V_o(x,t) = h_t + U h_x \quad . \tag{4. 2. 19}$$

Thus far the development has been general, and in particular no restrictions have been made on the amplitude of the motion. Taking the special case of small amplitude can easily be done now, and should compare to the results from small amplitude theory (Lighthill, 1960b, or Newman and Wu, 1973). Requiring the amplitude h to be of order b and h_x to be of order ϵ, the flow quantities in (4. 2. 11) - (4. 2. 16) become

$$V_n = -V_o , \qquad V_s = -U , \qquad \kappa = h_{xx} ,$$

$$\left(\frac{\partial V_n}{\partial t}\right)_s = -V_{ot} \qquad \left(\frac{\partial V_n}{\partial s}\right)_t = -V_{ox} \tag{4. 2. 20}$$

where V_o is given in (4. 2. 19). The sectional force (4. 1. 35) then reduces to

$$\underline{\mathcal{F}} = -\underline{e}_y \rho\pi b^2 \left(\frac{\partial}{\partial t} + U \frac{\partial}{\partial x}\right) V_o \tag{4. 2. 21}$$

which agrees with Lighthill's (1960b) result.

The next example was chosen to model the motion of a swimming eel or water snake. Observations have been made by Gray (1968) on the swimming motion of eels, and from these data and from our own observations in chapter VI a typical body centerline motion was chosen to be

$$h(x,t) = (a_o + a_1 x) \cos(kx - \omega t) \quad . \tag{4. 2. 22}$$

This motion corresponds to the propogation of an undulatory wave which increases in amplitude as it passes along the body from head to

tail, much the same as can be seen in figure 6. 1 for a swimming eel. The body cross section b(s) was assumed constant over the entire length of the body (i. e., b' = 0), except at the body ends where hemispherical caps were used to close the body. In calculating the forces on these hemispherical caps, potential flow over a sphere was used where results are well known and readily available. From an analysis of figure 6. 1 the following values were used in equation (4. 2. 22) and in the force and power calculations:

$$a_o = 0 \qquad bk = 0.15$$

$$a_1 = 0.1 \qquad \ell k = 11.0 \tag{4. 2. 23}$$

thus giving a slenderness ratio of $\epsilon = 0.014$.

In calculating the sectional force (4. 1. 35) for this body centerline motion the flow quantities (4. 2. 11) - (4. 2. 16) are needed and are all expressible in terms of h and its derivatives. It is necessary to perform the numerical integrations indicated in equations (4. 2. 9) and (4. 2. 10), and these integrals were done using Simpson's rule on an IBM 370/158 high speed computer. The sectional force $\vec{\mathcal{F}}$ is a function of s and t, and has components only in the x- and y-directions, since the z component must vanish by symmetry. In order to find the total mean force acting on the body by the fluid both a time average and an arc length integration must be carried out as was done in obtaining (4. 1. 36). These integrals were again performed using Simpson's rule, with the time average being taken first, followed by the integral over

the body length. Due to the symmetry of the flow and body undulations there cannot be a force in the y-direction, and the resulting mean force $\underline{F}$ has a nonzero component only in the x-direction. This total mean force is plotted in figure 4. 3 as a function of c/U, where c is the propulsive wave speed as seen in the body frame of reference ($c = \omega/k$). Since $\underline{F}$ is the force on the body a negative value indicates thrust and a positive value indicates drag, and has been rendered non-dimensional by $\frac{1}{2}\rho U^2 \pi b^2$. At $c/U = 0$ the motion is that of a rigid body being towed through the fluid at constant velocity U, and at $c/U = 1$ the motion is that of a sheath being pulled over a fixed track in space resulting in body material velocities being everywhere tangent to the body centerline. The latter case is similar to the motion of a snake moving on land over a rough surface. Within the constraints of potential theory both of these cases should exhibit no net force on the body.

Figure 4. 3 shows two regions where thrust is produced and one region where drag is produced. Having already imposed a uniform mean flow in the positive x-direction, an additional viscous drag is expected to occur acting in the same direction as the mean flow, and if there is to be any hope of obtaining a self propelling body a thrust must be generated by the body undulations to balance this viscous drag. For this reason the region between $c/U = 0$ and 1, where a drag is generated, is considered to be highly undesirable and incapable of sustaining steady swimming. However, it may be useful in decelerating and stopping maneuvers. The thrust generating region for $c/U < 0$ is

found to be unphysical since for body motion in this range of c/U there results a normal component of flow in excess of 0.7 U and at any reasonable Reynolds number for a swimming eel, say 10^4, the flow is almost certainly separated and our solution is no longer valid. The final region for $c/U > 1$ is of physical interest since a thrust capable of overcoming the viscous drag is produced, and indeed all high Reynolds number undulatory modes of propulsion operate in this range of c/U values (Webb, 1975).

Having found a range of c/U values for which self propulsion can occur there remains another important quantity to be calculated, namely the rate at which work is done by the swimming organism. The rate of work done by the fluid forces acting on the body must be equal to the rate of work done by the body musculature with some efficiency of the conversion, and hence the rate of work done by the fluid forces can be used as a measure of the power requirements placed on the animal during swimming. Thus the sectional power is recalled from equation (4.1.40), and since the cross sectional area is constant ($b' = 0$) the second term in (4.1.40) can be dropped to give the sectional power as

$$\mathcal{P} = -\underline{\mathcal{F}} \cdot \underline{V} \quad . \tag{4.2.24}$$

Work must also be done against the viscous forces and a corresponding sectional rate of work against these forces must also be included and is estimated as $C_D \frac{1}{2} \rho V^3 2\pi b$, where C_D was chosen arbitrarily as the drag coefficient for a flat plate in laminar flow for a Reynolds

number of 6×10^4, corresponding to that observed in figure 6.1. These two rates of work combine to give the total rate of work per unit arc length done by the eel. Time averaging and integrating over the body length gives the total mean rate of working which is plotted in figure 4.3, and which has been rendered nondimensional by $\frac{1}{2}\rho U^3 \pi b^2$. The mean rate of work is seen to have a relative minimum at $c/U = 0.6$ which occurs where steady forward swimming is impossible and in the interesting region ($c/U > 1$) there are ever increasing power requirements as c/U increases.

From figure 4.3 it is clear that if the eel wishes to increase his forward speed he need only increase his rearward wave speed, however doing this also causes an increased rate of work. At $c/U = 1$ work must be done but no forward thrust is produced, giving rise to a highly undesirable mode of operation, and as c/U increases without bound the rate of work rapidly increases without bound and is also a disadvantageous mode of operation. We may ask if there is an optimum value of c/U for which a forward thrust is generated at a moderate power output. To this end we introduce the nondimensional quantity

$$\mathcal{E} = \frac{P}{\underline{F} \cdot \underline{U}} \qquad (4.2.25)$$

called the specific energy cost of transport, and which provides a merit of the propulsive mode employed. The specific energy cost has been used by Gabrielli and von Karman (1950) to evaluate the comparative merits of fourteen classes of transportation vehicles, and by Schmidt-Nielsen (1972), Tucker (1970, 1975) and others for studies of

comparative physiology, and by Wu (1975) for studies of dynamic scaling in fish swimming and of indirect assessment on the flow character about fish. As defined in equation (4. 2. 25) the specific energy cost gives the rate of total energy expended in swimming per rate of useful energy expended toward propulsion. Figure 4. 4 shows the specific energy cost plotted as a function of c/U, and three branches occur. As discussed earlier only the branch for which $c/U > 1$ is of interest for steady swimming, and in this region there is a relative minimum at about $c/U = 2.6$. Checking to see if this value of c/U is within the physically meaningful range of our theory, we find that for values of $c/U > 2.5$ there exists local normal flow velocities in excess of the free stream velocity U, and as in the case of $c/U < 0$ separated flow is likely to exist. It seems reasonable that separated flow will alter the force, power and specific energy cost in a fashion to increase $\mathcal{E}$ and thus make the mode of propulsion less efficient, and we may expect to observe the organism employing a somewhat lower c/U value. The theory needs to be modified to include separated flow in the specific energy calculation, and since these alterations were not made the above conclusion should be regarded with caution. However, our observations in chapter VI and those of Gray (1933a, b) indicate that c/U is more typically equal to 1. 5 for swimming eels and indeed for a wide range of aquatic swimmers (Gray, 1968). This observation lends some confidence to the above claim that the swimming eel attempts to function in a mode where separated flow is held to a minimum, and thrust generation is accomplished by the potential flow forces.

A final calculation can be made using these results to assess the character of the flow encountered by a swimming eel (figure 6. 1). Since at high Reynolds number the viscous effects are confined to a thin boundary layer region, they can be considered separately from the pressure forces, and since a freely swimming body must have no net force on it, the thrust (4. 1. 36) can be equated to the viscous drag. That is,

$$F\ \frac{1}{2}\ \rho U^2 \pi b^2 \ = \ \pi b \ell\, \rho U^2 C_D \qquad (4.\ 2.\ 26)$$

where the thrust F is multiplied by $\frac{1}{2}\rho U^2 \pi b^2$ to render it dimensional, and where the drag is estimated by the right hand side where the eel surface area is approximated as $2\pi b\ell$. To cover the reasonable range of swimming modes we take $c/U = 1.5$ and 2.0, and for brevity in what follows the results at 2. 0 will be stated in parenthesis as $c/U = 1.5\ (2.0)$. Our prescribed motion (4. 2. 22) has at its worst point a local normal flow velocity of 0. 37U (0. 72U) giving a Reynolds number based on this velocity and on the body radius b of about 300 (600). At this value of c/U the corresponding mean force from figure 4. 3 is $F = 0.184\ (0.512)$, and using this value in equation (4. 2. 26) the drag coefficient can be estimated as

$$\begin{aligned} C_D &= \frac{F}{2}\,\frac{b}{\ell} \\ &= 0.00133\ (0.00369) \end{aligned} \qquad (4.\ 2.\ 27)$$

The Reynolds number based on length for the eel (figure 6. 1) is about 6×10^4 and the corresponding drag coefficients at this Reynolds

number for a laminar and a turbulent boundary layer on a flat plate are 0.00542 and 0.00820 respectively. In the advent of separated flow the drag coefficient is on the order of unity. Glauert and Lighthill (1955) have treated the boundary layer development and associated skin friction on a long thin cylinder in axial flow. Using their results (claimed to be accurate within 2 per cent) on an equivalent straight rigid body give a drag coefficient of 0.0069. The calculated value of C_D (4.2.27) is less than the drag coefficient corresponging to a laminar boundary layer and to an equivalent rigid cylinder by a factor of 4.1 (1.5) and 5.2 (1.9) respectively. This indicates that either the thrust force generated in this way is not sufficient to overcome the drag on the eel as estimated on an equivalent rigid body, or the drag experienced by the eel is less in this swimming mode than it would be on an equivalent rigid body. Thus we find ourselves faced with a similar paradox as Gray (1936) confronted in his dolphin studies. Due to the approximate nature of the body shape and the drag coefficient choice, precise agreement should not be expected and the result should be viewed only as an indication of the flow character. With this in mind it seems likely that the flow over such a swimmer would remain laminar with very little if any turbulent flow and almost certainly no separated flow is indicated.

It must be noted that the assumption of the equivalence of the unsteady swimming drag to the rigid model drag may lack general validity, since the pressure field and hence the boundary layer and resulting skin friction may differ substantially in the two cases. With

the proper body motion there could be a delay or an advancement of transition and more crucially a prevention of separation. There could also be a component of the unsteady skin friction which would aid in the propulsive force generation. Both mechanisms would result in a reduced drag and thus support the correctness of the above potential theory thrust result.

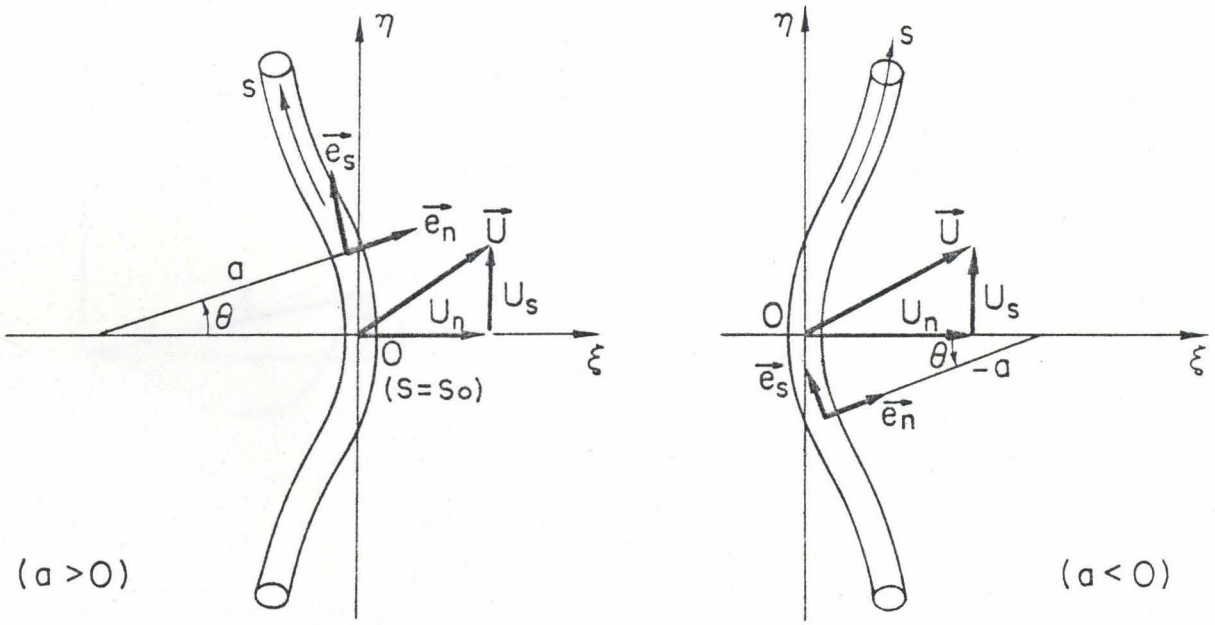

Figure 4. 1. The coordinate systems for a curved slender body.

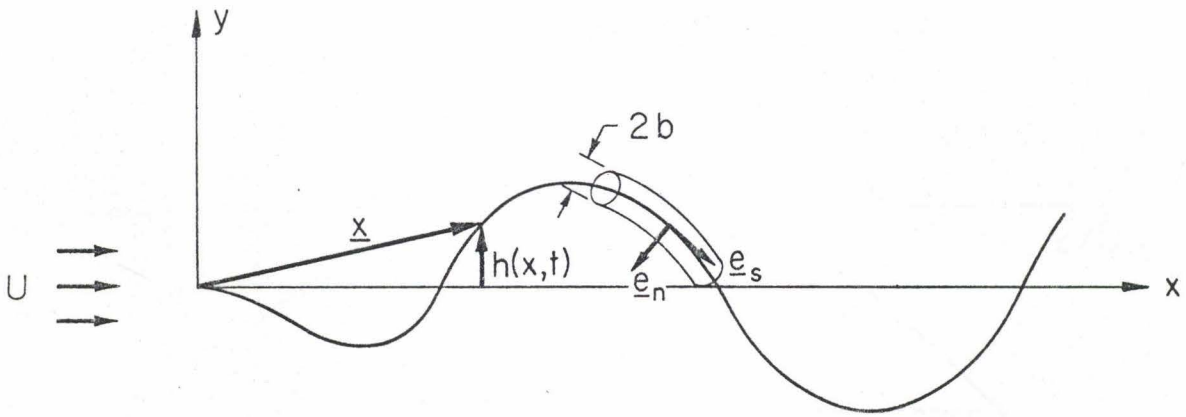

Figure 4.2. Coordinate system used illustrating the amplitude function h(x, t) for arbitrary body centerline motions.

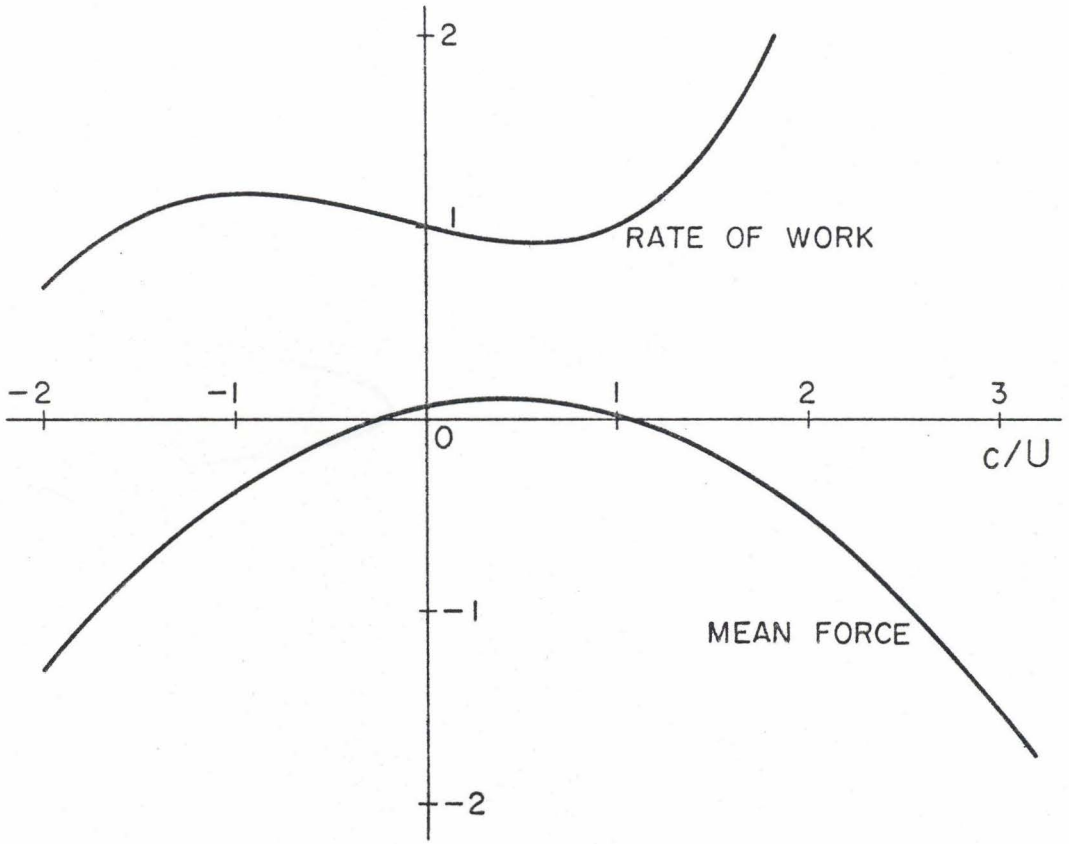

Figure 4.3. The total mean force on the body and rate of work done by the body as a function of c/U for a swimming eel.

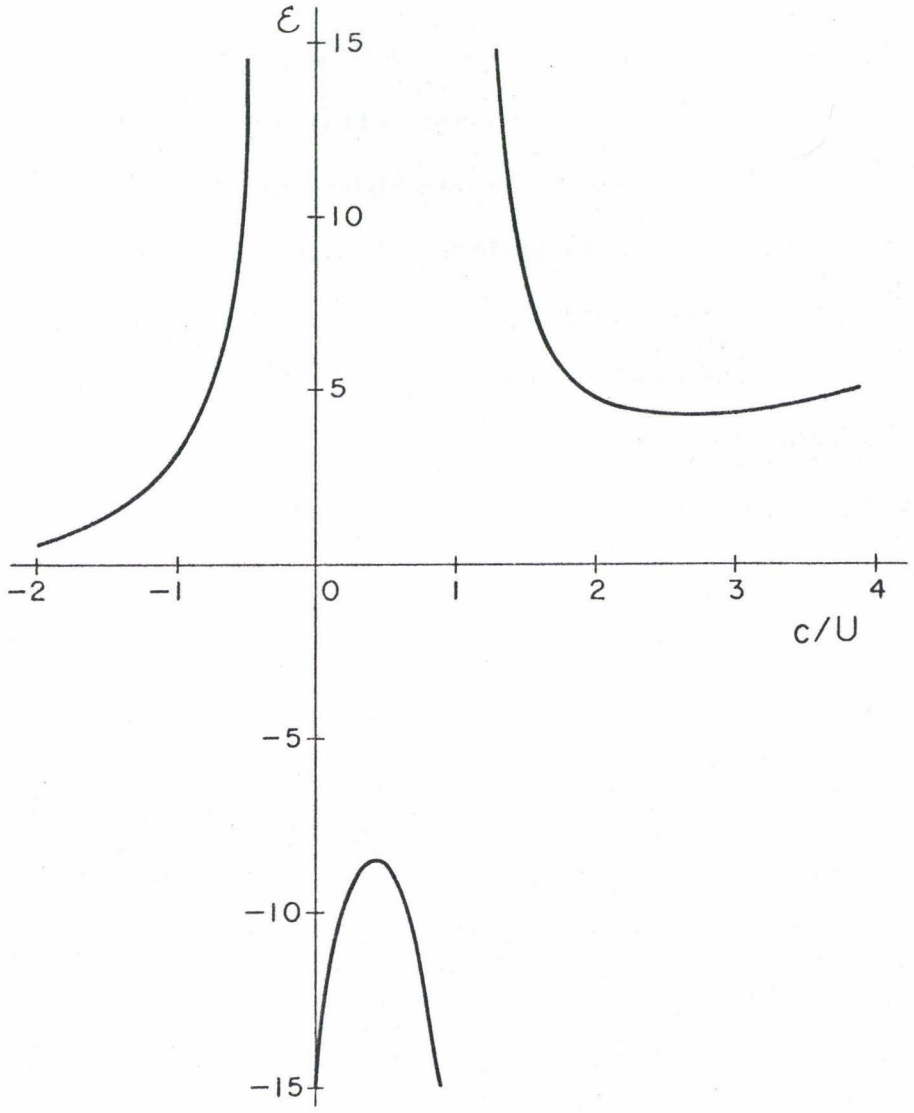

Figure 4.4. Specific energy cost of transport as a function of c/U for a swimming eel.

V. EXPERIMENTS ON FLOW PAST A SLENDER BODY

Experimental measurement of the pressure distribution over the surface of a slender body moving through a fluid (at high Reynolds number) is recognized as a difficult task, especially in the case when the body performs an unsteady, undulatory, flexible movement, and when the body is appended with side and tail fins like a fish. As a consequence, there has been no existing experimental results reporting data on velocity and pressure distributions in unsteady flow past a slender body of this type. Such experimental information is regarded as extremely valuable and necessary for providing a sound basis of estimating the validity of the simplifying assumptions that underlie various theories, as well as a reliable reference against which an error estimate can be obtained for different theoretical predictions.

5.1 Experimental apparatus

As a first step in obtaining experimental pressure measurements a rigid fiberglass model was constructed. The model consisted of two identical halves each constructed from the same mold, the dimensions of which were taken from a Chinook salmon. The resulting rigid model was closely elliptical in body cross section with major and minor axis given by $B(x)$ and $A(x)$ respectively, and the same coordinate system is used as in figure 2.1 where x is measured positive from the nose along the longitudinal axis of the model. Figure 5.1 shows the model used, and figure 5.2 gives measured values of the functions A and B. These data were fit by a least-square fit to a

fifth-order polynomial and to a triaxial ellipsoid for use in the theoretical calculations of pressures experienced by the model. It was not possible to fit the functions A(x) and B(x) with a polynomial over the entire length of the model since the body shape had infinite slope at the body extremities. Thus the body was broken up into three regions, and in each, the body shape conformed well to the fitted curve. At the boundary points between regions, the functions A(x) and B(x) were required to be continuous and to have continuous first derivatives. The functions A and B are given below, where all lengths have been rendered nondimensional by the body length (23.25 inches):

for $0 \leqslant x \leqslant 0.0430$ $\quad (0 \leqslant x \leqslant 1 \text{ in.})$

$$A(x) = 0.0477 \left[1 - \left(\frac{x - 0.0559}{0.0559}\right)^2\right]^{\frac{1}{2}} \tag{5.1.1}$$

$$B(x) = 0.0623 \left[1 - \left(\frac{x - 0.0808}{0.0808}\right)^2\right]^{\frac{1}{2}} \tag{5.1.2}$$

for $0.0430 \leqslant x \leqslant 0.968$ $\quad (1 \text{ in.} \leqslant x \leqslant 22.5 \text{ in.})$

$$A(x) = 0.0361 + 0.282\,x - 1.05\,x^2 + 1.97\,x^3 - 1.98\,x^4 + 0.749\,x^5 \tag{5.1.3}$$

$$B(x) = 0.0348 + 0.543\,x - 1.76\,x^2 + 3.25\,x^3 - 3.41\,x^4 + 1.38\,x^5 \tag{5.1.4}$$

for $0.968 \leqslant x \leqslant 1.0$ $\quad (22.5 \text{ in.} \leqslant x \leqslant 23.25 \text{ in.})$

$$A(x) = 0.0182 \left[1 - \left(\frac{1 - 0.0394 - x}{0.0394}\right)^2\right]^{\frac{1}{2}} \tag{5.1.5}$$

$$B(x) = 0.0384 \left[1 - \left(\frac{1 - 0.0333 - x}{0.0333}\right)^2\right]^{\frac{1}{2}} \tag{5.1.6}$$

The model was towed down a twenty-five-foot-long towing tank, using a variable speed control motor to drive an overhead carriage. The tank was thirty inches wide and twenty-four inches deep, with sidewalls and bottom of glass, for observation purposes. The top remained uncovered allowing a strut to penetrate the free surface and attach the model to the carriage (figure 5. 3).

In all data taken the tank was filled to capacity. This gave a cross sectional area of about 700 square inches and the model projected area amounted to only two per cent of this. The resulting solid blockage corrections (Pope, et al., 1966 and Pankhurst, et al., 1952) in the pressure coefficint measurements were less than four per cent and no blockage corrections were made since errors in calibration and chart reading exceeded this value.

Above the tank and supported on a track running the entire length of the tank was a carriage. The carriage straddled the tank and ran freely on wheels along this track. At one end of the tank was a 1/4 horsepower motor used to move the carriage along the track by means of a cable drive. The carriage speed was controlled remotely with the aid of a Minarik variable speed control. The carriage could be brought up to speed within 2 to 4 feet of its rest position and maintained a constant velocity for the length of a data run (10-15 feet). The maximum speed obtainable was five feet per second, limited by the tank length and time needed to accelerate and decelerate the carriage. Speed was checked initially in two ways. The first was the use of a time lapse photograph taken under stroboscopic lighting. This method was used only as a check and was not continued after verification of the

second method. In this second method, a switch was arranged so as to close at equal distances along the tank, and as the switch closed a marker was made on a strip chart recorder used in recording data. Typical carriage speeds ranged from 1 to 4 ft./sec. giving a Reynolds number range of 1.8×10^5 to 7.2×10^5 based on model overall length. Data was taken at two and sometimes three different speeds and averaged to get the plotted pressure coefficients. No noticeable velocity dependence was observed in the data and hence higher carriage speeds were used when the pressure became small, in order to obtain better accuracy.

From the carriage a streamlined strut was suspended into the water and served as support for the model being tested. The strut had an internal hole along its length which was used to pass tubes into the model from above the water level. The carriage-strut assembly was capable of varying the model angle of attack. The entire assembly including carriage, strut, and model was found to have a natural frequency of about 4 cycles per second. During the data runs the natural frequency was only slightly or not at all excited and caused no problems.

Miniature flush mounted pressure transducers were used at the outset of the experimental investigation. In order for the units to be mounted inside the model, water proofing and miniature size (1/8 inch diaphram) were needed. A high sensitivity of about 20 mm H_2O full scale was needed and obtained with the aid of high gain carrier amplifiers and piezoresistive (semiconductor strain gage) pressure transducers manufactured by Entran Devices, Inc., model EPS-1032

(figure 5. 4). The accuracy of these transducers in measuring pressure was found to be greatly influenced by heat-conduction and forced convection effects when the model was towed through water. Since we were already pushing the sensitivity of the units and because of the complex gage geometry, these anomalies were unable to be overcome, and remote variable reluctance transducers with fluid filled tubes were used.

The inductance type pressure transducers were Validyne model MP45-4 (figure 5. 5), and although they provided the needed sensitivity, liquid filled tubes were required, so that the transducers could be located on the carriage above the tank water line. The tubes used were high compliance polyethylene and care was taken to bleed the tubing and transducer prior to each run. A wash with alcohol followed by a rinse in distilled water was found to help in bleeding the tubes and transducer. In order to check for air bubbles which may have been caught in unseen corners of the transducer or tubing an impulsive load was given the transducer and tubing combination. When air pockets existed the response time was greatly lowered and in these cases the tubes were re-bled until a satisfactory response was obtained. Standard treatments of response times and natural frequencies of liquid filled tubes are available (Doebelin, 1966) and reasonable agreement was obtained with measured tube frequencies in the range of 50-80 cycles per second. It is noted here that this is well above the observed structural natural frequency and is sufficiently high so as not to interfere with the steady measurement taken. The transducers were positioned on the carriage just above the water line

and the necessary wires were then led off the carriage and allowed to hang freely on the laboratory floor. Twenty feet of cable was used allowing ample length for carriage traverse since the recording equipment was midway along the tank.

The recording equipment used consisted of a Sanborn eight channel thermal writing recorder model 358-100A, a Sanborn eight channel low-gain amplifier bank, model 958-2900, and a Hewlett-Packard bank of eight carrier preamplifiers model 8805A (figure 5. 6). The carrier preamplifier provided a 5 volt 2400 Hz excitation signal to the transducers, and demodulated and amplified their output. The low-gain amplifiers provided additional amplification and served as an interface for the recorder. The recorder had eight channels, one of which was used to monitor the carriage position and hence gave the model speed, leaving seven channels available for data.

The output of the pressure transducers was monitored on this recorder. A calibration was done on the entire system at the end of each test, and frequently also at the beginning. Sample data runs and calibration runs are shown in figures 5. 7 and 5. 8 respectively.

The measurements of the pressure coefficient on the body surface were made relative to the static pressure port of a Pitot-static tube of the Prandlt design. The Pitot-static tube was suspended from the carriage and towed alongside the model. A test was made to determine the interference between the model and the Pitot-static tube. The Pitot-static tube was then positioned sufficiently far from the model to minimize these interactions (about eight inches). The

resulting pressure measurements are shown in figures 5. 9, 5. 10, and 5. 11 and are discussed in the next section.

If there exists a depth difference between the Pitot-static tube and the measuring station due to wave action in the tank this will show as erroneous data. A depth difference of only 0. 5 mm can cause an error in the Cp reading of 0. 01 for a carriage speed of 3 ft. /sec. A disturbance of this magnitude would not be detected visually and no other measuring devices were available to measure any such wave heights.

Direct measurements of the pressure difference across the body were subsequently made and thus eliminated the need for a remote reference pressure. Some results of these experiments are shown in figures 5. 12, 5. 13, and 5. 14 for several different locations on the model. The slight negative pressure at zero angle of attack may be explained by the difference in tank boundaries. The lower boundary is a solid surface while the upper is a free surface, and blockage effects indicate an asymmetry in the zero angle of attack case similar to those observed in figures 5. 12 and 5. 13.

5. 2 Discussion of experimental results

The results of the experimental pressure measurements are summarized in figures 5. 9 through 5. 14, where both the absolute pressure and the pressure difference across the body are plotted. Three sets of theoretical curves are also presented in these figures, and are designated throughout with the following notation: — — — — exact potential theory for ellipsoidal bodies as outlined in section 2. 2,

—— – —— slender body theory presented in section 2. 1, and

—— – – —— center plane singularity method outlined in section 2. 3. In figures 5. 12, 5. 13, and 5. 14 the center plane singularity method results lie very close to the slender body theory curves and were omitted there to retain clarity in the plots. The angle of attack is defined positive when the nose is raised toward the free surface as in figure 5. 3. For plots 5. 9, 5. 10, and 5. 11 the point of pressure measurement is then on the lower side of the model facing the tank bottom and hence the oncoming flow at positive angle of attack. For plots 5. 12, 5. 13, and 5. 14 this same convention is retained and

$$\Delta Cp = C_p(\alpha) - C_p(-\alpha)$$

$$= C_p(z) - C_p(-z) \quad .$$

Due to the elliptic nature of the Laplace equation there is continuous dependence of the velocity potential and hence the pressure, on the domain (Courant and Hilbert, 1962). By choosing an ellipsoid which is enclosed by the body and another which enclosed the body it was hoped to find an upper and a lower bound on the solution. However, the pressure was found to be very sensitive to the body shape functions $A(x)$ and $B(x)$ and their derivatives and it was not possible to easily find an ellipsoid which had general applicability as an upper or lower bound for the entire body length. An ellipsoid with nearly the same cross section and longitudinal rate of change of cross section at

a specified x was chosen, and reasonable results are expected from the exact potential theory, since the slender body theory solution indicates a more sensitive dependence on the local body shape functions than on the distant body shape. With this in mind the exact potential solution for an ellipsoid is also plotted, even though the model shape is not ellipsoidal. The ellipsoid shown in figure 5. 1 was used and agreed closely with the model shape near the mid section, deviated somewhat in the nose region, and was grossly in error in the tail region.

Upon comparison of the exact ellipsoid solution with the data it is seen to be largely in error (as much as 50 per cent). It appears from these limited results that the pressure distribution is very sensitive to the body geometry and the use of such an exact potential solution is limited to order of magnitude estimates of flow quantities when used for more general body shapes. The real value of such an exact theory is that it serves as a guide in the investigation and development of new theories as was demonstrated in section 2. 3 for the center plane singularity method.

For the positions near the body center, where the cross sectional area is changing slowly, the results of the slender body theory and the center plane singularity method are in very good agreement with each other and with the data (figures 5. 10 and 5. 11). In the nose region the slender body theory departs from the data while the center plane singularity method continues to follow the data. For an x-position of 15 per cent of the model overall length (figure 5. 9), there is a 25 per cent error in C_p for the slender body theory. This error

is expected since the theory does not have general validity near the body ends, and especially as in our case when the ends are blunt.

The C_p versus α data shows a tendency to be high for positive angles of attack and low for negative angles of attack. Two possible explanations are offered for this observation. The first has already been mentioned in section 5. 1 and relies on a difference in hydrostatic pressure between the model pressure port and the static pressure port on the Pitot-static tube. As mentioned at that time a wave height difference of only 0. 5 mm is sufficient to explain the deviations observed. A dependence on the angle of attack is expected, since for positive angle of attack the model nose and indeed the entire model is positioned closer to the free surface than in the zero angle of attack situation. Whereas in the negative angle of attack case the model nose was positioned closer to the tank bottom, and an asymmetry of the character seen in the data may be expected.

A second possible cause of this trend in the data is boundary wall effects. For the positive angle of attack case, we expect open tunnel blockage corrections to be used since the model is closer to the free surface. Open tunnel blockage indicates that the measured pressure coefficient should be slightly increased in magnitude due to a decrease in the apparent free stream velocity at infinity. For negative angles of attack the model is closer to the tank bottom and solid blocking corrections are more appropriate. These corrections should lead to a somewhat higher free stream velocity than is actually measured by the carriage speed, thus causing a decrease in the pressure

coefficient. The trends in both of these explanations are consistent with the observations, and the roll of each is not clearly specified.

In order to eliminate the possible hydrostatic wave height anomaly the pressure difference across the model at a given x location was measured directly. At zero angle of attack these two ports were in direct vertical alignment, and at eight degrees angle of attack they were horizontally separated by at most 7/16 inches. It is assumed that any waves generated by the motions of the model through the initially quiescent tank have a wave length on the order of the body overall length and over a distance of 7/16 inches the depth change (or wave height) is insignificant. The results of these tests are seen in figures 5. 12, 5. 13, and 5. 14, and slopes are listed for comparison in table 5. 1.

TABLE 5. 1

Theory / Position	Exact Ellipsoid $x10^{-3}(deg.)^{-1}$	Slender Body Theory $x10^{-3}(deg.)^{-1}$	Center Plane Singularity $x10^{-3}(deg.)^{-1}$	Experiments $x10^{-3}(deg.)^{-1}$
x = 3. 45 in. y = 0	22. 2	18. 9	18. 4	19. 1 (22. 1)
x = 7. 2 in. y = 0	4. 86	3. 21	3. 91	6. 02 (5. 89)
x = 7. 2 in. y = 1. 60 in.	4. 84	6. 19	6. 31	9. 54 (9. 47)

A second reason for taking ΔC_p measurements was that the slender body theory predictions of ΔC_p should be less sensitive to

overall body geometry than the C_p predictions and more dependent on local body shape, and hence give a wider range or validity for the theory. Table 5. 1 illustrates this feature and better agreement is seen with the center plane singularity method. For the position $x = 3.45$ in. the two theories and the experimental result agree to within 4 per cent. However there is substantial error (up to 40 per cent) in the last two cases where $x = 7.2$ in. It should be noted that at these two locations (i. e., at $x = 7.2$ in.) the full scale pressure readings were on the order of 2 mm H_2O, and at this low pressure level an uneven blockage effect need only amount to a fraction of a mm H_2O to account for the departure from the theories. Since the measurements rule out the hydrostatic pressure difference, we conclude that the discrepancy must be due to differences in the wall effects as just discussed.

From the C_p versus α data of figures 5. 9, 5. 10, and 5. 11 we can further plot ΔC_p versus α. The resulting straight line slopes are 0. 0221, 0. 00589, and 0. 00947 respectively and are listed in parentheses in table 5. 1. These last two (for $x = 7.2$ in.) agree within two per cent of the results of figures 5. 13 and 5. 14, but the first case is in error by 15 per cent. This discrepancy at $x = 3.45$ in. is attributed to an angle of attack dependent wave height between the pressure station on the model and the Pitot-static reference pressure.

5. 3 Concluding remarks

From the experimental pressure measurements and the theoretical pressure calculations and their comparison, we can make several concluding remarks. The first conclusion is that the use of the exact triaxial ellipsoid solution does not appear to have a uniformly high accuracy when used to approximate the detailed pressure distribution on a body of general shape. The real value of this class of exact solutions is in suggesting theoretical techniques of solution and in supplying an exact solution for special geometries to which theories of more general applicability must reduce. Next, as seen from the C_p vs. α plots, good agreement is obtained between the data and the center plane singularity method and the slender body theory, with the only exception being in the nose region where the slender body theory becomes less accurate, as indicated by its departure from the data. Since computations are more easily carried out using the slender body theory, it is suggested for use in predicting pressures away from the body ends. When the distance from the nose (or tail) is of the same order as the body cross sectional dimension, departure of the slender body theory from the data is seen (figure 5. 9) and in these regions a more exact solution (e. g. , the center plane singularity method) is required.

A great deal of effort was devoted to the pressure measurements, especially in overcoming the problems associated with the sensitivity at extremely low pressure levels, the minute hydrostatic pressure differences, and the thermal convection from the pressure transducers. The system which is described above was found to be

adequate for measuring the steady pressures, but serious problems will arise when the present experimental system is applied to investigate flow involving unsteady pressures. Measurement of such unsteady pressures on an accelerating body remains as a formidable problem for which future developments in flush mounted pressure transducer design are almost essential. Such developments are regarded as important not only in the present application but throughout the field of hydrodynamics where unsteady local flow quantities are of growing concern.

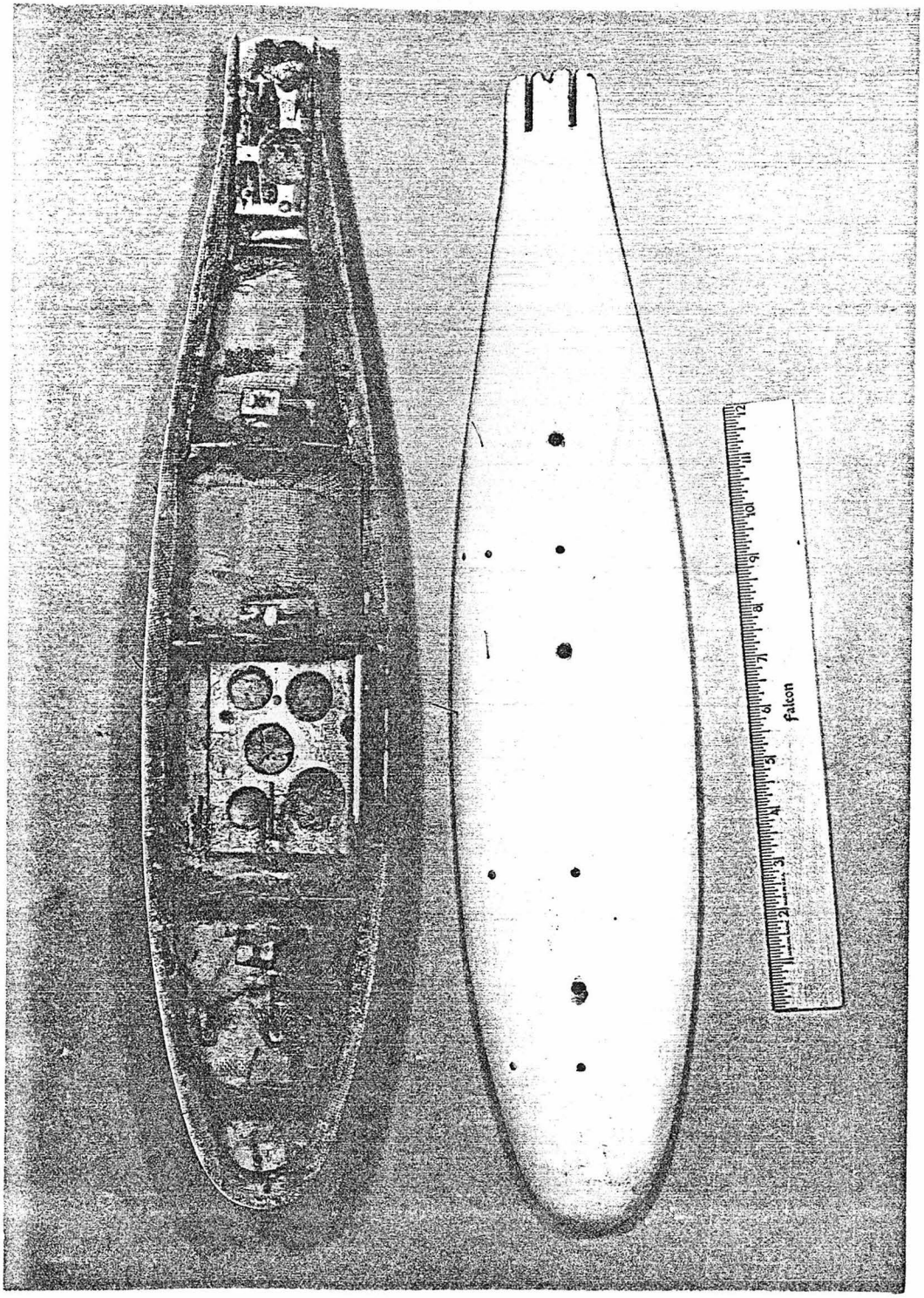

Figure 5.1. Fiberglass model molded after a Chinook salmon and used in towing tank tests.

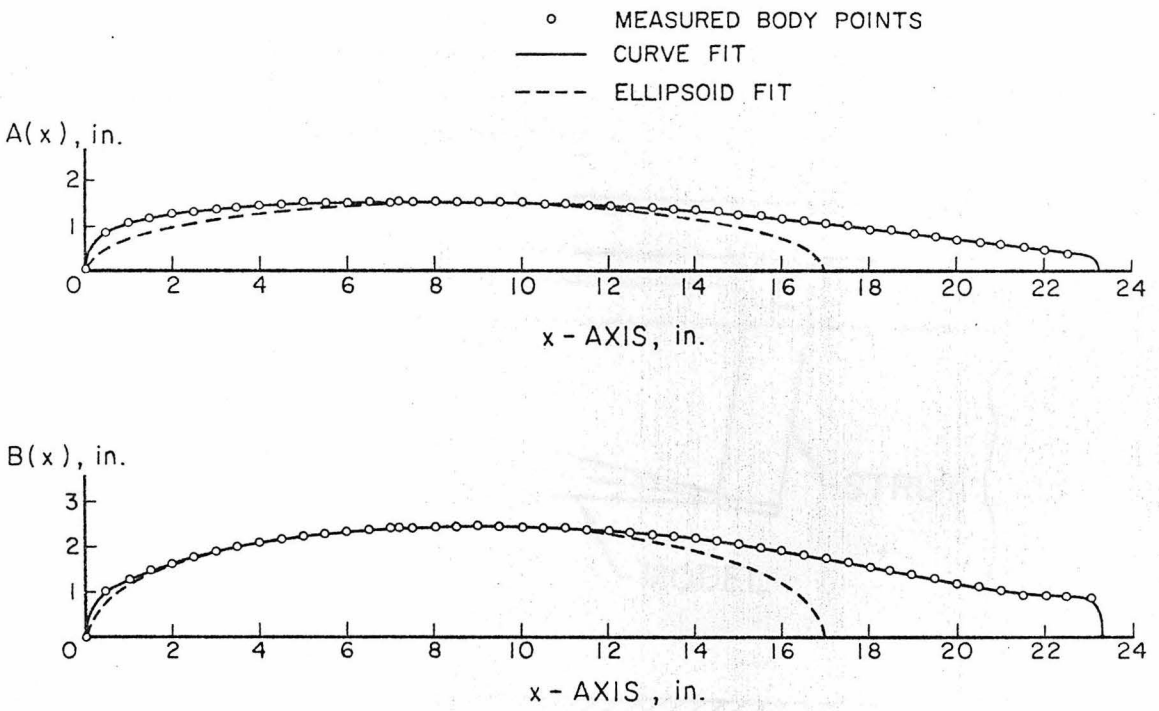

Figure 5. 2. Curve fits to the fiberglass model of figure 5. 1.

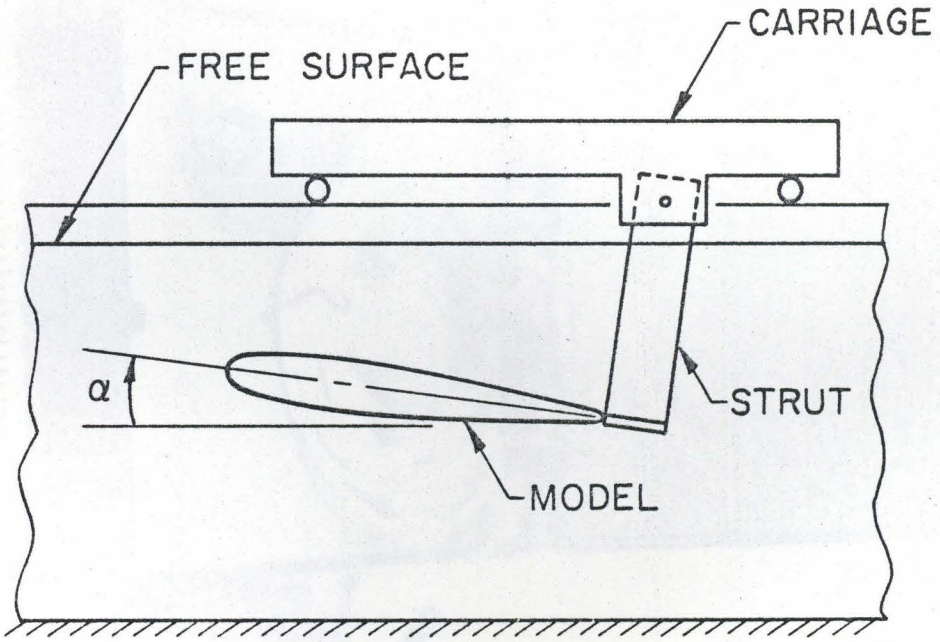

Figure 5. 3. Side view illustration of experimental setup with model at a 7 degree angle of attack.

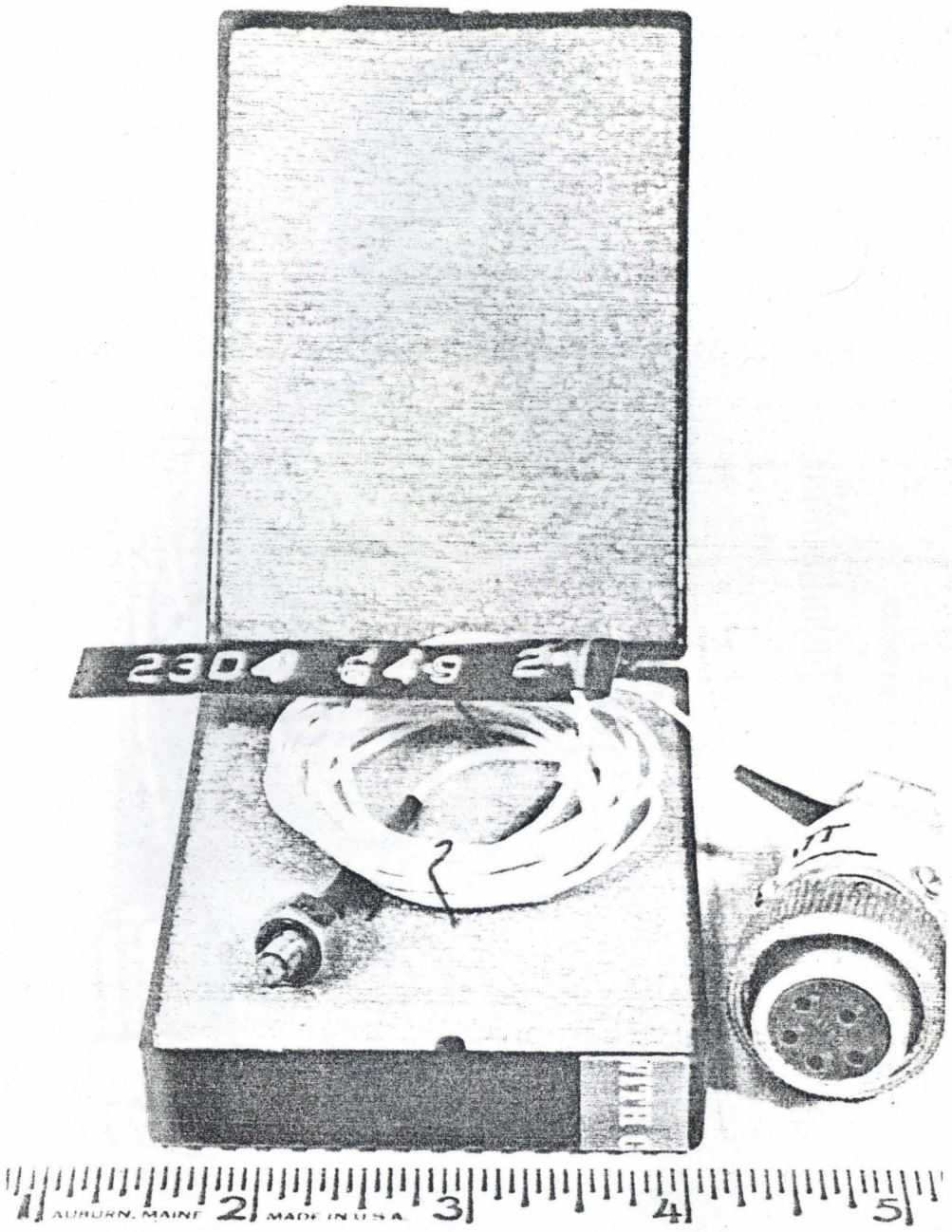

Figure 5. 4. Miniature flush mounted pressure transducer (Entran Devices model EPS-1032).

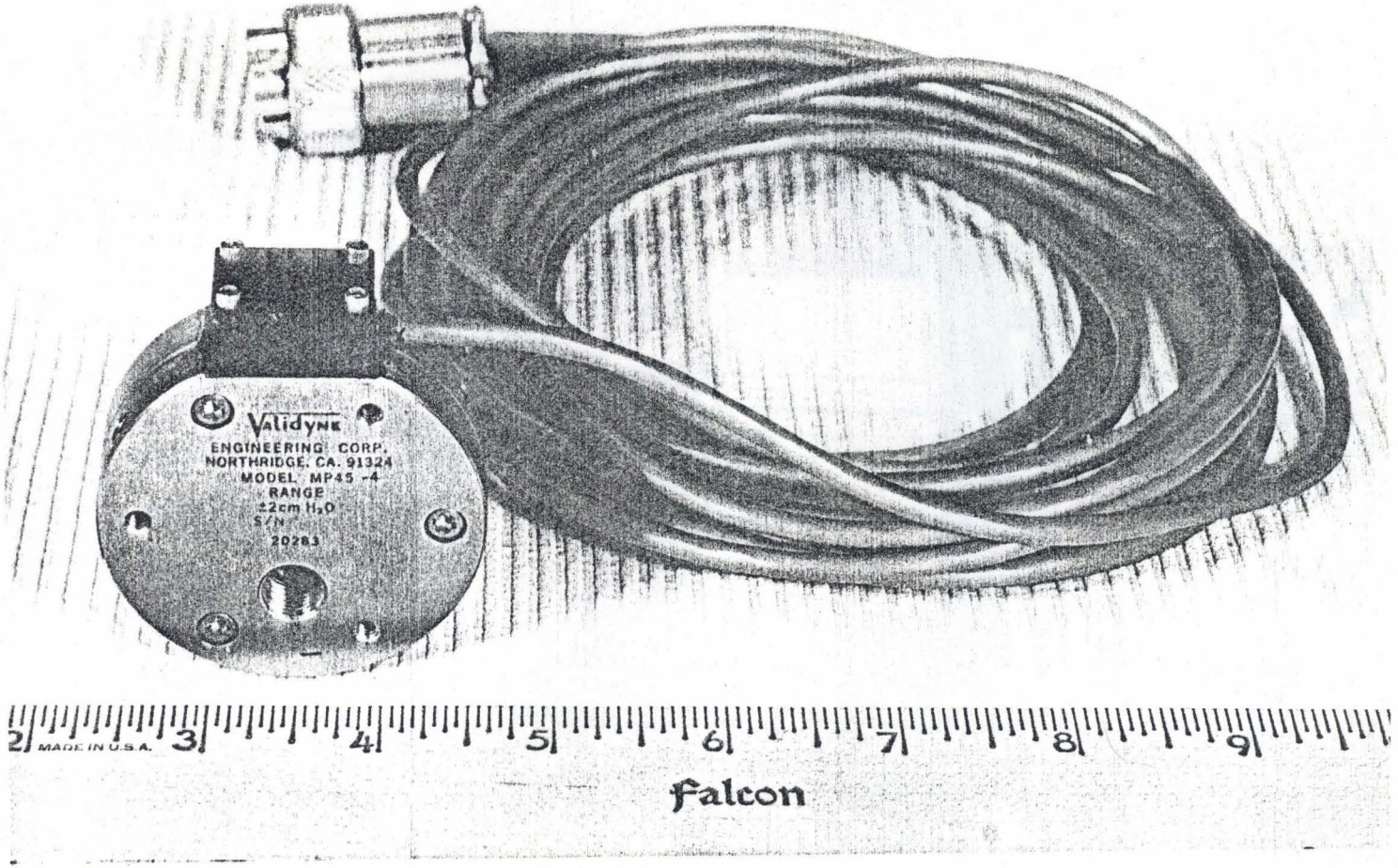

Figure 5. 5. Validyne model MP45-4 high sensitivity pressure transducer.

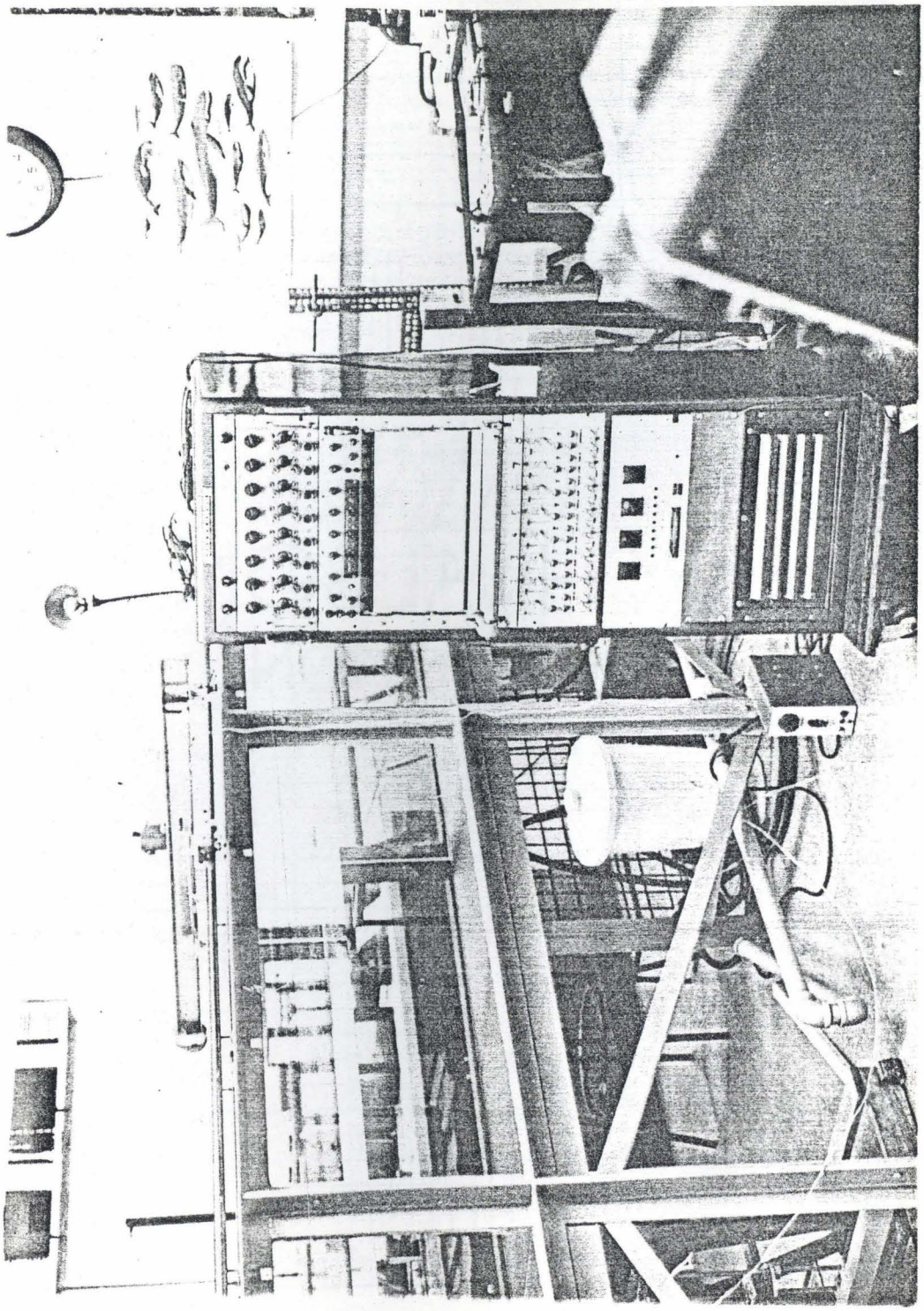

Figure 5.6. Section of the 25 foot towing tank, with overhead carriage and chart recorder.

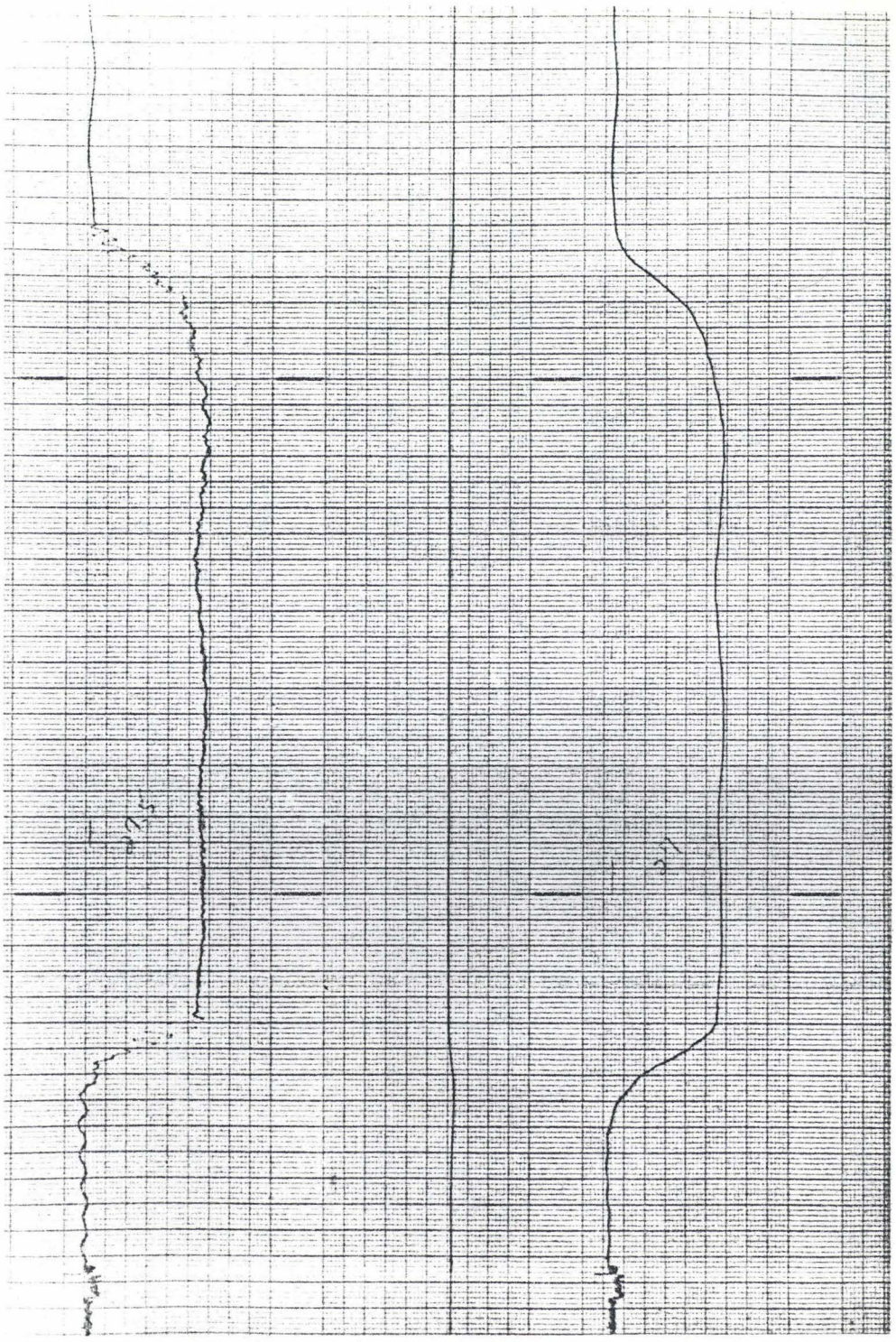

Figure 5.7. Chart recording of data, time runs from right to left (0.2 sec/div.) pressure runs vertical (1 mm H_2O/div.).

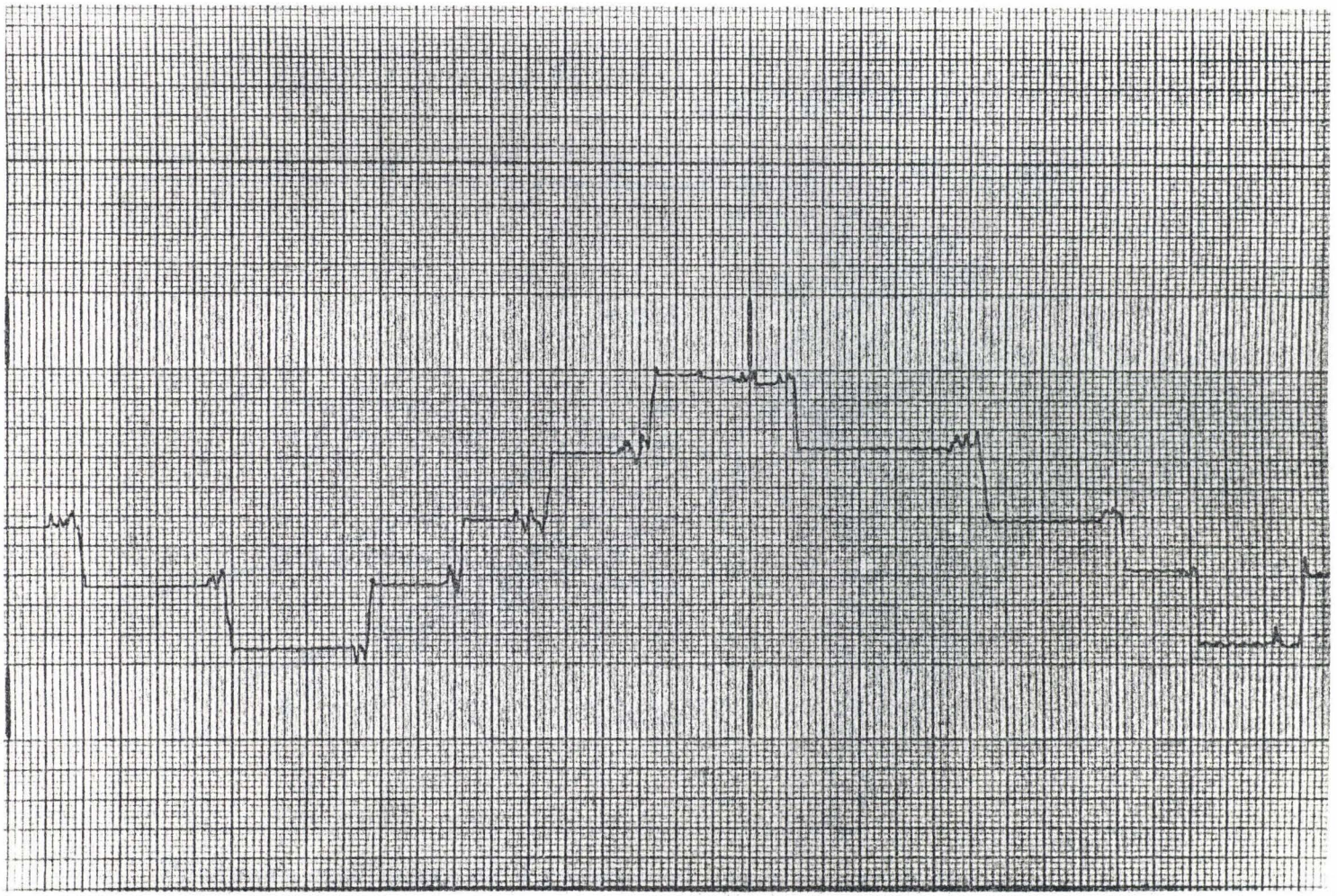

Figure 5. 8. Calibration of Validyne pressure transducer, done in increments of 1 mm of water.

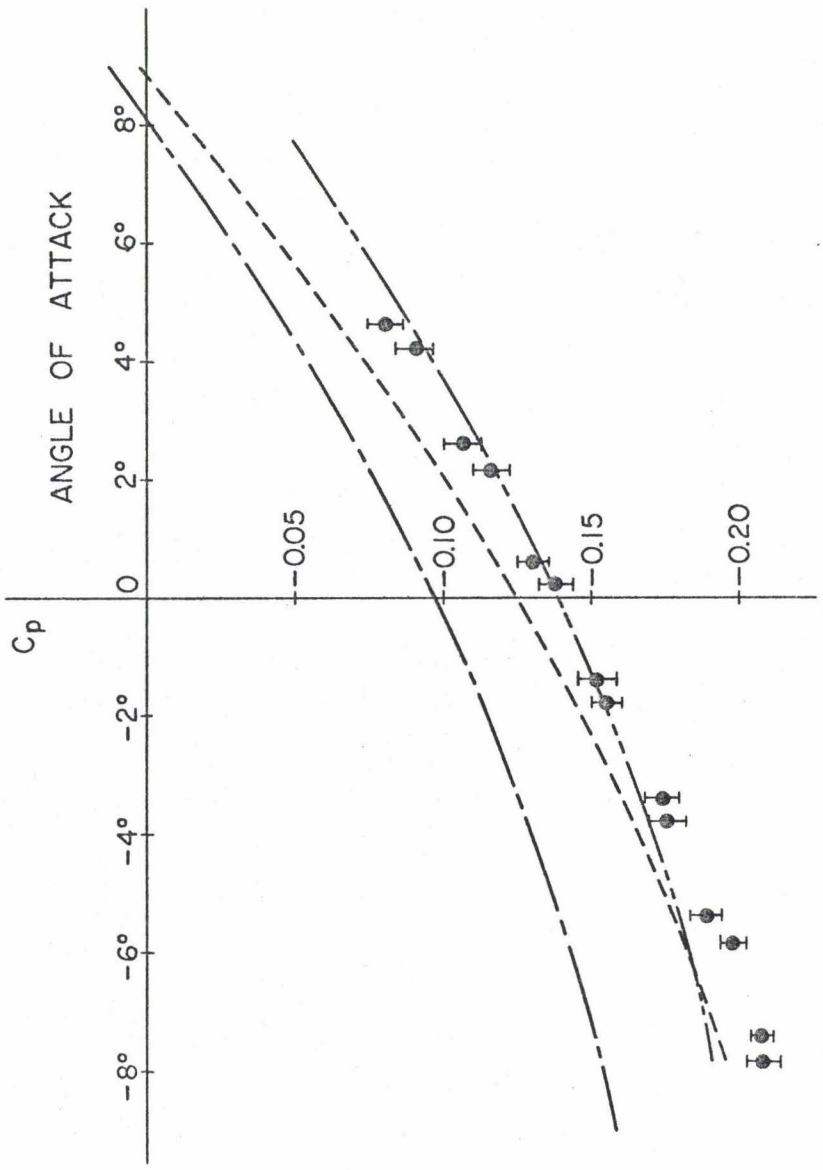

Figure 5.9. Pressure coefficient as a function of angle of attack for a point on the body surface at x = 3.45 in. and y = 0.

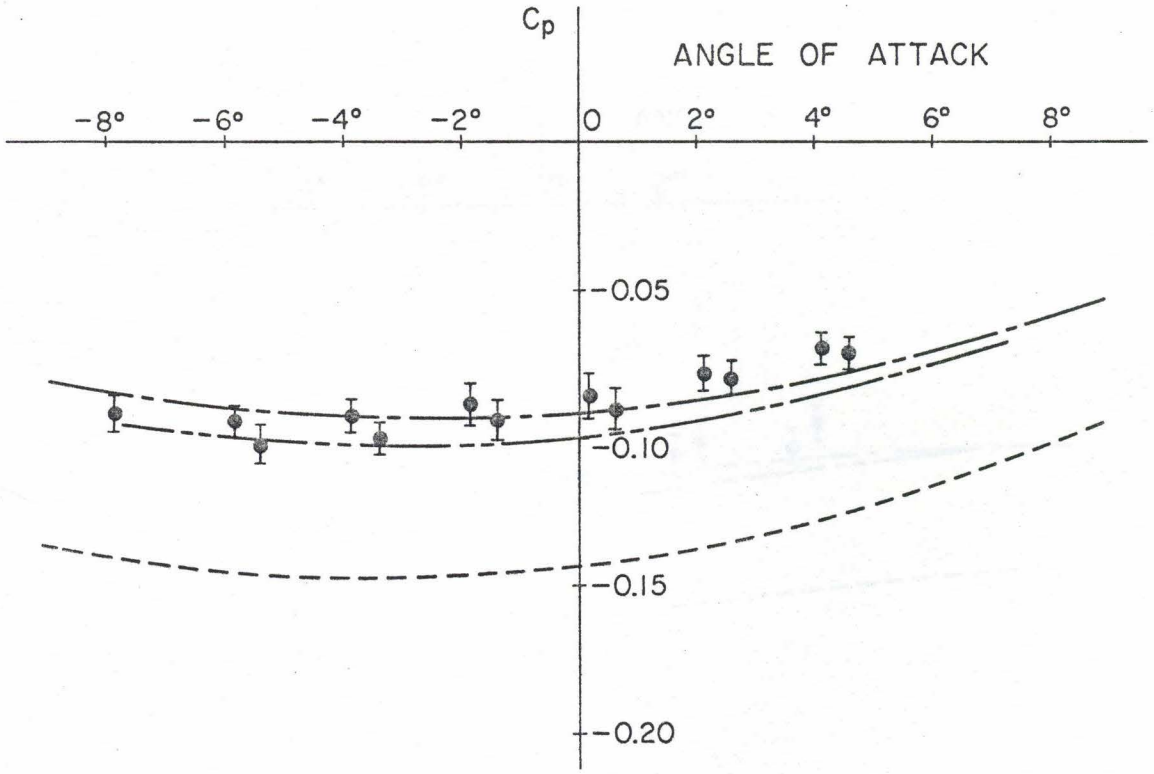

Figure 5.10. Pressure coefficient as a function of angle of attack for a point on the body surface at x = 7.2 in. and y = 0.

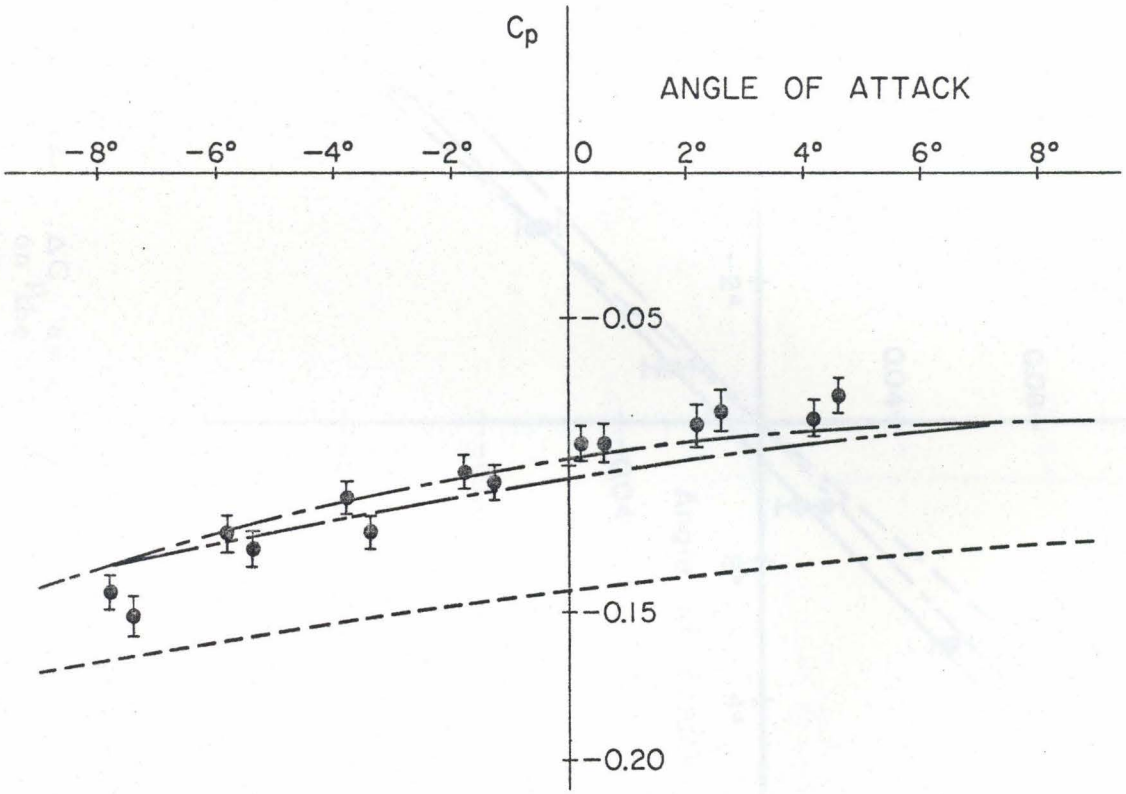

Figure 5.11. Pressure coefficient as a function of angle of attack for a point on the body surface at x = 7.2 in. and y = 1.60 in.

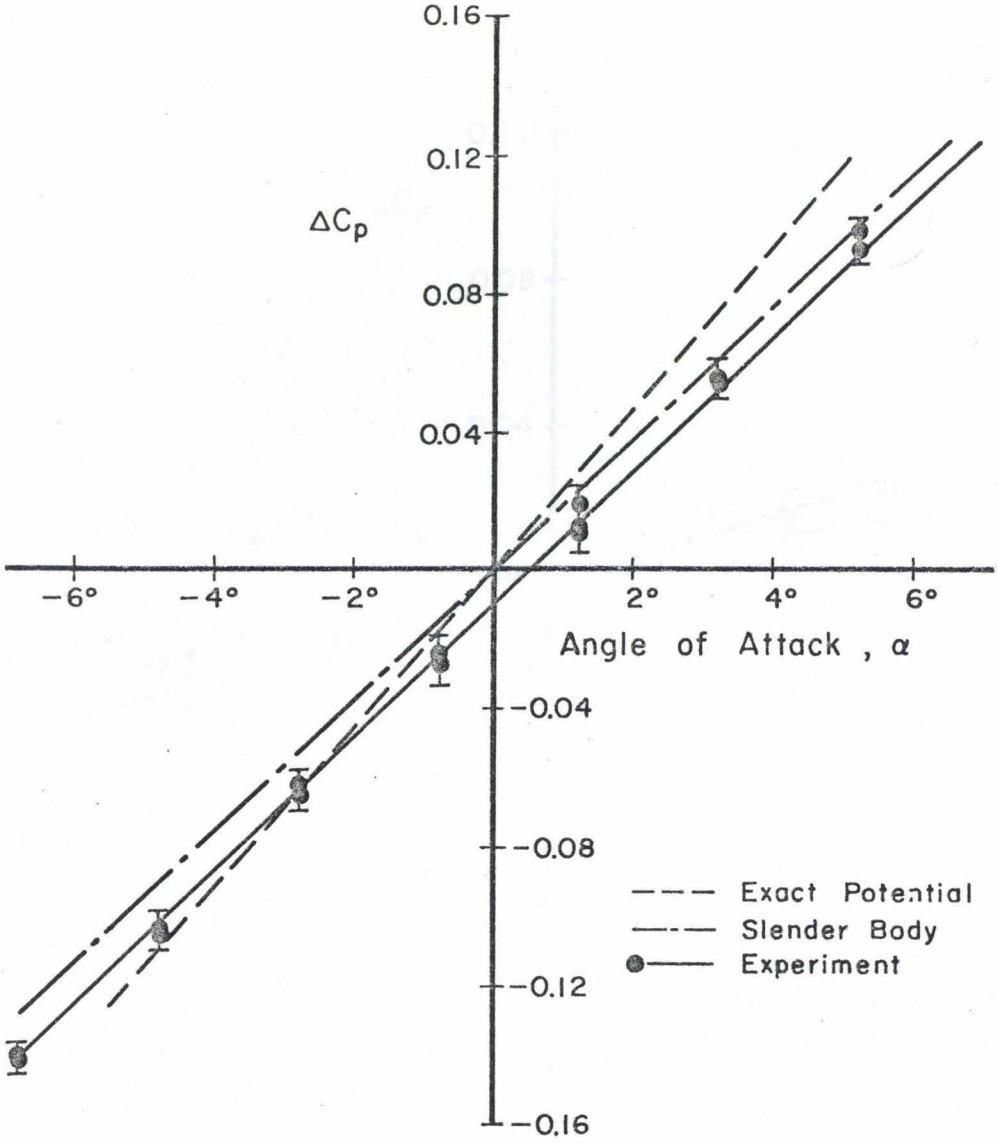

Figure 5. 12. ΔC_p as a function of angle of attack for a point on the body surface at x = 3. 45 in. and y = 0.

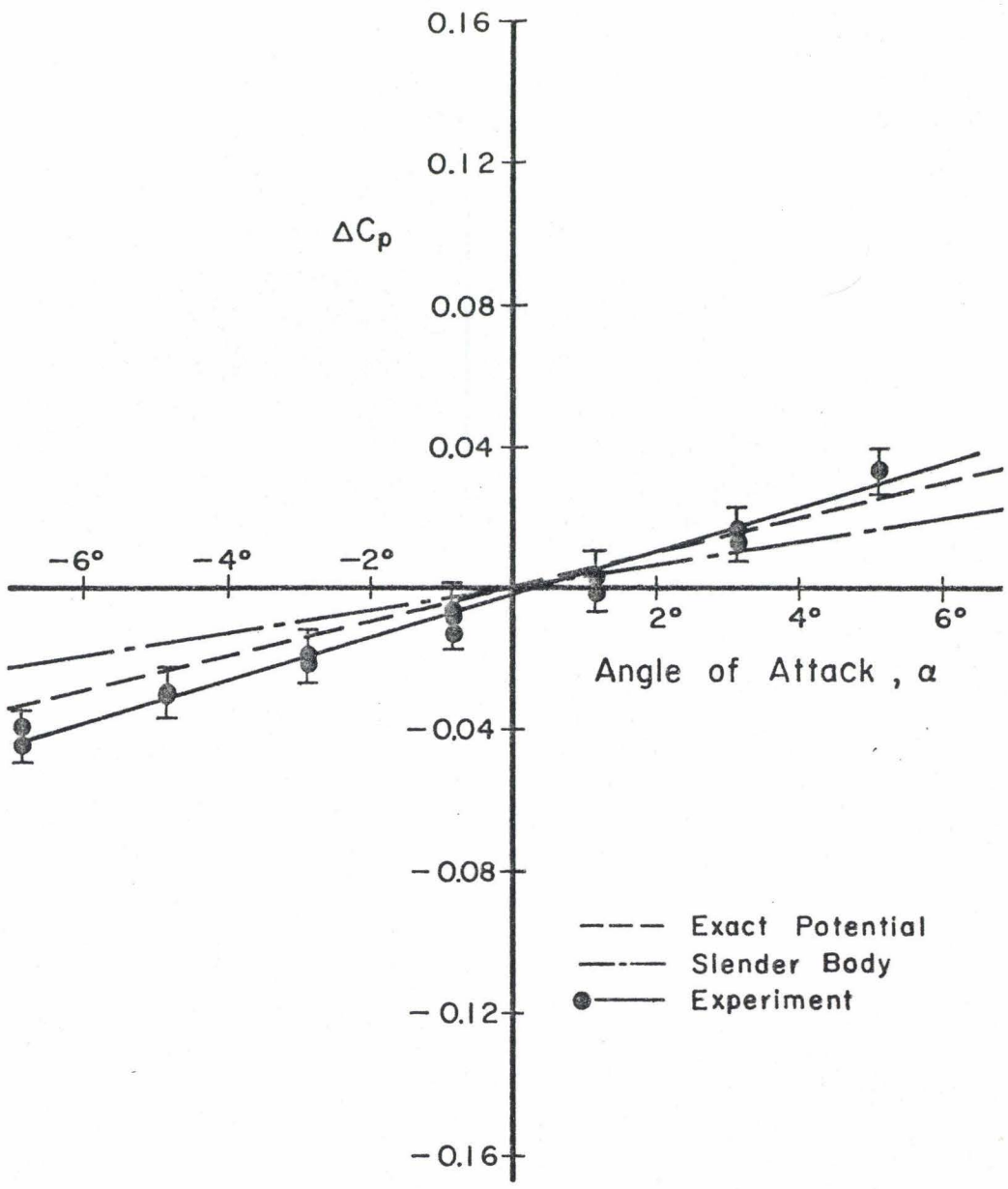

Figure 5.13. ΔC_p as a function of angle of attack for a point on the body surface at $x = 7.2$ in. and $y = 0$.

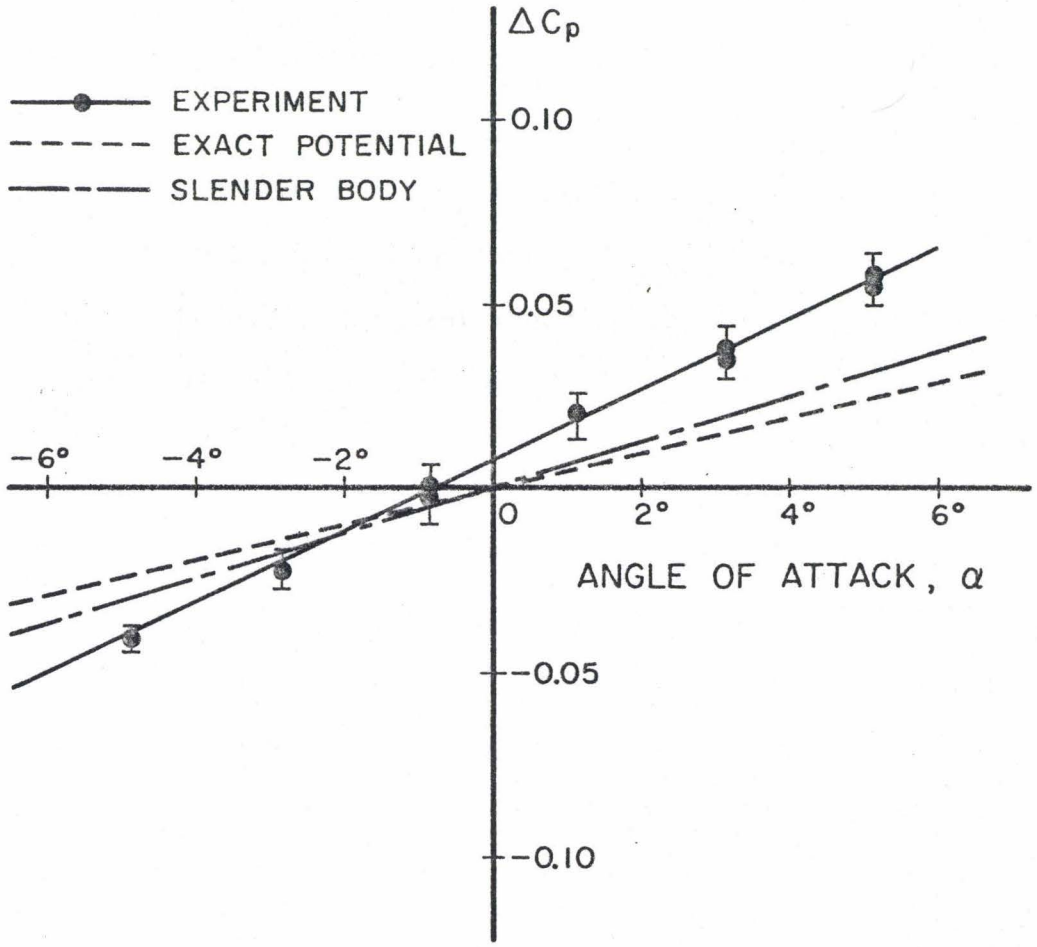

Figure 5.14. ΔC_p as a function of angle of attack for a point on the body surface at $x = 7.2$ in. and $y = 1.60$ in.

VI. OBSERVATIONS ON THE SWIMMING OF ELONGATED BODIES

Observations of the swimming motion of two aquatic animals were made, with special interest in their applications to the theory developed in chapter IV. Such data were found useful in choosing reasonable parameters in the theoretical calculations and in viewing the validity of the theory. In light of the developments in chapter IV an elongated swimmer was sought which had a circular body cross section, exhibited finite amplitude body undulations, and lacked body appendages from which vortex shedding might be expected. Two such organisms were found and their swimming motion documented.

6.1 Leech

The first organism investigated was a common leech (Hirudo medicinalis). Although the leech has a highly extensible body, capable of altering its overall body length many-fold, the body length remained constant during steady swimming maneuvers. The leech had an overall length of 4 cm (as measured during steady swimming) and hence was swimming at a Reynolds number of 1.4×10^3. Observations were made in a shallow (1.5 cm deep) plastic dish with a 1/2 in. square grid placed beneath for a length scale. The leech was viewed from above with a Shibaden model HV-15S television camera and the motion was recorded on a Sanyo model VTR video tape recorder. The framing rate of the recorder was thirty frames per second, which was sufficient to catch 17 frames for each beat cycle. A frame by frame analysis gave the data listed in table 6.1.

6.2 Eel

Observations were also made on a fresh water eel (Synbranchus marmoratus). This species lacks dorsal and ventral fins and has a nearly circular body cross section except in the posterior third of the body where it showed a lateral flattening. The eel was allowed to swim in an aquarium 25 cm wide by 120 cm long with a water depth of only 6 cm to ensure that the eel would swim in a horizontal plane. Using a 16 mm Photosonics model 1P movie camera, motion pictures were taken from above at about 50 frames per second, and a frame by frame analysis gave the data listed in table 6.1. Figure 6.1 shows a series of successive frames (0.0356 seconds between frames) corresponding to sequence 2 in table 6.1, with a grid having 2 cm squares placed on the tank bottom to provide a length scale.

TABLE 6.1

	Leech	Eel (seq. 1)	Eel (seq. 2)
body length, ℓ [cm]	4.0	19.42	19.42
body radius, b [cm]	0.079	0.28	0.28
mean speed, U [cm/sec]	3.39	30.45	33.90
wave speed, c [cm/sec]	5.61	45.54	49.96
wave length, λ [cm]	3.4	11.24	11.39
frequency, f [cycle/sec]	1.76	3.61	4.68
head amplitude [cm]	0.78	0.33	0.65
tail amplitude [cm]	1.33	4.47	4.19
mean head to tail separation [cm]	3.45	18.0	18.0
Reynolds number, $U\ell/\nu$	1.356×10^3	5.91×10^4	6.58×10^4
specific speed, U/ℓ	0.85	1.57	1.75
c/U	1.65	1.50	1.47
slenderness ratio, $\epsilon = \ell/b$	0.0198	0.0144	0.0144

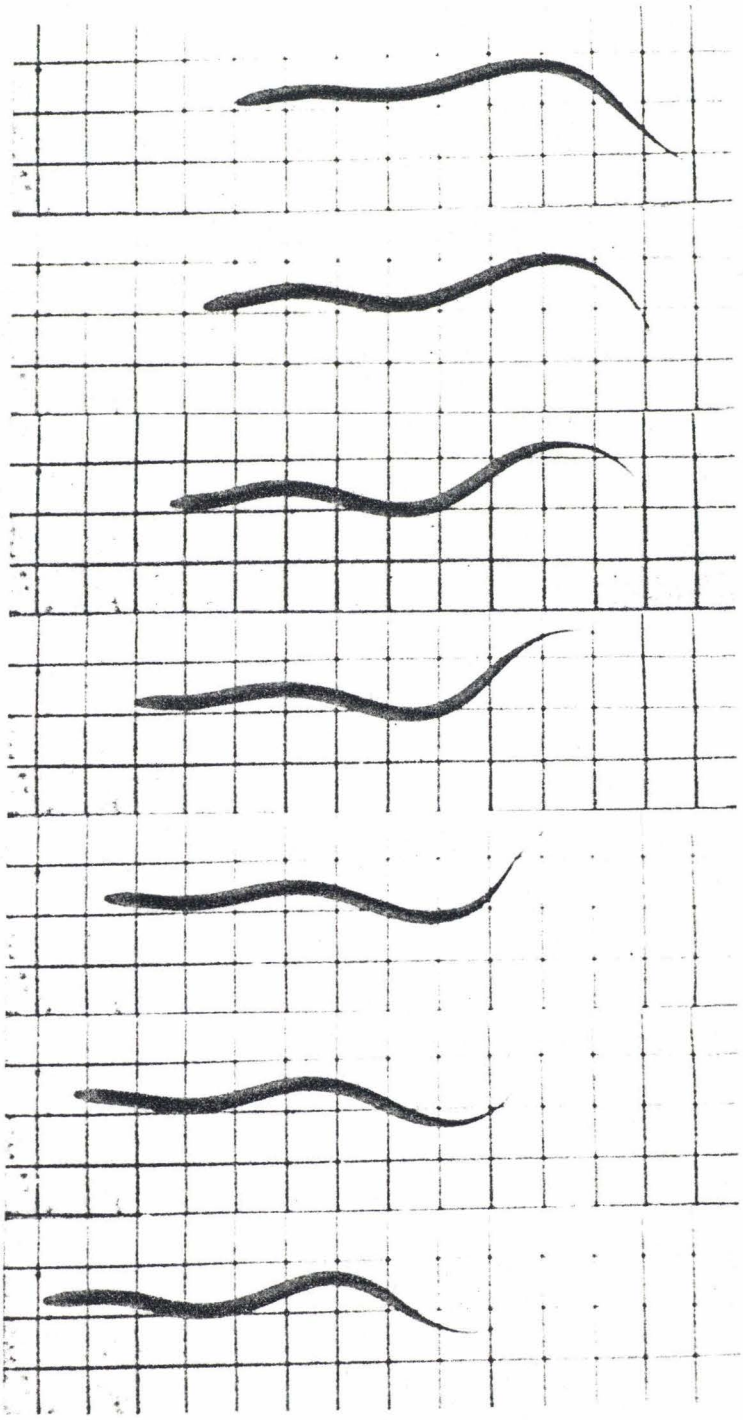

Figure 6. 1. Swimming of a fresh water eel (Synbranchus marmoratus). Grid is 2 cm square and 0. 0356 sec. between frames (see table 6. 1, seq. 2).

REFERENCES

Courant, R. and Hilbert, D. 1962 Methods of mathematical physics. Vol. II, Interscience Publishers, a division of John Wiley & Sons, New York.

Doebelin, E. O. 1966 Measurement systems application and design. McGraw-Hill Book Co.

Gabrielli, G. and von Karman, T. 1950 What price speed? Specific power required for propulsion of vehicles. Mechanical Engineering, 72, 775-781.

Glauert, M. D. and Lighthill, M. J. 1955 The axisymmetric boundary layer on a long thin cylinder. Proc. Roy. Soc. London Series A 230, 188-203.

Gray, J. 1933a Studies in animal locomotion I. The movement of fish with special reference to the eel. J. Exp. Biol., 10, 88-104.

Gray, J. 1933b Studies in animal locomotion II. The relationship between the waves of muscular contraction and the propulsive mechanism of the eel. J. Exp. Biol., 10, 386-390.

Gray, J. 1936 Studies in animal locomotion VI. The propulsive powers of the dolphin. J. Exp. Biol., 13, 192-199.

Gray, J. 1968 Animal locomotion. World Nat. Ser., Weidenfeld & Nicolson, London.

Havelock, T. M. 1931 The wave resistance of an ellipsoid. Proc. Roy. Soc. A, 132, 480-486.

Jones, R. T. 1946a Properties of low-aspect-ratio pointed wings at speeds below and above the speed of sound. NACA TN 1032.

Jones, R. T. 1946b Properties of low-aspect-ratio pointed wings at speeds below and above the speed of sound. NACA Report 835.

Letcher, J. S. 1975 Sailing hull hydrodynamics, with re-analysis of the Antiope data. Trans. SNAME, 83, 1-17.

Lighthill, M. J. 1960a Mathematics and aeronautics. J. Roy. Aero. Soc., 64, 375-394.

Lighthill, M. J. 1960b Note on the swimming of slender fish. J. Fluid Mech., 9, 305-317.

Lighthill, M. J. 1969 Hydromechanics of aquatic animal propulsion. Annu. Rev. Fluid Mech., 1, 413-446.

Lighthill, M. J. 1970 Aquatic animal propulsion of high hydro-mechanical efficiency. J. Fluid Mech., 44, 265-301.

Lighthill, M. J. 1971 Large-amplitude elongated-body theory of fish locomotion. Proc. Roy. Soc. Lond. B, 179, 125-138.

MacMillan, W. P. 1958 The theory of the potential. Dover Publications, Inc., New York, New York.

Munk, M. M. 1924a Note on the pressure distribution over the hull of elongated airships with circular cross section. NACA TN 192.

Munk, M. M. 1924b The aerodynamic forces on airship hulls. NACA Report 184.

Newman, J. N. 1975 Swimming of slender fish in a nonuniform velocity field. J. Austral. Math. Soc., 19 (Series B), 95-111.

Newman, J. N. and Wu, T. Y. 1973 A generalized slender body theory for fish-like forms. J. Fluid Mech., 57, 673-693.

Pankhurst, R. C. and Holder, D. W. 1952 Wind-tunnel technique; an account of experimental methods in low - and high-speed wind tunnels. Pitman & Sons, London.

Pope, A. and Harper, J. J. 1966 Low-speed wind tunnel testing. John Wiley & Sons, Inc., New York.

Saffman, P. G. 1967 The self-propulsion of a deformable body in a perfect fluid. J. Fluid Mech., 28, 385-389.

Schmidt-Nielsen, K. 1972 Locomotion: Energy cost of swimming, flying, and running. Science, 177, 222-228.

Tucker, V. A. 1970 Energetic cost of locomotion in animals. Comp. Biochem. Physiol., 34, 841-846.

Tucker, V. A. 1975 The energetic cost of moving about. Am. Scientist, 63, 413-419.

Ward, G. N. 1955 Linearized theory of steady high-speed flow. Cambridge, University Press, London, New York.

Webb, P. W. 1975 Hydrodynamics and energetics of fish propulsion. Bulletin 190, Fish. Res. Board Can., Ottawa, Canada.

Wu, T. Y., Brokaw, C. J. and Brennen, C. (editors) 1975 Swimming and flying in nature, Vols. 1 & 2. Plenum Press, New York and London.

Wu, T. Y. and Chwang, A. T. 1974 Double-model flow theory: A new look at the classical problem. Contribution to the Tenth ONR Symposium on Naval Hydrodynamics, June 24-28, Massachusetts Institute of Technology.

Wu, T. Y. 1975 Introduction to the scaling of aquatic animal locomotion. Cambridge Symposium, Biodynamics of animal locomotion, 1-5 September, England.